THE INTERACTIONS OF PRESSURE SENSITIVE ADHESIVE WITH PAPER SURFACES

By

BOXIN ZHAO, B. Eng., M. Eng.

A Thesis

Submitted to the School of Graduate Studies

In Partial Fulfillment of the Requirements

For the Degree of

Doctor of Philosophy

McMaster University

THE INTERACTIONS OF PRESSURE SENSITIVE ADHESIVE WITH PAPER SURFACES

DOCTOR OF PHILOSOPHY — MCMASTER UNIVERSITY

(Chemical Engineering) — Hamilton, Ontario

TITLE: The Interactions of Pressure Sensitive Adhesive with Paper Surfaces

AUTHOR: Boxin Zhao

B. Eng. (Central South University of Technology, China)

M. Eng. (Institute of Chemical Metallurgy at Chinese Academy of Science, China)

SUPERVISOR: Professor Robert Pelton

NUMBER OF PAGES: xiii, 136

Abstract

The interactions of pressure sensitive adhesive (PSA) with paper surfaces were investigated by using peel adhesion testing as a probe. The objectives of this work were to reveal the fracture mechanism of paper/adhesive laminates and establish the links between paper properties and the performance of PSA tapes.

Particular attention was given to analyzing paper/adhesive peel curves. It was found that the peak peel force (i.e. the maximum force in a peel curve) was more effective for analyzing peelings from paper than the conventionally used steady-state force. Based on this, we developed a new peel data analysis method by which the overall peel behavior of a paper/adhesive combination is conveniently summarized by plotting the log peak peel force as a function of the log peel rate. This approach yielded a generalized peel curve consisting of a rate-dependent interfacial domain and a rate-independent failure domain.

The force generated at the paper surface in peeling was analyzed; it was found to be proportional to the overall peel force. By varying peel rates, the two types of forces were shown to have a linear relationship for the two tape types and two paper types investigated. This result justifies the use of the easily measured peel force as an estimate of the real force at the interface.

Rapid peelings induce paper delamination in which paper is separated into two layers. Microscopic analysis revealed that there are three sub-processes: 1) initially, the top layer of fibers, beneath the peel front, is lifted; but, 2) it must be fractured in order for the fiber layer to be peeled from the paper sheet; and, 3) in the steady-state delamination region, the top layer of paper fibers are peeled from the paper. Processes 1 and 2 only occur initially, whereas delamination (process 3) occurs continuously during peeling. The initiation of paper delamination from the surface was found to require more than double the steady delamination force because of the need to fracture the top fiber layer (process 2).

For the first time, links between paper properties and the performance of PSA have been identified by the use of advanced statistical analysis and the newly developed approach for analyzing paper/adhesive peel curves. The paper properties influencing peel force in the interfacial failure domain are, primarily, the paper surface chemistry characterized by oxygen/carbon ratio (determined by X-ray photoelectron scanning analysis) and, secondarily, the surface roughness. The governing paper property in the paper failure domain is the paper internal (Scott) bond strength. The log-log slope in the interfacial failure domain is independent of paper properties, and it is found to be governed by adhesive rheology.

Finally, the fundamental research was extended to solve a practical problem. We developed a new peel-based test for paper surface strength, in which the force required to initiate paper delamination when peeling a strip of adhesive tape is proposed as a measure of paper surface strength. This method makes it possible to compare surface strength with

other strength properties of paper. Further, this surface strength was found to be independent of peel rate and strongly correlated to the IGT strength (an industrial measure of paper surface strength).

Acknowledgements

Firstly, I wish to thank my advisor Dr. Robert Pelton for his guidance and encouragement. He has also given me many opportunities to network with industry, attend conferences and meet other experts in the field. All these have helped me grow as a scientist and scholar. I would like to thank the members of my academic committee Dr. An-Chang Shi and Dr. Philip Wood for their support and valuable input, and 3M Canada and the National Science and Engineering and Research Council for funding the research.

My appreciation goes to Dr. Mark Kortschot (University of Toronto), Dr. Sören Östlund and Dr. Lars Wågberg (KTH, Sweden), and Dr. Kaarlo Niskanen (KCL, Finland) for their useful discussion and constructive suggestions on paper physics; to Dr. John Vlachopoulos (McMaster University) for suggestions on polymer rheology; to Dr. Honglu Yu and Dr. John MacGregor (McMaster University) for helping with the statistical analysis; to Dr. Atsushi Tanaka, Mr. Rolf Wathen, and Ms. Malin Eriksson for helping organize my European trips.

This work required a large number of tape and paper samples as well as some specialized testing. For these, I thank 3M Canada for providing many adhesive tapes, Dr. Bruce Arnold (Chair of the ASTM Paper Aging Research Program) for providing pilot machine-made fine paper samples, Domtar's Donohue Mill for providing newsprint samples, and Dr. Joseph Aspler and Mr. Anthony Manfred for helping with IGT testing on paper surface strength in the Paprican printability laboratory in Montreal.

I would also like to thank all my colleagues at the McMaster Center for Pulp and Paper Research for their friendship and support which made my time in the laboratory so enjoyable. Special thanks go to my summer students Elaine Miasek, Alison Banks and Luis Anderson for their excellent assistance on conducting experiments and kind help with my English. The departmental staff, Doug Keller, Paul Gatt, Kathy Goodram, Julie Birch and Lynn Falkiner, are thanked for their technical and administrative assistance.

I am grateful to my parents, sisters, brothers-in-law for their love and support. Most of all, I would like to thank my wife Zhiyu Gong for her love and encouragement.

TABLE OF CONTENTS

LIST OF FIGURES

LIST OF TABLES

Chapter 1 Introduction

The interactions of pressure sensitive adhesive with paper surfaces are important for many applications such as packaging and lamination, where a proper control of adhesion at the interfaces is required. For example, the splicing tapes used to join paper rolls require rapid adhesion giving a strong splice at paper machine speeds which are usually more than 1000m/min [1].

Although it has long been realized that paper properties affect tape adhesion, the detailed links between properties of paper and those of paper/adhesive laminates are unknown. In contrast to the huge literature on both paper and adhesive technologies, there is only a few research papers [2,3,4,5] describing paper/adhesive interactions. This is partly because of the complicated nature of paper and adhesives and partially because of the lack of an appropriate method to analyze the interactions between adhesives and paper. The objective of this thesis is to investigate the interplay between paper and adhesive tape.

This chapter provides some background knowledge for the rest of the thesis. It has three sections: paper, adhesive tape and fundamentals of adhesion, and concludes with an outline of the thesis.

1.1 Paper

1.1.1 Paper as a fiber network

Paper is a network of fibers which are isolated either mechanically or chemically from wood. In papermaking, wood fibers are initially suspended in water; this fiber suspension flows onto the wire mesh of a paper machine where water drains through the wire leaving the fibers on the wire surface. Upon drying, adhesion develops in the overlapping zone of two fibers forming *the interfiber bond.* It is the interfiber bonds that hold the fibers together to form a macroscopically continuous material. The average fiber length is about 2mm which is much greater than the thickness of a paper sheet (around 100μm for uncoated paper), so the fiber network is planar and almost two-dimensional.

P*ulp beating* and *wet pressing* are used in the papermaking to improve the extent and strength of interfiber bonds. The main function of pulp beating is to improve fiber flexibility by partly delaminating the fiber cell walls whereas wet pressing helps force the fibers together before drying.

1.1.2 Paper as a composite material

The major component of paper fibers is cellulose. Besides that, paper contains many other components, either natural, or deliberately added to improve its performance.

For example, paper from mechanical pulp, such as newsprint, contains lignin and natural hydrophobic resinous components. The surface of fine paper made from chemical pulp, such as copy paper, is usually treated with hydrophobic chemical sizing molecules to reduce water and ink penetration. In addition, fillers are often added to paper so as to reduce the cost and improve its appearances. All these chemical additives contribute to the paper properties, turning paper into a complicated composite so as to meet the demands of various applications.

Paper products can be divided into two categories – coated and uncoated. Properties of uncoated paper are mainly determined by the fiber properties, their structural arrangement and the presence of functional additives. Examples of uncoated paper are newsprint, printing/writing paper and packaging paper. For coated paper such as magazine paper, there is a coating layer (mainly pigments and polymer binders), so the surface properties depend largely on the nature of the coating layer.

1.1.3 Paper structural properties

The structural properties of paper depend upon the spatial arrangement of fibers in the paper sheet. Some common characteristics are paper basis weight or grammage, thickness, density, relative bonded area (RBA), formation, sidedness, porosity and paper directionality. These properties are described in many textbooks in paper science such as *Properties of Paper: An Introduction* (Tappi Press, 1995) [6] and *Paper Physics* (Fapet Oy, 1998) [7]. The paper properties relevant to this thesis are briefly reviewed in the following.

Basis weight, or grammage, is defined as mass per area. It depends mainly on the amount of fibers per unit area of paper, although other papermaking additives, such as fillers, affect this value. Paper basis weight is important for at least two reasons: firstly, the trading of paper products is mostly based on weight; and secondly, there is no absolute value for paper thickness.

Paper thickness is only a relative parameter because paper is compressible. So paper thickness is always measured under a specified pressure. The value of paper thickness is often used to calculate paper density – see next. In addition, paper stiffness depends on its thickness; the thicker the paper, the stiffer it is.

Paper density is the ratio of paper basis weight to paper thickness. It is a fundamental material property. Most paper strength properties are related to paper density. It is usually called "apparent paper density" because of the relative nature of paper thickness.

Paper directionality refers to its anisotropic structure. Figure 1.1 illustrates three major directions of paper: machine direction (MD), cross direction (CD) and Z-direction (ZD). This arises from the process of papermaking, in which fibers tend to form layers and to be aligned parallel to the paper machine direction (MD). In addition, fibers ends are found to be orientated up or down in the z-direction although their mean direction is in the plane of the paper sheet [8,9]; apparently this is because of the hydrodynamic effects in papermaking, but its precise cause is still unknown.

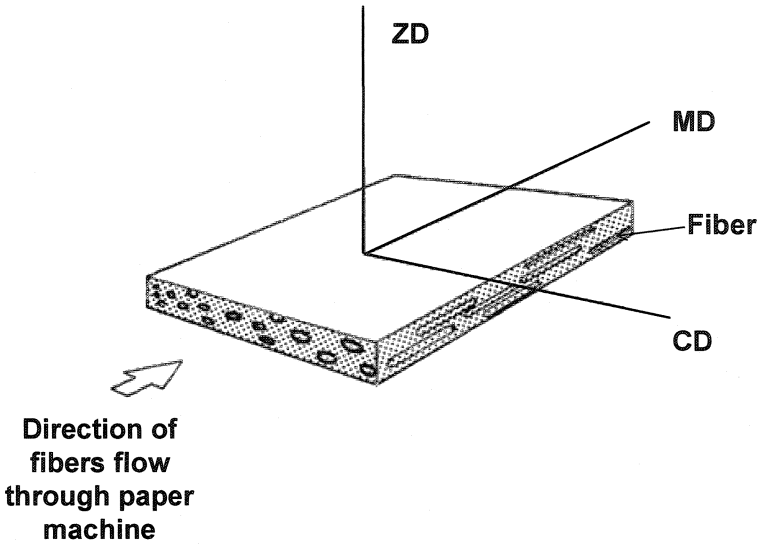

Figure 1.1 Paper anisotropic structure (from the *Handbook of Physical Testing of Paper* [10])

1.1.4 Paper surface properties

Paper surface properties include optical properties, surface roughness and surface chemistry or energy [11]. The latter two aspects are most relevant to this thesis, so they are reviewed in the following.

Surface roughness is important for it affects the contact area between paper and other materials. It is often categorized into three types according to the scale of observations [12]: 1) *optical roughness* at scales of less than 1μm, referring to the roughness of individual fibers or pigment particles; 2) *micro roughness* at scales of 1μm - 100μm, referring to the roughness of the fiber network; 3) *macro roughness* at scales of 0.1mm-1mm, referring to the roughness of paper as a continuum.

Paper roughness can be measured by either a mechanical or an optical profilometer. The resulting surface profiles are usually characterized by three parameters: the arithmetic roughness R_a, the root-mean-square roughness R_{rms} or the maximum roughness R_z. Of these, R_a is calculated as the average of height deviations from the mean line of the profile; R_{rms} is calculated as the root mean square of height deviations from the mean line; and R_z is the maximum height deviation from the mean line.

The **surface chemistry** of paper is also important. Borch [13] reviewed aspects of paper adhesion with polymers and concluded that the variation of paper adhesion depends on the chemical nature of surfaces. Because of this importance, many methods have been developed for characterizing paper surface chemistry [11]. Of these, the method of *X-ray photoelectron spectroscopy* (XPS) analysis is used in this thesis.

The principle underlying XPS is the interaction between X-rays and the electrons of the sample surface. XPS detects the binding energy of the electrons of the surface

atoms, and provides detailed information on surface elemental compositions and even the different bonding states of the elements. In a series of paper [14,15,16], Dorris and Gray demonstrated the feasibility of applying the XPS analysis to paper and wood fibers. Particularly, they analyzed the carbon signal and divided its fine structure into four categories (C1– C4) according to the oxidation level of carbon. C1 refers to un-oxidized carbon (C-C/C-H), C2 refers to carbon with one bond to oxygen (C-O), C3 refers to carbon with two bonds to oxygen (O-C-C or C=O), and C4 refers to carbon with three bonds to oxygen (O-C=O). Recently, XPS was also applied to investigate the influence of paper chemical and physical treatments on paper surface chemistry [17,18,19].

1.1.5 Paper strength

Paper strength properties are usually divided into two categories: *in-plane strength* and *out-of-plane strength*. The first one measures how much load a paper specimen can withstand before it breaks, whereas the second one measures paper resistance to delamination (i.e. the separation of a material into two layers). In addition, there are many other paper strength properties such as tear and burst strength; most of them are related to paper end-use. The common paper strength properties are reviewed in the following.

Paper in-plane strength properties are usually measured by tensile testing. A typical tensile stress/strain curve is illustrated in Figure 1.2, where paper stress increases with paper strain until paper breaks. The initial slope of the stress/strain curve is paper elastic modulus (E). The stress at the breaking point is paper tensile strength. The area under the tensile curve (i.e. the shadowed area) is the total energy consumed and this is called *tensile energy adsorption* (TEA).

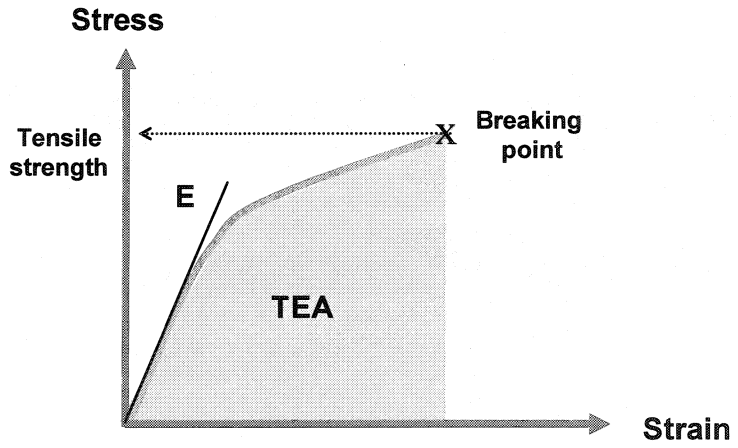

Figure 1.2 Illustration of paper tensile test. The X-axis corresponds to paper strain, and Y-axis corresponds to paper stress. E stands for the elastic modulus of paper, which is the initial slope of the tensile curve. TEA stands for tensile energy absorption, which is the shadowed area.

Page developed a theory for paper tensile strength [20]. He proposed that the reciprocal of the tensile strength is proportional to the sum of the reciprocals of the interfiber bond strength and the fiber strength. In the simplest form, the relationship was expressed in the following equation.

$$\frac{1}{T} = \frac{1}{F} + \frac{1}{B}$$

where T is the tensile strength; F is the fiber strength; and B is the interfiber bond strength.

The Page theory provides a simple picture of the relationship between the tensile strength of paper and those of fiber and interfiber bond. It predicts the fact that the strength of weakly-bonded paper is controlled by the interfiber bond strength, while the fiber strength becomes important for well-bonded paper. However, this theory ignored the behavior before the tensile break point, and its validity has been debated [21]. Therefore the Page model should only be regarded as a semi-empirical theory.

Paper out-of-plane strength measures the strength in the paper thickness direction, also called the paper Z-strength. This is usually much less than its in-plane strength. The elastic modulus in a Z-tensile test was found to be only about 1% of that in an in-plane tensile test [22]. More often, paper Z-strength is measured by delamination tests such as internal (Scott) bond test, peel test and cantilever beam technique. Of these methods, the Scott bond test appears to be the most popular one and was used in the research for this thesis.

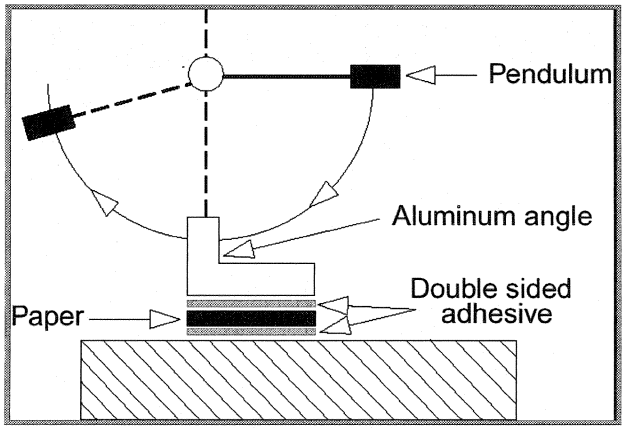

Figure 1.3 Illustration of a Scott bond tester

Figure 1.3 illustrates the essential features of a Scott bond tester. The paper sample is mounted on an aluminum angle using a double-sided adhesive tape. A pendulum with a fixed weight is released from the horizontal position. The pendulum impacts the aluminum angle causing the paper to delaminate. The released energy from the pendulum is calculated from the maximum height after impact. Note that the force is indirectly applied to the paper sample by using adhesive tape with the assumption that the

adhesive has no effect on paper strength. This is a common feature for almost all paper Z-strength measurements.

The paper Z-strength properties measured from different methods were found to be closely correlated [23]; however, their values were significantly different. Of them, the Scott bond method gives the highest value, while the peel test gives the lowest. The differences were attributed to variations in the extent of microscopic damage by [24] because delamination angles vary in the different methods.

1.2 Adhesive tape

Many adhesive tapes and labels used with paper are pressure sensitive or self-adhesive. Packaging tape, splicing tape and Post-It® notes are common examples. Pocius [25] described the Pressure Sensitive Adhesive Tape Council's definition for the pressure sensitive adhesive (PSA); PSAs are materials which

- Have aggressive and permanent tack
- Adhere with no more than finger pressure
- Require no activation by any energy source
- Have sufficient ability to bond onto the adherend
- Have enough cohesive strength to be able to remove cleanly from the adherend

1.2.1 Chemical nature of PSA

To fulfill the above requirements, PSA products need to be carefully formulated. The two major components are elastomers and tackifiers. The elastomer, the backbone of a PSA, comes mainly from four families of polymers: natural rubber, acrylics, styrene-containing copolymers or silicone-containing polymers. Tackifiers are various small molecular additives used to help adjust the transition temperature and interfacial adhesion properties [26,27].

1.2.2 Adhesion mechanism

In a broad sense, adhesives function because of their propensity to consume a large amount of energy in the separation of two bonded materials. This resistance energy to debonding can be measured by either peeling or probe-tack experiments. In practice, the peeling performance of adhesives is commonly reported because it resembles practical applications and is easy to perform.

In peeling, adhesives are stretched between the substrate and adhesive backing. These stretched adhesives form a peeling zone, whose size depends on the adhesion to the substrate and its own rheology. Within the peeling zone, the stress distribution is complicated as described by Kaelble [28]. The measured peel energy is the energy dissipated when the peeling zone moves by one unit area.

One significant phenomenon in the peeling zone is the formation of adhesive fibrils. The detailed processes were revealed mainly by probe-tack experiments [29,30,31,32], and the mechanism of fibrillation, as proposed by Zosel [30], involves three steps: *cavitation*, *fibril growth* and *separation*. These are illustrated in Figure 1.4,

in which an adhesive film is confined between two bonded surfaces. In debonding, some cavities are generated at the interface, and then propagate along both vertical and horizontal directions until the stress generated by the deformed adhesive fibrils reaches its adhesion strength, at which point separation occurs. The formation and growth of fibrils consume a large amount of energy, and it was found that these processes are mainly governed by the adhesive rheology.

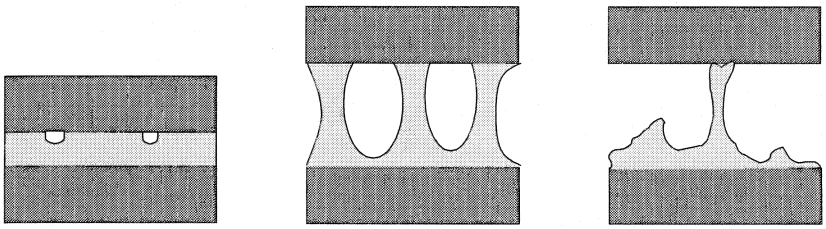

Figure 1.4 Illustration of adhesives' debonding processes (redrawn from *Zosel, 1998*)

The prerequisite for high energy consumption during fibrillation is to have a good adhesion between an adhesive and its substrate. High adhesion between PSA and substrate limits the horizontal propagation of cavities and results in PSA fibrillations. By contrast, low adhesion causes faster horizontal propagation and even the coalescence between the neighboring cavities, resulting in a "brittle" debonding which consumes much less energy.

1.3 Fundamentals of Adhesion

1.3.1 Adhesion theories

Fundamentally, adhesion is a molecular phenomenon. All atoms and molecules adhere to one another with considerable force. When two solid bodies approach to nanometer order distance, they will jump into contact as a result of molecular adhesion [33]. However, the adhesion phenomena are diverse, and many of them are related to the specific properties of the adhesion substrates. There are five theories in the adhesion science proposed to explain various adhesion phenomena [25,34]: *electrostatic theory, diffusion theory, mechanical interlocking theory, adsorption theory, and weakest layer theory*.

The electrostatic theory proposes that surfaces adhere to each other by forming a double layer of electrical charge at the interface. This theory is effective to materials with substantially different electronegativities such as metals, but not very applicable to paper and polymers.

The diffusion theory was proposed for explaining the adhesion phenomena between polymers, particularly for two identical polymers. It states that the adhesion between two polymers is due to the mutual diffusion of polymer molecules across the

interface. This requires that the chains of polymers in contact are sufficiently mobile and mutually soluble. As a result of the diffusion, there is no longer an interface, but rather an interphase, i.e. a solution of molecules from the two contacting materials.

The mechanical interlocking theory proposes that the mechanical interlocking between adhesives and the irregularities of a substrate surface is the major source of adhesion. This theory is particularly applicable when applying liquid adhesives to porous materials. Liquid adhesives easily interlock with the irregularities of material surface, which could result in sufficient adhesion strength after they are solidified. Dickson [35] studied the adhesion between paper and its coated layer, and found that adhesion strength increased with the intensity of interlocking between paper and solidified coated layer.

The adsorption theory is the most popular theory in adhesion science. It proposes that materials with an intimate contact adhere to one another through molecular interactions such as van der Waals bonds, hydrogen bonds, acid-basic interactions, and covalent bonds. In this theory, the two important concepts are surface tension and the work of adhesion. The former is a direct measure of intermolecular forces within one material. A good contact of an adhesive with its substrate requires a low surface tension for the adhesives, but a high surface tension (often called surface energy for solid surface) for the substrate. The work of adhesion is the minimum energy required to separate two surfaces in intimate contact; and it was found that the measured adhesion strength is proportional to the work of adhesion – see the section of *practical adhesion.*

The weakest layer theory is actually a debonding theory which concerns the locus of bond failure. This theory proposes that the measured bond strength is determined by the strength of the weakest layer in the bonded structure. Therefore, it is important to determine the locus of adhesive failure in any adhesion test. In practice, it is always desirable to remove the weak bonded materials from adhering surfaces to ensure a stronger bond.

1.3.2 Practical adhesion

The fracture energy required to overcome the adhesion is often called *practical adhesion* [25]. Measuring the practical adhesion always involves a mechanical test in which an external force is applied some distance away from the interface. Therefore practical adhesion is related to the fundamental intermolecular interactions by complex mechanisms involving interfacial chemistry, rheology of inelastic materials and fracture mechanics [36].

Much research effort has been devoted to identifying the relationship between practical adhesion and the intrinsic adhesion energy (i.e. the thermodynamic work of adhesion). The practical adhesion (G) was proposed by Gent et al. [37] and later theoretically justified by Andrews [38] as a product of two terms, the intrinsic adhesive fracture energy (G_0) and a mechanical loss factor (ϕ), i.e. $G = G_0 \cdot \phi$. The mechanical loss factor was found to be a function of separation rate (V), temperature (T) and strain level (ε). Owning to this factor, practical adhesion is usually much greater than the work of adhesion; however, when mechanical losses are negligible, i.e. $\phi \approx 1$, the practical

adhesion equals the work of adhesion in the case of pure interfacial failure. Furthermore, this mechanical loss factor accounts for the effects of peel rate and temperature on the practical peel energy: typically a high velocity and / or low temperature result in a high peel energy.

One elegant example of this relationship was demonstrated by Li et al. [39] who conducted low-rate contact mechanics measurements based on the JKR theory [40] and the standard peel measurements for acrylic pressure sensitive adhesives. They showed that the adhesion energy obtained at low separation rate by contact mechanics measurements is equal to the work of adhesion and governed by the surface energy of contact surfaces; whereas at the usual separation rate by peeling measurements, the adhesion energy is much higher than the work of adhesion. They fitted their experimental data into the following relationship

$$G = G_0\left(1 + \left[\frac{v}{v^*}\right]^n\right)$$

where G is the measured adhesion energy, G_0 the work of adhesion, v the separation rate, v^* a critical separation rate and n is an empirical (fitting) parameter. This fit was good, as shown in Figure 1.5. The fitting parameter n has recently been attributed to the rheology of adhesives as discussed by Shull [41].

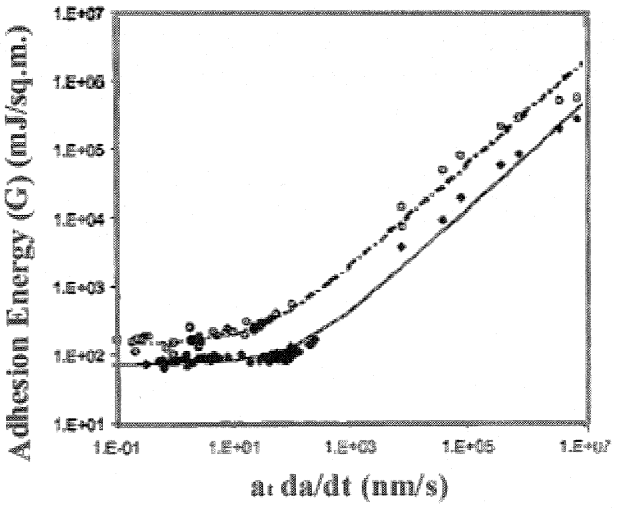

Figure 1.5 Adhesion energy as a function of reduced crack propagation rate (da/dt is the crack propagation rate and a_t is the WLF shift factor). Open points are for material containing 10% AA (acrylic acid) while closed points are for material containing 0% AA. ***(Li, et al., 2001)***

1.3.3 Peel adhesion testing

Peel adhesion testing is often employed to assess the bonding strength of laminated materials when at least one of the layers is flexible [42]. It is one of the

commonest methods to evaluate the performance of adhesive tapes. Indeed, the formulation of PSA tapes involves balancing the cohesive strength of the adhesive, measured by a shear test, to the adhesion strength, measured by peeling [42].

In a peel test, the adhesive tape and substrate are laminated under pressure; after setting, peeling is carried out at a fixed peel angle as illustrated in Figure 1.6. The measured force depends on the peel angle. The relationship between peel force and the work required to separate one unit bonding area can be deduced from the peel geometry as

$$\frac{F}{b} = \frac{G}{1-\cos\theta}$$

where F is the peel force; b is the width of the peel strip; θ is the peel angle and G is the total peel work. This equation predicts that the peel force should be inversely proportional to $(1\text{-}\cos\theta)$. Satas in the *Handbook of Pressure Sensitive Adhesive Technology* [42] reviewed many investigations on this relationship, and concluded that the above equation was generally satisfied. It has also been noted that the peel work G may include many components, and may change with peel angle when the deformation of the peel strip reaches its plastic yield point [43,44]. It is well known in literature [42] that the peel force increases with increasing adhesive thickness and eventually levels off. On the other hand, the energy dissipated in a thin adhesive layer is negligible.

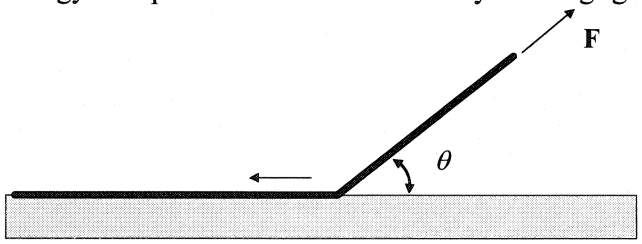

Figure 1.6 Illustration of a general peel geometry where F is the peel force and θ is the peel angle

To summarize, the practical adhesion strength is always proportional to the intrinsic adhesion strength between adhesive and substrate although there are many contributing factors from both adhesive and substrate. Indeed, if there was no adhesion at all, the measured adhesion force would be zero. This is the justification for using the peel test to evaluate the performance of adhesive tapes.

1.4 Objectives and research approach

The objectives of this thesis are to characterize the fracture mechanisms of adhesive/paper laminate; and to relate paper properties to the performance of pressure sensitive adhesives. For these, we employed peel adhesion testing as a probe. Many commercial acrylic adhesive tapes were tested, and one of them was chosen as the standard tape to investigate the effects of paper properties. The paper samples employed were uncoated since the surface properties of coated paper depend to a large extent on the nature of the coating layer.

1.5 Thesis outline

This thesis consists of one introductory chapter, five research chapters and one concluding chapter. The five research chapters include two published papers (Chapter 2), one submitted paper (Chapter 6), and three manuscripts. Following is an outline of the chapters.

Chapter 1 Introduction. This chapter sets a context for the research chapters by providing the basic knowledge, describing the experimental methods used in the research, and reviewing the current studies. It concludes with the research objectives and an outline of the thesis.

Chapter 2 Peel adhesion to paper – Interpreting peel curves. In this chapter, the peeling behavior of adhesive/paper laminates is analyzed, and a new data analysis method is developed, by which the peeling behavior can be summarized in a generalized peel curve. The influence of paper type, PSA type and peel angle on the generalized peel curve is also determined. The contents of this chapter were published in the *Journal of Material Science Letter*, 22:265-266 (2003) and the *Journal of Adhesion Science and Technology*, 17(6):815-830 (2003).

Chapter 3 Surface peel force. This chapter clarifies the relationship between *overall peel force* (i.e. the measured peel force) and *surface peel force* (i.e., the force generated at paper surface in peeling). For this, we developed a technique to analyze the induced paper strain in peeling. The surface peel force was obtained through independently calibrating that paper strain. The revealed linear relationship between the overall peel force and surface peel force justifies our using peeling as a probe to study the adhesive/paper interactions.

Chapter 4 The paper delamination in peeling. This chapter focuses on the process of paper delamination, particularly its initiation. The delamination process was directly observed with a video camera fitted with a microscope lens. The factors influencing delamination were studied by peeling from a series of randomly oriented paper sheets (handsheets) made in the laboratory. In addition, the influence of papermaking variables, including beating, wet pressing and fiber length, on the tendency of the resulting paper towards delamination were examined.

Chapter 5 Paper properties affecting tape adhesion. Presented in this chapter are the results of an experimental study which identify the key paper properties influencing paper adhesion to pressure sensitive adhesives tape. The critical features of this work are the use of advanced statistical analysis and a newly developed approach for analyzing adhesive/paper peel curves.

Chapter 6 Using peel as a measure of paper surface strength. This chapter is an application of the above fundamental research to a practical problem. We propose using peel as a measure of paper surface strength. For this, the paper surface strength of many paper samples was measured by both the proposed peel method and the present industrial method (IGT paper surface strength test). The contents of this chapter were submitted to the *Tappi*.

Chapter 7 Conclusions and suggestions. This chapter summarizes all research in this thesis and provides some comments and suggestions for future work.

1.6 References

1 W.J. Goetz, R.J. Alheld, H.G. Ehrnrooth, and P.A. Landskroener, *Tappi,* 68(2):113-115 (1985).

2 J.J. Bikerman, *Tappi* 44(8):568-571 (1961).

3 T. Yamauchi, T. Cho, R. Imarnura, and K. Murakarmi, *Nordic Pulp Paper Res. J.,* 3 (3):128-131 (1988).

4 T. Yamauchi, T. Cho, R. Imarnura, and K. Murakarmi, *Nordic Pulp Paper Res. J.,* 4 (1):43-47 (1989).

5 R. Pelton, W. Chen, H. Li, and M.R. Engel, *J. Adhesion*, 77:285-308 (2001).

6 W.E. Scott, J.C. Abbott, and S. Trosset (ed.), *Properties of Paper: An Introduction*, Tappi Press (1995).

7 K. Niskanen (ed.), *Paper Physics*, Fapet Oy (1998).

8 E.R. Finger, and Z.J. Najewsk, *Tappi*, 37(5):216-224 (1954).

9 K. Niskanen, I. Kajanto and P. Pakarinen, "Paper structure", In: *Paper Physics*, edited by K. Niskanen, Fapet Oy, p. 47 (1998).

10 R.E. Mark, C.C. Haberger, J. Borch and B.M. Lyne (ed.), *Handbook of Physical Testing of Paper*, 2nd edition, Volume 1, Marcel Dekker, New York (2002).

11 T.E. Conners and S. Banerjee (ed.), S*urface Analysis of Paper, CRC Press* (1995).

12 I. Kajanto, J. Laamanen and M. Kainulainen, "Paper bulk and surface", In: *Paper Physics*, edited by K. Niskanen, Fapet Oy, p. 100 (1998).

13 J. Borch, *J. Adhesion Sci. Tech,* 5(7):523-541 (1991).

14 G.M. Dorris and D.G. Gray, *Cell. Chem. Technol.*, 12:9-23 (1978).

15 G.M. Dorris and D.G. Gray, *Cell. Chem. Technol.*, 12:721-734 (1978).

16 D.G. Gray, *Cell. Chem. Technol.*, 12:735-743 (1978).

17 A. Koubaa, B. Riedl, and Z. Koran, *J. Appl. Polym. Sci.* 61:545-552 (1996).

18 M. Kazayawoko, J.J. Balatinecz, R.T. Woodhams and R.N.S. Sodhi, *J. Wood Chem. Technol.* 18(1):1-26 (1998).

19 S. Chen and H. Tanaka, *J. Wood Sci.* 44:303-309 (1998).

20 D.H Page, *Tappi* 52(4):674-680 (1969).

21 D.G. Williams, *Tappi*, January: 100 (1983).

22 I. Kajanto, "Structural mechanics of paper and board", In: *Paper Physics*, edited by K. Niskanen, Fapet Oy, p. 214 (1998).

23 A. Koubaa and Z. Koran, *Tappi*, 78(3):103-111 (1995).

24 A. Tanaka, H. Kettunen, K. Niskanen and K. Keitaanniemi, *J. Pulp Paper Sci.*, 26(11):385-390 (2000).

25 A.V. Pocius, *Adhesion and Adhesives Technology*, 2nd edition, Carl Hanser Verlag, Munich, Germany (2002).

26 I. Benedek and L.J. Heymans (ed.), *Pressure Sensitive Adhesives Technology*, Marcel Dekker, New York (1996).

27 D. Satas (ed.), *Handbook of Pressure Sensitive Adhesive Technology*, Van Nostrand Reinhold, (1989).

28 D.H. Kaelble and R.S. Reylek, *J. Adhesion*, 1:124-134 (1969).

29 A. Zosel, *J. Adhesion*, 30:135-149 (1989).

30 A. Zosel, *Int. J. Adhes. Adhes.*, 18:265-271 (1998).

31 C. Creton, J. Hooker and K.R. Shull, *Longmuir*, 17:4948-4954 (2001).

32 A.J. Crosby and K.R. Shull, *Adhesives Age*, 42(7):28-33 (1999).

33 K. Kendall, *Molecular Adhesion and its Application*, Kluwer Academic/ Plenum Publishers, p. 46 (2001).

34 A.J. Kinloch, *Adhesion and Adhesives*, Chapman and Hall (1987).

35 R.J. Dickson and P. Lepoutre, *Tappi*, 80(11):149-157 (1997).

36 A.N. Gent, *Plastics Rubber Int.*, 6:151 (1981).

37 A.N. Gent, and J. Schutz, *J. Adhesion*, 3:281 (1972).

38 E.H. Andrews, *J. Mater. Sci.*, 9:887-894 (1974).

39 L. Li, G.L. Kobra and A.V. Pocius, "Surface energy and adhesion studies on acrylic pressure sensitive adhesives", In: *Adhesion society 24th conference proceeding*, pp. 274-276 (2001).

40 K.L. Johnson, K. Kendall and A.D. Roberts, *Proc. R. Soc. Lond.* A, 324:01 (1971).

41 K.R. Shull, *Mat. Sci. and Eng. R.* 36(1):1-45 (2002).

42 D. Satas (ed.), In: *Handbook of Pressure Sensitive Adhesive Technology*, pp. 61-96, Van Nostrand Reinhold (1989).

43 A.N. Gent and G.R. Hamed, *J. Appl. Polym. Sci.*, 21:2817-2831 (1977).

44 J.G. Williams, *J. Adhesion*, 41:225-239 (1993).

Chapter 2

Peel Adhesion to Paper - Interpreting Peel Curves

Abstract

Peel experiments involving three PSA tapes and three paper substrates were employed to develop a general approach for the analysis of peeling from paper. Plotting the logarithm of the peak peel force (i.e. the maximum value) versus the logarithm of the peel rate yielded a generalized peel curve which illustrated transitions from interfacial to paper failure. The general peel curve consisted of linear segments (on the log/log plots) which intersected when the failure mode changed from interfacial to paper failure. The influence of paper type, PSA type, and peel angle on the generalized peel curve was determined.

2.1 Introduction

Peel adhesion testing is often employed to assess the bonding strength of laminated materials when at least one of the layers is flexible [1]. Peel tests are easy to perform and the resulting peel trace contains useful information about both the adherate and substrate. For example, pressure sensitive adhesives (PSAs) are routinely evaluated by peeling from stainless steel. The experimental variables are peel rate and peel angle. The output of a peel test is an average peel force and a qualitative assessment of the failure mode, which is usually interfacial or cohesive failure in the PSA. The formulation of PSA tapes involves balancing the cohesive strength of the adhesive, measured by a shear test, to the adhesion strength, measured by peeling [1].

In this work we report the use of peel measurements to characterize the interactions of PSA tapes with paper. The tape/paper system is challenging because the failure can occur within the paper structure as well as in the adhesive or at the adhesive/substrate interface. Our longer term interests are in understanding how paper properties influence the performance of taped structures, whereas this work focuses on the characterization of PSA/paper peel curves.

Bikerman [2] was one of the first authors to discuss peeling from paper. He focused on paper as a porous medium and discussed the flow of adhesives into the paper structure. Key observations from this work involved the details of the peel force versus peel distance curves. Specifically, it was reported that the peel force often reached a maximum value which decayed to a steady-state value. Herein we call this maximum peel force the peak peel force, Fp (N/m). Bikerman also noticed that if a tape was peeled from the edge of a sheet of paper, the peak peel force was lower than if the peeling started away from the paper edge.

More than twenty years later, Yamauchi and coworkers [3,4] reported the first systematic peel studies involving paper properties. They identified three modes of peel failure: interfacial, paper and mixed failure. The mode of peel failure changed from paper failure to interfacial failure by either increasing paper density or decreasing peel rates.

Paper delamination in peeling has been used to estimate the z-direction strength of paper [5,6,7]. In a series of papers Yelon and coworkers analyzed the mechanics of paper bending and peel delamination [8,9,10]. They proposed measuring delamination force as a function of the minimum radius of curvature of the paper. The peel work, extrapolated to zero curvature, is a measure of the true delamination work.

Previous studies in our laboratory extended the pioneering work of Yamauchi and coworkers by including the effects of lamination pressure, paper surface energy and peeling direction [11]. Paper properties were proposed to fall into two categories: surface chemical properties and paper structural properties. The paper structural properties, such as surface roughness and porosity, seemed more important than surface chemistry for the initiation of paper failure in peeling. Furthermore, it was realized that the conventional peel data analysis of plotting the steady-state peel force versus peel rate was not a good way to characterize the peel behaviors of PSA tapes from paper because the onset of paper failure gave discontinuities in the peel curves which were difficult to predict or

model. In a recent note, we suggested that by plotting peak peel forces versus peel rates, discontinuities in the peel curves did not occur and changes in failure were more tractable [12]. In this work we report the results of a systematic investigation of paper properties on peeling with emphasis on peak peel forces.

2.2 Experimental

2.2.1 Materials

Two types of papers (newsprint and filter paper) and three commercial pressure sensitive adhesive tapes were employed in this work. The commercial tapes were Scotch Brand 3M tape No 9974B, No 400 and No 410 (3M London, Ontario, Canada). 3M No 9974B tape was the major tape used in this work; it consists of a blue 77 μm adhesive layer coated on both sides of a bleached tissue carrier and was provided with a white backing (90μm). The other two kinds of tape No 400 and No 410 consist of a white adhesive layer (106μm) coated on both sides of a bleached tissue carrier and were provided with a white backing (80μm). The three paper samples were newsprint paper (Donohue, Ontario, Canada) and filter papers No1 and No 4(Whatman International Ltd. Maidstone, England.).

2.2.2 Methods

All paper samples were conditioned in a constant temperature (23°C) and relative humidity (50%) room for at least one week before testing; the testing was performed in the same conditions. The paper density was determined by measuring the paper caliper (thickness) and grammage (mass per unit area). The average values were used by measuring the caliper (Precision Micrometer, Testing Machines Inc.) and mass (Mettler Toledo, Laboratory& Weighing Technologies) of a pile of 5 sheets. Mechanical strengths of paper were measured based on TAPPI test methods (T494 and T833): Paper in-plane strength was measured in an Instron tester in terms of maximum tensile stress; the paper z-strength was measured by internal bond strength (Internal Bond Tester HUYGEN Corporation, Illinois , U.S.A.).

The surface roughness of paper was characterized by root mean square (RMS) roughness measured by an optical profilometer (WYKO surface profiler). The samples were measured on the smooth side with an evaluation area of 459μm x 603μm. At least four specimens were measured for each sample; the average values were reported. In addition, the microscopic structures of the paper samples were observed under an optical microscope (ZEISS, West Germany), and the typical images were captured by the connected camera.

The peel test samples were prepared following the work of Pelton et al. [11]. First the PSA white tape backings were replaced by strips of Canon copy paper. For this, tape strips 2.5cm x 4cm were placed across a sheet of copy paper. The paper was trimmed to 2.5 cm yielding a paper tail which extended about 10 cm beyond the tape. This tail was used to attach the strip to the clamps of the tensile machine.

The other white backing was removed from the other surface of the test tape. Then a strip of single sided transparent tape (Grand &Toy Ruban Invisible) was placed on the front edge of the PSA surface to serve as a separation layer or release layer to help initiate the peel crack (see Figure 2.1).

For 180° peel tests the paper substrate (i.e. the newsprint or filter paper) was fixed to a 7.5 cm x 10cm stainless steel panel with double-sided tape 9974B. The Canon paper backed strip was placed onto the paper substrate and a 2.04kg rubber coated roller (ChemInstruments, Mentor Ohio) was hand rolled over the sample ten times. A schematic illustration of the 180° peel samples is shown in Figure 2.1. Note that the tape was placed so that it was not near an edge of the paper substrate. In the final step, the top copy paper backing was gently folded back at the position of the "separation tape". Peel tests were performed within two minutes of lamination.

The 90° peel test was conducted by mounting the test paper substrate onto a free-rotating wheel as shown in Figure 2.2. The construction of the wheel, based on a PAPRICAN design, was described previously [11]. The construction of the 90° peel test sample was similar to that of 180° peel test except that the metal plate in Figure 2.1 was replaced by the surface of the free-rotating wheel. As before, the dimensions of the paper substrate were greater than the tape strip (25mm width) to avoid edge effects.

The peel tests were performed by an Instron Corporation Series IX automated material tester located in a constant temperature (23°C) and humidity (50%) room. A 50N load cell was used in all experiments. A computer interface was used to control the peel conditions and restore the peel data in the form of force versus displacement. Peel rates ranged from 2mm/min to 500mm/min. Normally paper substrates were peeled in the "machine direction".

Many of the results were plotted as the logarithm of the peel force versus the logarithm of the peel rate. The error bars were calculated as $\log(F \pm SD) / F)$ where F is the mean peel force based upon at least 5 measurements and SD is the corresponding standard deviation.

2.3 Results

The properties of two filter papers and the newsprint substrates are listed in Table 2.1. Optical micrographs taken with transmitted light are shown for the three paper samples in Figure 2.3. The filter papers, based on only very long cotton fibers, had a very open structure which was reflected in the low density values. By contrast, the newsprint is made from mechanical pulp which has many small fibers and fines. Thus newsprint was denser and smoother than the filter paper. Inspection of the images in Figure 2.3 reveals that the newsprint fibers tended to be aligned in the papermachine direction whereas the filter paper sheets showed no orientation.

Figure 2.4 shows two typical examples of peel force versus distance curves when peeling tape 9974B at 180° from newsprint surface. The lower peel rate gave interfacial failure whereas the higher peel rate caused the paper to fail. In the case of interfacial failure, the peel curve is noisy but approximately constant, resembling the peeling from stainless steel. The peel curve at the higher peel rate is more complicated. The peel force

initially rises to a maximum point and then drops to a low steady-state value, corresponding to catastrophic delamination (paper failure). Figure 2.5 shows the corresponding tape surfaces after peeling. In the case of interfacial failure, the tape surface after peeling looked clean. However, microscopic examination of the tape surface after peeling revealed small debris on the adhesive surface. In the paper technology literature this situation is called "picking" and is a source of contamination during some printing operations.

The paper failure case in Figure 2.5 is obvious and unequivocal; at lease one layer of fibers was embedded in the tape after peeling. Some insight into the failure initiation mechanism is also given by the image in Figure 2.5. In this case paper failure appears to start at three points which then broaden and merge with further peeling to cover the tape with at least one layer of fibers. The term mixed failure (see Figure 2.5) denotes this transition region between interfacial and paper failure. At very high peel rates, the paper fails immediately and there is no transition region.

An idealized peel curve is presented in Figure 2.6. It is useful to divide peel curves into three regions: the initial increase, the transitional decline and the steady-state propagation region. Four peel characteristics can be extracted from the curves: the Peak Peel Force (F_p), the Steady-state Force (F_{ss}), Initiation Distance (D_i) and the Transition Distance (D_t) – see Figure 2.6. The peak force, F_P, is the force required to initiate peeling. The steady-state peel force, F_{ss}, corresponds to the mean force value in the steady-state region.

The idealized peel curve in Figure 2.6 does not resemble the interfacial curve in Figure 2.4. The interfacial failure can be regarded as a special case of a general peel behavior in which $F_p = F_{ss}$ and $D_t = 0$.

Figure 2.7 shows nine repeated 180° peel curves for 9974B tape on filter paper No 1. The curves labeled Mean and Standard Deviation were calculated from replicated data at each peel distance. Table 2.2 summarizes the peel curve characteristics from Figure 2.7. The transition distance, D_t, showed a far greater sample-to-sample variation than either the steady-state or peak peel forces. We noticed that the initiation distance, D_i, was often influenced by the amount of slack in the mounted sample before peeling. Thus D_i values were not considered further.

The effect of peel rate on the peel behavior is shown in Figure 2.8 which shows both the mean peel curves at each peel rate and the corresponding standard deviation curves based on at least five repeated measurements. As reported by Yamauchi et al.[3] and our previous work [11], the failure mode changes from interfacial to paper failure when the peel rate is increased. An interesting feature revealed in Figure 2.8 (B) is that variation in the duplicated curves expressed as the standard deviation curve was the lowest at both the highest and lowest peel rates. By contrast, the intermediate 25 mm/min peel rate experiments had the greatest standard deviation. It seems that near the critical peel rate, the peel force is sensitive to subtle variations in paper surface properties.

Many 180° peel experiments were conducted with tape 9974B and the three types of paper. The resulting characteristic peel curve parameters (see Figure 2.6) are plotted as functions of peel rate. Figure 2.9 shows the steady-state peel force, F_{ss}, versus peel rate on logarithmic scales. At low peel rates in the interfacial failure domain, F_{ss} increases

with peel rate – this is a typical behavior for PSA peeling from steel and other hard surfaces. At higher peel rates, the transition from interfacial to paper failure causes a discontinuity in these curves – this has been reported before [3,11]. The filter paper curves clearly show a slight positive slope in the paper-failure domain. This reflects the complicated viscoelastic nature of paper. The adhesive technology literature generally presents peel results as an average value in the steady-state part of the peel curve, (i.e. they use F_{ss}). F_{ss} was a useful parameter when one only focused on either interfacial failure domain or paper failure domain. However, the complex nature of the F_{ss} curves in Figure 2.9 renders them not effective in terms of significant scientific interpretation. In a previous note, we claimed that F_p was a more relevant parameter to characterize peeling from paper [12].

Figure 2.10 shows the corresponding F_p data. Three curves display the same tendency. The peak peel force monotonically increases with peel rate until the paper fails and then becomes constant. The increasing slopes for the three papers are the same. Because the transition in failure modes is clear, values can be assigned for the critical peak force F_{pc} for paper failure, and the corresponding critical peel rate, V_c, around which paper failure occurred.

Figure 2.11 shows the transition distance D_t values as a function of peel rate. In all cases D_t decreases with peel rate. The D_t values range from about 3 to 35mm. For comparison the length scale of individual fibers is about 2 mm. Furthermore, in the papermaking process fibers clump together in flocs which can persist in the final paper structure [13]. The size scale of most fiber flocs is 2-20mm. Note that the newsprint paper has a significantly greater transition distance than the two filter papers, perhaps reflecting differences in fiber arrangement within the paper sheet.

All the previous results were obtained with one tape, 3M 9974B, at a peel angle of 180°. Figure 2.12 shows the results of peeling three different tapes from newsprint. The three tapes display similar overall behavior in the log F_p vs log peel rate plots. In the paper failure domain, the three tapes gave approximately the same F_p value indicating that this was dominated by paper properties. By contrast, in the interfacial failure domain both the slopes and the critical peel rate, corresponding to the initiation of paper failure, are sensitive to the properties of the PSA. For example, consider a horizontal line at log(Fp/Nm-1)= 2.5 in Figure 2.12 intersecting the peel curves in the interfacial domain. The line intersects the tape 410 curve at an order of magnitude lower peel rate than tape 400, reflecting the different properties of PSA tapes.

There is significant literature on the peel mechanics from hard surfaces [1,14,15]. It is well established that measured peel forces are a function of peel angle. A simple energy balance for peeling a linear elastic strip predicts that the peel energy at the peel front is equal to the measured force times (1-cosθ) where θ is the peel angle [16]. Thus, the peel force should decrease with increased peel angle for a linear elastic system. Figure 2.13 compares log peel force versus log peel rate for experiments using 90° and 180° peel angles. The two curves are parallel in both the interfacial and paper failure regions with the180° peeling always giving the higher force values. This reflects the fact that more energy is consumed in bending the peel strip at the higher peel angle, indicating

that the present peeling system is not a linear elastic system. Note that the critical peel rate values for the initiation of paper failure were not very sensitive to the peel angle.

2.4 Discussion

This paper is the first in a series exploring how paper properties influence the peel behavior of PSA tapes. The primary focus of the current work was to identify the most useful parameters to characterize peel behavior. Future work will reveal the role of papermaking parameters, paper properties and the paper failure initiation mechanism.
The most important conclusion of this work is that the peak peel force, F_p, particularly when plotted against peel rate, is a most useful approach to display the features of peeling.

The power of this approach is illustrated by the results in Figure 2.10. In the interfacial failure domain, the F_p actually equaled the F_{ss} because there was no peak occurring in the peel curve. The two filter paper curves overlap in the interfacial failure domain indicating that they have the same adhesion to the tape. This reflects the fact that both filter papers are based upon pure cotton fibers. On the other hand, for a given peel rate in the interfacial failure domain, the F_p value for newsprint is much lower than for filter paper. This seems reasonable since the chemical composition of newsprint is significantly different from that of the filter papers (Table 2.1). The filter papers consist of pure cellulose which has a relatively high surface energy. By contrast, newsprint is made from mechanical pulp which contains about 30 wt% lignin instead of 100% cellulose in filter paper. Lignin is a complex aromatic polymer, more hydrophobic than cellulose [17]. Newsprint surfaces also contain a few percent of pitch, which consists of hydrophobic fatty and resin acids and esters.

Figure 2.10 also shows that newsprint is more resistant to delamination than filter paper 1, which in turn is more resistant than filter paper 4. This is the same order as density, z-directional strength and surface roughness (Table 2.1). Future work involving many more paper types will help clarify the links between conventional paper properties and the initiation of paper delamination.

The results in Figure 2.10 suggest the applicability of a generalized peel curve shown in Figure 2.14 which consists of three straight line segments on the log/log plot. The segments correspond to the three main failure modes when tapes are peeled from papers. The commercial tapes used in this work were strong so we were unable to peel slowly enough to induce cohesive failure. However, we reported cohesive PSA failure in previous work involving experimental adhesives of low cohesive strength [11]. From a practical perspective, the complete curve illustrated in Figure 2.14 could be drawn with six data points – two per straight line segment. The roles of experimental parameters on the generalized peel curve are now considered.

The paper cohesive failure segment in the schematic generalized curve (Figure 2.14) was drawn as a horizontal line because the experimental curves were independent of peel rate in the paper failure domain. Indeed, the comparison of the three tapes, shown in Figure 2.12, suggests that the peak peel force corresponding to paper failure was approximately independent of the PSA properties. Note that the tested tapes had the same

paper backing and were of similar thickness. Variation of the tape backing stiffness or the PSA thickness is likely to influence the peak peel force corresponding to paper failure.

Interpretation of the peak peel forces in the interfacial failure domain is a challenging problem which one would expect to involve both the PSA/paper work of adhesion and the viscoelastic properties of the PSA. If we consider only the slopes of the log F_p vs log V curves, some insights are obtained from the current results. The slopes of the three interfacial failure segments in Figure 2.10 are approximately equal, even though we know that newsprint has a lower surface energy than cotton. Thus, it would seem that the slopes are not very sensitive to the work of adhesion. By contrast, the slopes of the interfacial failure segments are sensitive to variations in the PSA (see Figure 2.12). Thus, it seems that the PSA viscoelastic properties dominate the slope of the log-log peel curves in the interfacial failure domain.

Peeling tapes from papers, like peeling from any other surface, is sensitive to peel angle. However, the results in Figure 2.13 suggest that the generalized peel curve is only displaced vertically with peel angle. The major features are preserved.

Finally, paper is a complex material so the initiation of paper failure in peeling is a complex problem at the fundamental level. This work suggests that the critical peak force, F_{pc}, is a measure of the minimum force required to initiate delamination. Furthermore, the transition distance may reflect the scale of paper features controlling delamination initiation. Future work will address these issues.

2.5 Conclusions

The main conclusions from this work follow. The first two confirm previously published work whereas the final four are new.

1. Peeling tapes from uncoated paper usually results in interfacial failure or delamination of the paper. Weak adhesives or very low peel rates can give PSA cohesive failure.
2. Paper failure is characterized by a high peak force, a relatively low propagation force and a transition distance over which the failure mode changes from mixed to paper failure.
3. Peak peel forces and steady-state delamination forces are reproducible quantities showing a small dependence on peel rate, whereas the transition distance shows significant sample-to-sample variation.
4. The critical peel rate for paper failure, V_c, is a property of both the PSA and the paper whereas the critical peak force for paper failure, F_{pc}, is mainly a paper property and is independent of peel rate.
5. The overall peel behavior of a PSA/paper combination is conveniently summarized by plotting the log peak peel force as a function of log peel rate. Transitions between failure modes are obvious in this form of data analysis.
6. The critical peel force for paper failure, F_{pc}, and the transition distance as function of peel rate are measurable parameters influencing the initiation of paper failure.

2.6 Acknowledgments

This work was supported by 3M Canada and the Natural Science and Engineering Research Council of Canada. Acknowledgments were given to Mr. Chris Mao for helping with paper roughness measurements, and Mr. Steve Dillon for carrying out peel tests on filter papers.

2.7 References

1 D. Satas, In: *Handbook of Pressure Sensitive Adhesive Technology*, D. Satas (Ed), pp. 61-96. Van Nostrand Reinhold (1989).

2 J.J. Bikerman, *Tappi* 44 (8):568-571 (1961).

3 T. Yamauchi, T. Cho, R. Imarnura, and K. Murakarmi, *Nordic Pulp Paper Res. J.,* 3 (3):128-131 (1988).

4 T. Yamauchi, T. Cho, R. Imarnura, and K. Murakarmi, *Nordic Pulp Paper Res. J.,* 4 (1): 43-47 (1989).

5 A. Koubaa and Z. Koran, *Tappi*. 78 (3): 103-111 (1995).

6 J. Skowronski and W. Bichard, *J. Pulp Paper Sci.* 13, (5): 65-169 (1987).

7 J. Skowronski, *J. Pulp Paper Sci.* 17 (6): 217-222 (1991).

8 A. El Maachi, S. Sapieha, and A.Yelon, *J. Pulp Paper Sci.* 21(10): 362-366 (1995).

9 A. El Maachi, S. Sapieha, and A.Yelon, *J. Pulp Paper Sci.* 21(12):401-407 (1995).

10 A. El Maachi, S. Sapieha, and A.Yelon, *Nordic Pulp Paper Res. J.* 14 (1):17-22, 29 (1999).

11 R. Pelton, W. Chen, H. Li, and M.R. Engel, *J. Adhesion*, 77: 285-308 (2001).

12 B. Zhao and R. Pelton, *J. Mater. Sci.* (accepted 2002).

13 K. Niskanen, I. Kajanto and P. Pakarinen, In: *Paper Physics*, K. Niskanen(Ed), Fapet Oy, Helsinki, Finland, pp. 14-53 (1998).

14 A. N. Gent and G. R. Hamed, *J. Appl. Polym. Sci.* 21 (10): 2817-2831(1977).

15 J. Kim, K. S. Kim and Y. H. Kim, *J. Adhesion Sci. and Tech.* 3 (3): 175-187 (1989).

16 J. G. Williams, *J. Adhesion* 41: 225-239 (1993).

17 S. B. Lee and P. Luner, *Tappi* 55 (1): 116-121 (1972).

2.8 Tables and figures

Table 2.1 Paper properties

Physical Properties of Paper Samples					
Sample	Composition	Density (kg/m^3)	Roughness (μm)	Tensile Strength (MPa)	Z-strength (J/m^2)
Filter Paper No. 4	100% cotton fiber	458.8	13.26	5.25	141
Filter Paper No. 1	100% cotton fiber	504.6	9.27	11.66	191
Newsprint Paper	Mechanical softwood fiber	661.7	4.32	20.9	223

Note: the roughness is the root mean square (RMS) roughness measured by the WYKO surface profiler.

Table 2.2 Peel curve characteristics for the results in Figure 2.7

	Mean	Standard Deviation
F_p, N/m	407.6	31.6
F_{ss},N/m	207.9	45.0
D_t, mm	5.1	2.2
D_i, mm	2.3	0.2

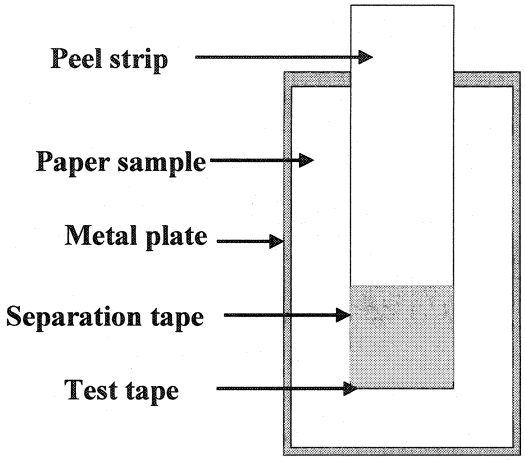

Plain View

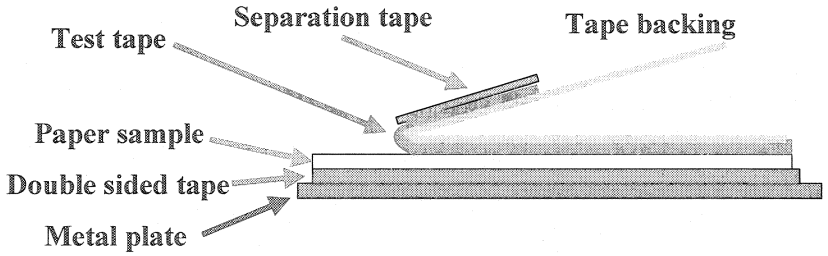

Side view

Figure 2.1 The construction of 180° peel samples

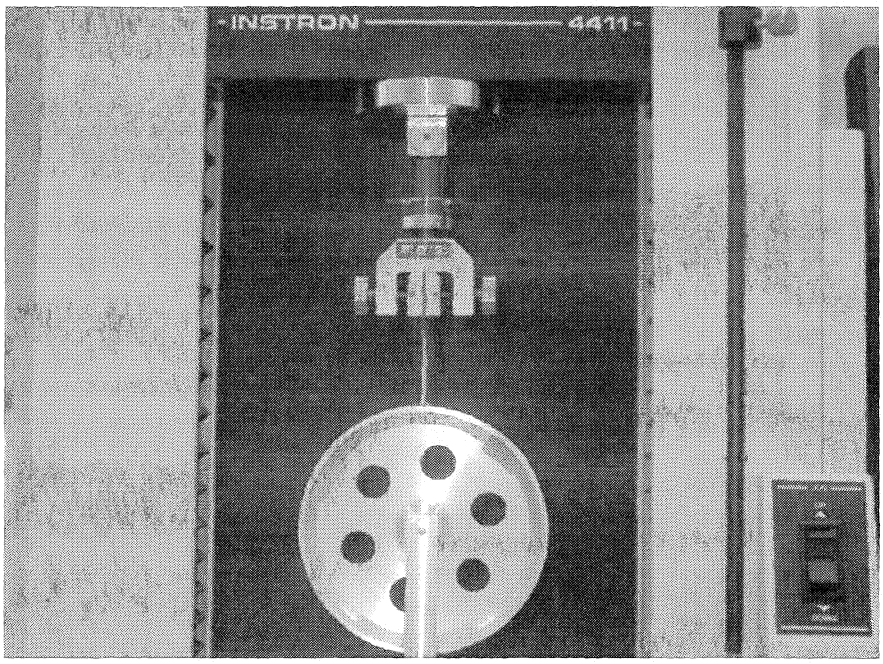

Figure 2.2 Experimental setup for 90° peel test

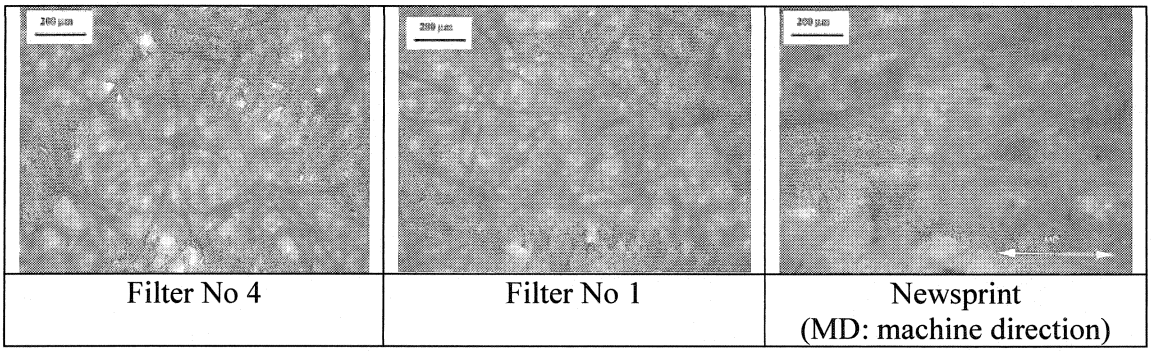

Filter No 4	Filter No 1	Newsprint (MD: machine direction)

Figure 2.3 Microscopic structures of paper samples

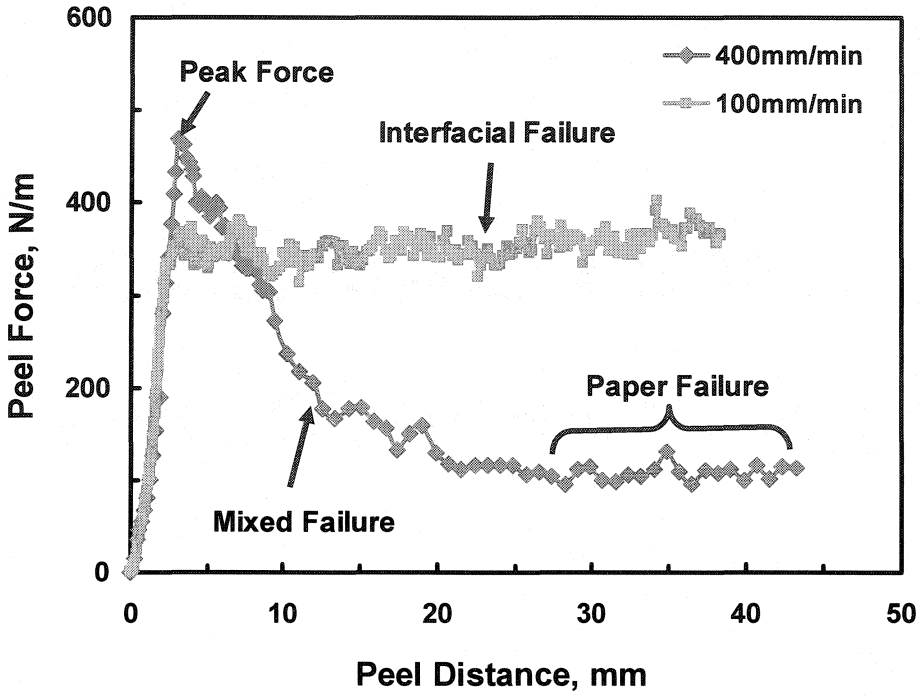

Figure 2.4 **Typical peel curves and failure modes for peeling PSA tape 9974B from newsprint paper at peel rates of 100mm/min and 400mm/min.**

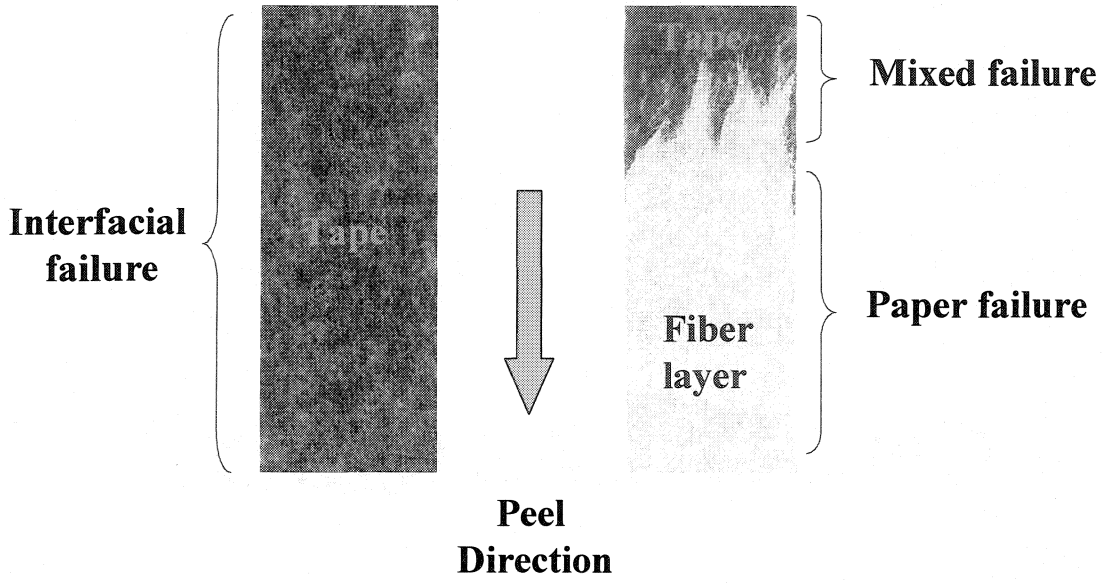

Figure 2.5 **PSA tape surfaces after peeling from newsprint paper at 100mm/min (left) and 400mm/min (right) corresponding to the peel curves in Figure 2.4.**

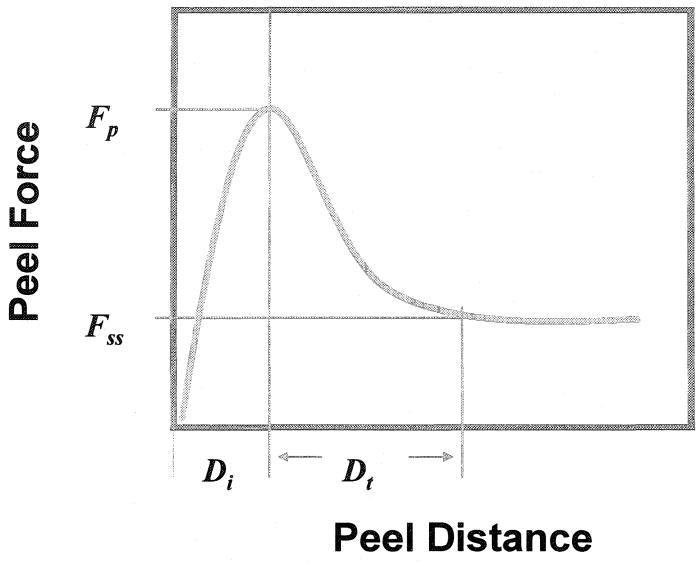

Figure 2.6 **Illustration of an idealized peel curve with four parameters: Peak peel force (F_p), Steady-state force (F_{ss}), Initiation distance (D_i), and Transition distance (D_t).**

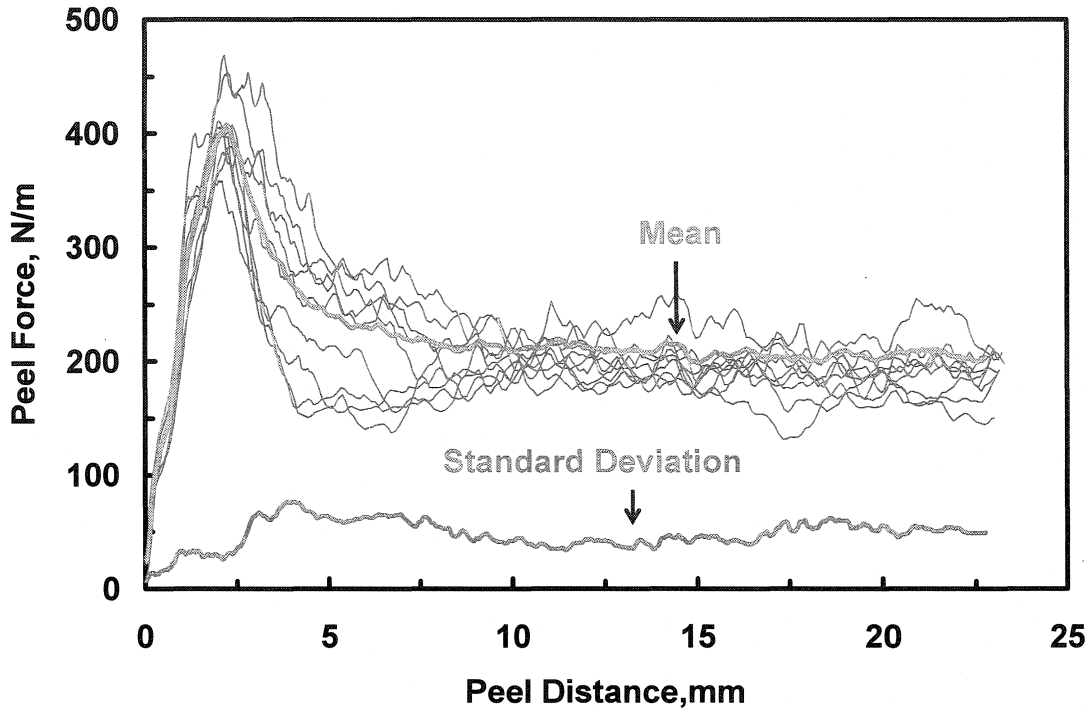

Figure 2.7 **An example of peel curve reconstruction: Peeling PSA tape 9974B from filter paper 1 at 50 mm/min.**

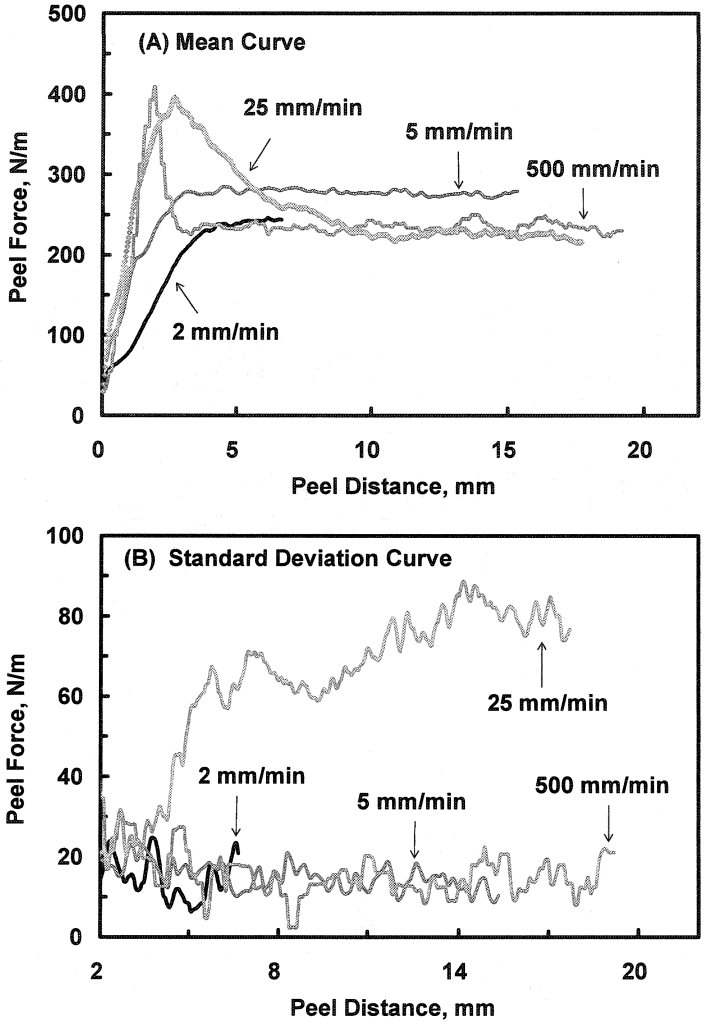

Figure 2.8 **The influence of peel rate on peel behavior. 180° peeling of PSA 9974B from filter paper 1. Interfacial failure was observed at peel rates of 2 and 5mm/min whereas paper failure occurred at 25 and 500mm/min.**

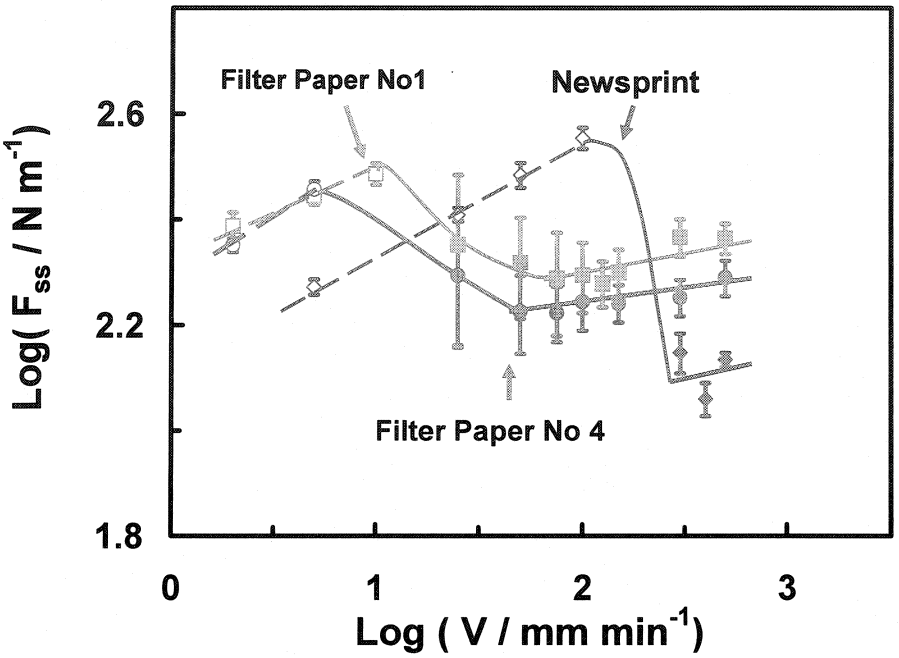

Figure 2.9 **Steady-state peel force versus peel rate. Open symbols are for interfacial failure; filled symbols are for paper failure. 180° peeling of tape 9974B**

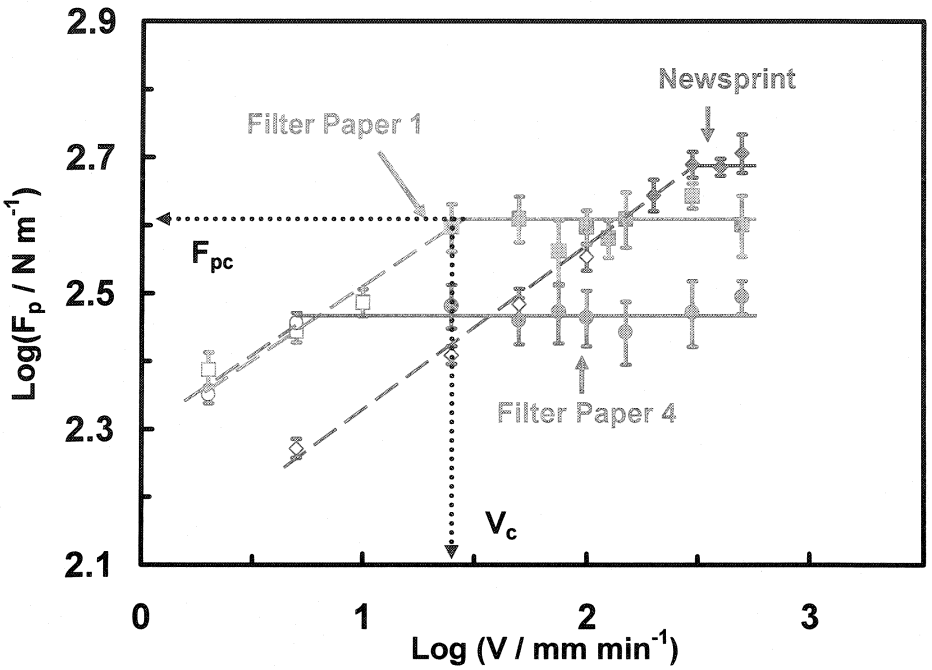

Figure 2.10 **The influence of peel rate on the peak peel force (F_P). Open symbols are for interfacial failure; filled symbols are for paper failure. 180 ° peeling of tape 9974B**

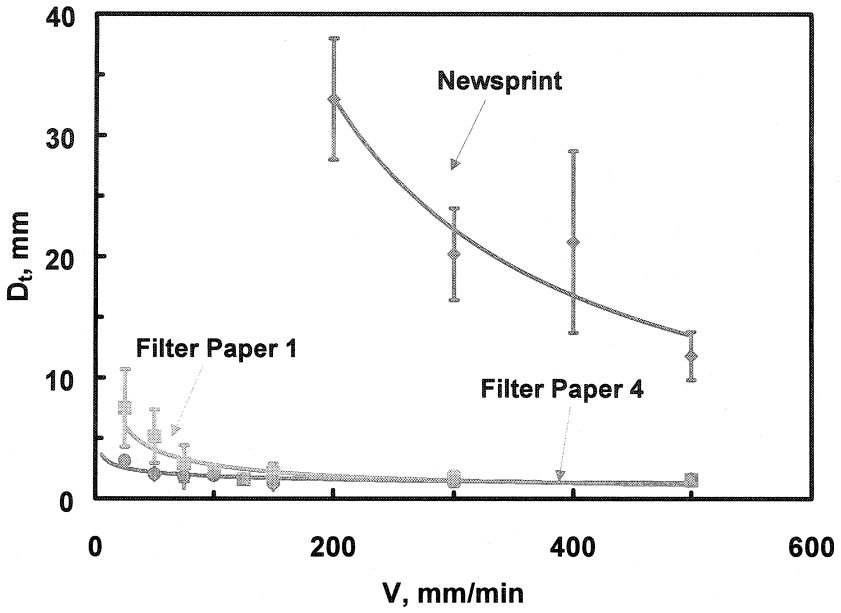

Figure 2.11 **Transition distances. D_t is the mean of at least five repeated tests, the error bar is the standard deviation of D_t. 180 ^{o} peeling of tape 9974B**

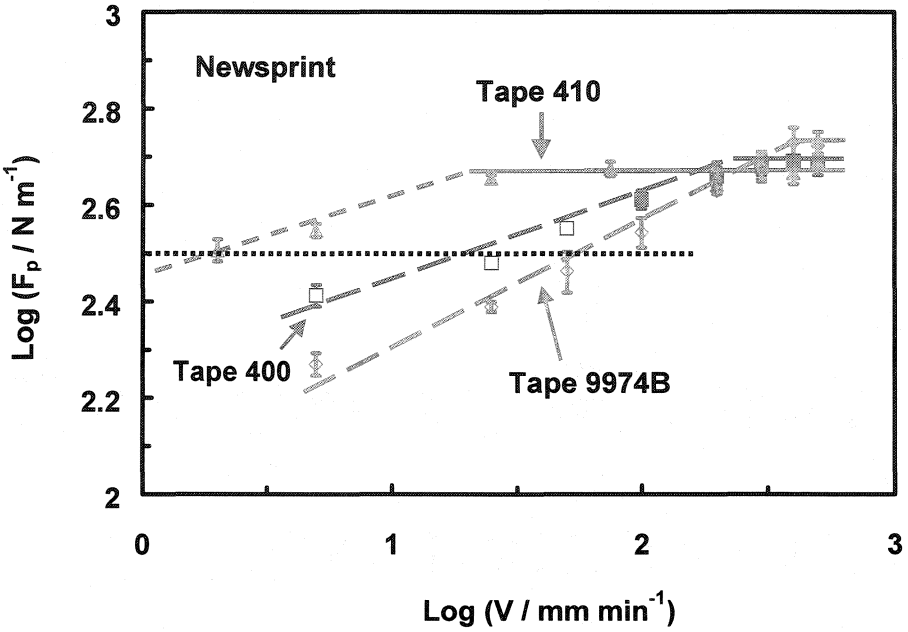

Figure 2.12 Peeling different tapes from newsprint. Open symbols are for interfacial failure; filled symbols are for paper failure.

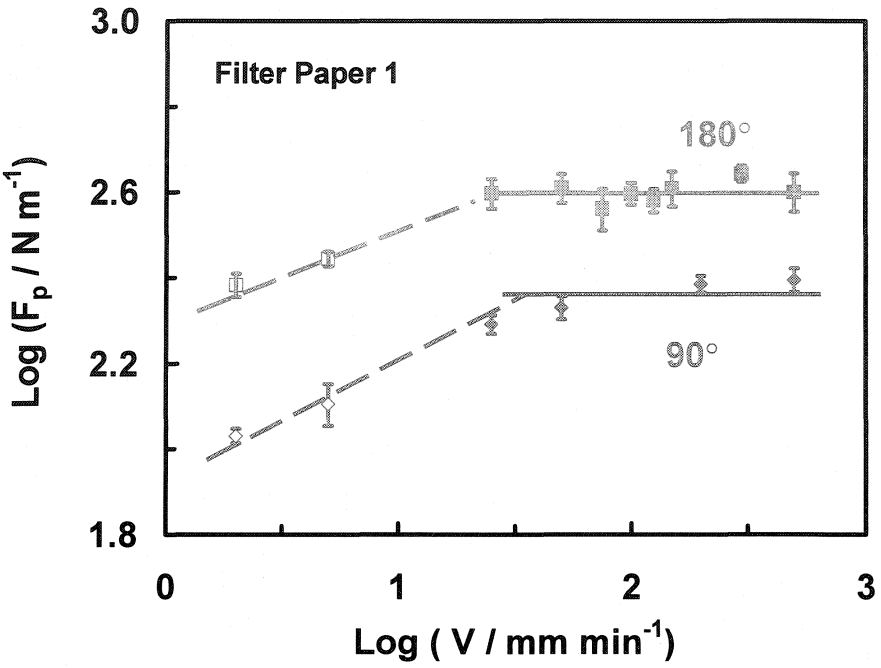

Figure 2.13 **The effect of peel angle for peeling tape 9974B from filter paper 1. The open symbols indicate interfacial failure; filled symbols indicate paper failure.**

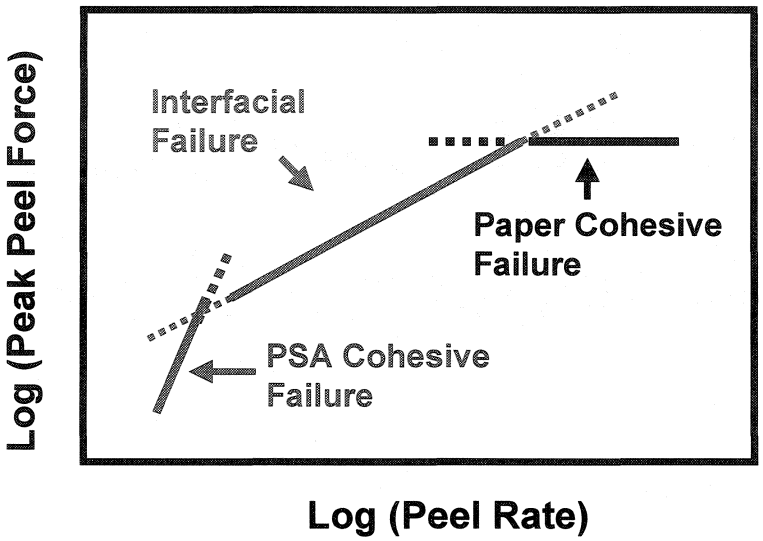

Figure 2.14 **A schematic illustration of a generalized peel curve. Transitions between failure modes correspond to intersections in the curves.**

2.9 Appendix: the effect of lamination time on peel force

A series of preliminary tests were conducted to investigate how peel force varies with lamination time. Figure 2.15 plots the interfacial peel force against the lamination time for the laminate of newsprint/adhesive 9974B on logarithmic scales; the failure mode was interfacial failure. As expected, the peel force increased only slightly with the lamination time. In the thesis work, we kept the lamination time constant.

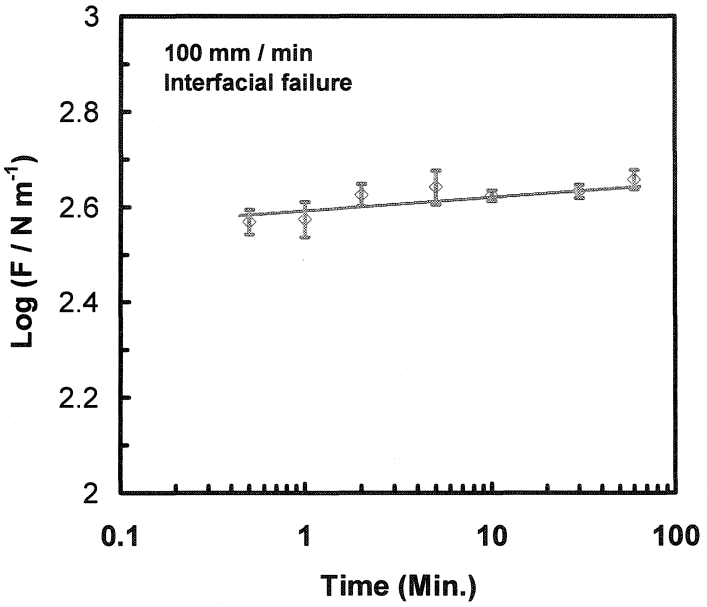

Figure 2.15 the effect of lamination time on peel force. Peeling tape 9974B from newsprint along paper machine direction at 100mm/min. Interfacial failure

Chapter 3 Surface Peel Force

Abstract

Peel experiments involving two pressure sensitive adhesive tapes and two kinds of paper were employed to illustrate a new approach to measure the forces transmitted to paper surfaces during peeling. Peeling a pressure sensitive adhesive tape from a paper surface causes the paper to stretch. The degree of that stretch is a measure of the force applied to the paper surface. Thus, paper was employed as a force transducer, which was calibrated by independent experiments.

The surface peel forces experienced by the paper surface were found to be up to 25% less than the overall peel forces measured by load cell. And this surface force increased with peel rate showing the same dependence as the overall peel force until the onset of paper failure. It was concluded that conventional peel force measurements could be used to evaluate paper surface strength since most of the measured peel force was transmitted to the paper surface and because the ratio of the surface peel force to the overall peel force was independent of peel rate.

3.1 Introduction

Modern papers and paperboards are complex engineered composite materials whose mechanical properties are sensitive functions of the arrangement of fibers, fillers and polymers. The paper science and technology community has established various standard testing methods for measuring many paper properties; in North America the methods are described in TAPPI and PAPTAC testing manuals. However, paper surface strength, which is important for printing and adhesion, has not been captured in a simple, well established test. Currently, wax pick (Tappi T459) and IGT pick tests (Tappi T499) are the most routinely used. However the former is crude and the latter is sensitive to the complex rheology of test fluids.

Everyone who has unwrapped a gift knows that peeling a pressure sensitive adhesive (PSA) tape from wrapping paper can cause it to rip. At very low peel rates a PSA tape may cleanly separate from a paper surface, whereas at high peel rates, the paper fails. Thus there exists a transitional peel rate and peel force corresponding to the onset of paper surface failure. Furthermore, for a given type of tape, this transitional force or peel rate should be a relative measure of paper surface strength. One of the ultimate goals of our work is to develop a simple peel-based measurement of paper surface strength.

In a conventional peel experiment, one measures the *overall peel force* required to pull a tape from a substrate while controlling the macroscopic peel angle and the peel rate. Such tests are easy and rapid to perform. However, there are two factors which complicate relating the measured peel force to the force actually experienced by the paper surface. The first factor is the complexity of the peel front. Microscopic evaluation of the peeling front reveals very complex structures which include strands of PSA spanning between the tape backing and the paper surface. These strands are called fibrils in the PSA technology literature. The second factor is absorption of energy by tape backing when it is bent and by the PSA when it stretched. The net affect of these two factors is that it is not possible to derive a fundamental relationship between the overall peel force and the *surface peel force* experienced by a paper surface. The goal of this work was to measure the surface peel force and to compare it to the overall peel force with a view to the development of a peel-based surface strength measurement for paper.

The fundamental idea of the work described in this paper is that when a tape is peeled from a paper surface, the paper stretches in response to the applied surface force. By measuring this stretch, it is possible to obtain the surface peel force transmitted to the paper during peeling. Results are presented illustrating the role of paper and tape type on overall peel force and surface peel force. However, before proceeding to new results it is instructive to review the main behaviors exhibited when tapes are peeled from paper surfaces.

The peel test is widely used to assess the adhesion when at least one substrate is flexible because the measurements are easy to make and the results are reproducible. Common examples of the application of peel testing include the characterization of pressure sensitive adhesive (PSA) tapes [1] and the z-direction strength of paper [2,3,4].

We have employed the peel test to characterize the interactions of PSA tape with paper [5,6].

From a more fundamental perspective, peel testing is complicated because energy is often consumed in a variety of poorly defined processes. It is generally accepted that peel energy is a product of the work of adhesion and a dissipation factor, which is a function of peel rate, and temperature [7,8]. The effects of peel geometry have also been investigated [9,10,11,12,13] mainly focusing on the plastic bending of the peel arm or the adherent. Kinloch defined a geometry-independent parameter, the adhesive fracture energy, to characterize the fracture of the laminate by theoretically deriving the dissipated energy terms [13].

In a series of papers, Yelon and coworkers analyzed the mechanics of paper bending and peel delamination [14,15,16]. They measured the work of peeling as a function of the minimum radius of curvature of the paper and extrapolated this peel work to zero curvature to give the true delamination work. According to their results, the paper delamination work at 90° peeling accounted for about 60% of the total peel work.

Our interests involve the peel behavior of tapes from paper. This is a challenging system because failure often occurs in the paper substrate. In our previous work [6,17] we showed that a series of peel experiments was best analyzed by plotting the peak peel force, F_p, versus the peel rate on logarithmic axes where the peak peel force was defined as the maximum point in a peel force versus peel distance curve. The resulting logarithmic plot was a straight line with a positive slope at lower peel rates when the failure mode was interfacial. At a critical peel rate, the paper failed and the F_p versus peel rate logarithmic plot became a horizontal line.

It seems reasonable to propose that the critical peel rate and the corresponding peak peel force are measures of paper surface strength. In this paper we move towards the ultimate goal of developing a peel-based test for surface strength. The main issue addressed herein is the relationship between the overall peel force measured in a peel test and the actual force experienced by the paper surface.

3.2 Experimental

3.2.1 Materials

Two types of paper and two commercial pressure sensitive adhesive (PSA) tapes were employed in this work. The two types of paper were Masterpak™ glassine paper #2-11 (New York, USA) and newsprint (Donohue, Ontario, Canada). Some physical properties of the paper are listed in Table 3.1. The paper density was determined by measuring the paper caliper (thickness) and grammage (mass per unit area). Average values were obtained by measuring the caliper (Precision Micrometer, Testing Machines Inc.) and mass (Mettler Toledo, Laboratory & Weighing Technologies) of a pile of 5 sheets. The elastic moduli of the papers were determined, according to TAPPI method (T494), at 25mm/min with an Instron Model 4411 Universal Testing System (Instron® Corporation).

The commercial tapes were Scotch Brand 3M tapes No 9974B and No 400, provided by 3M London, Ontario, Canada. They consisted of adhesive layers coated on both sides of a bleached tissue carrier and were provided with a white backing. The thicknesses of the adhesive layers were 77 μm for tape 9974B, and 106 μm for tape 400. The tape samples were stored in sealed plastic bags.

3.2.2 Methods

Peel test samples were prepared following the work of Pelton et al. [5]. First the backings on double-sided PSA tapes were replaced by strips of Canon copy paper. For this, tape strips 2.5cm x 4cm were placed across a sheet of Canon copy paper. The paper was trimmed to 2.5 cm yielding a paper tail which extended about 10 cm beyond the tape. This tail was used to attach the strip to the clamp of a tensile machine.

The original white backing was removed from the other surface of the test tape. Then a strip of single-sided transparent tape (Grand &Toy Ruban Invisible) was placed on the front edge of the PSA surface to serve as a separation (release) layer to help initiate the peel crack. The peel strip construction is illustrated in Figure 3.1.

The peeling apparatus (see Figure 3.2) consisted of a free-rotating wheel, a tensile testing machine (Instron® 4411 Universal Tester), and a video camera fitted with a macroscopic lens. The peel wheel (25mm wide, 142 mm in diameter with a SKF 6, 8-2 RSI radial bearing) was based on a PAPRICAN design [3]. The video camera was placed behind the wheel focusing on the peeling region, and it was directly lined to a computer in which video clips were collected and analyzed with Ulead VideoStudio 4.01 software.

The tape strip was placed on top of the sample paper on the wheel and was laminated by ten passes with a 2.04 kg rubber coated roller (ChemInstruments, Mentor Ohio). In the final step, the top copy paper backing was gently folded back at the position of the "separation tape" and clamped by the upper clamp of the Instron.

The peel tests were performed with the Instron tester located in a constant temperature (23°C) and humidity (50%) room. A 50N load cell was used in all peel experiments and the peel rates ranged from 5mm/min to 500mm/min. Video images of the peel front were recorded and analyzed to give the degree of paper stretch during peeling. The image analysis was accurate to 0.03mm.

Calibration Experiment

Independent experiments were conducted to permit conversion of the extracted paper stretch information into force values. The experimental setup, shown in Figure 3.3, mimicked the peel apparatus except that the force was applied to the underside of the paper with a steel bar (3mm x 3mm) which initially was set in a notch (4mm wide, 4mm deep and 25mm long) running across the peel wheel. The paper strip was half covered with tape to mimic a peel sample. A calibration experiment consisted of measuring the applied force as a function of displacement at constant strain rates of 5 mm/min to 350 mm/min.

3.3 Results

When tapes were peeled from paper at a superficial angle of 90° using a peel wheel, the paper was observed to be raised from the wheel surface. Figure 3.4 shows a typical frame from a peel video and the symbol *d,* which we call the *separation distance*, denotes the vertical distance between the paper surface and the aluminum peel wheel. The following sections will relate *d* to the actual surface peel force experienced by the paper during peeling. Two paper types were employed – glassine and newsprint (Table 3.1). Following the classic studies of Yamauchi et al. [18], we showed in previous work that peeling from glassine, a dense smooth paper, usually gives interfacial failure with occasional "picked fibers". Peeling from newsprint gives interfacial failure only at low peel rates, with catastrophic paper delamination occurring at high peel rates [6].

Figure 3.5 shows the peel force, *F*, and separation distance, *d*, versus peel distance for peeling tape 9974B from glassine paper. In this case, the failure mode was interfacial failure, meaning that the pressure sensitive adhesive cleanly separated from the paper surface. The peel force, *F*, curve reached a plateau value which was noisy but approximately constant. In this case, the plateau force value equaled the peak peal force, F_p. Note that the initial rise in peel force corresponded to the removal of slack in the sample.

The corresponding separation distance, *d*, curve is also plotted in Figure 3.5. Although superficially similar in shape to the peel force curve, the separation distance had a small positive slope when the peel force was constant.

Figure 3.6 shows results of peeling from newsprint which displayed paper failure. In this case, the peel force curve was more complicated; peel force rapidly increased to a peak and then dropped to a much lower steady-state region corresponding to paper delamination. The separation distance curve displayed a similar shape to that of the peel force curve.

Figures 3.5 and 3.6 show that the separation distance was a function of peel distance and the failure mode. To facilitate comparison of different peel experiments, a single parameter called the peak separation distance, d_I, was chosen to represent separation distance curves. Figure 3.6 illustrates the definition of d_I, which is the separation distance corresponding to the peak force.

Peel experiments were conducted as a function of peel rate for three paper/tape combinations. Figure 3.7 shows the peak peel force, F_p, as a function of peel rate on logarithmic axes; the error bars were calculated from the formula of $\log((F_p \pm SD)/F_p)$ where F_p is the mean of three repeat experiments, and *SD* is the standard deviation of F_p. The corresponding failure modes are depicted by the type of fill in the plotted data points: open symbols denote interfacial failure; gray-filled points denote fiber picking; and black-filled points correspond to complete paper failure.

A general feature of Figure 3.7 is that Log (F_p) linearly increased with Log (V) while the failure mode changed from interfacial failure to fiber picking. At high peel rates, newsprint displayed paper failure and the corresponding peel force, F_p was independent of peel rate. By contrast the very dense glassine paper only showed fiber picking (Table 3.1). This is consistent with our previous results [6]. Peeling tape 9974B

from different types of paper gave similar initial slopes, whereas peeling tape 400 gave a different slope. We believe that the different initial slopes of the two PSA tapes reflect differences in the adhesive properties. Furthermore, peeling tape 400 gave greater peel forces than did tape 9974B, indicating a stronger adhesion for glassine/tape 400 than glassine/tape 9974B. In addition, peeling with tape 9974B caused newsprint to fail at a lower peel rate than glassine, reflecting the fact that the z-direction surface strength of glassine is greater than that of newsprint.

The corresponding peak separation distance, d_l, values are shown in Figure 3.8 as a function of log peel rate. The peak separation distance increased with peel rate until fiber picking occurred, after which d_l declined with increasing peel rate. In the interfacial failure region, the newsprint gave a greater d_l than glassine paper perhaps reflecting its lower elastic modulus (see Table 3.1 for paper properties).

Tape type also influenced the peak separation distance. Tape 400 with stronger adhesion energies as indicated in the peel force curve, also gave higher peak separation distances than tape 9974B.

One of the goals of this work was to estimate the forces actually applied to the paper surface during peeling. For this, a relationship between separation distance and surface force was required. This relationship was obtained by two ways. First, a simple model was derived to predict surface force as a function of separation distance and conventional paper properties. Second, direct mechanical measurements were made of the force required to stretch paper in the same peel geometry to give a direct calibration curve. The direct calibration forces were used to give surfaces force, F_s, values whereas the model was derived to illustrate the role of experimental parameters. The model is now described.

Calculating Surface Force from Separation Distance

A schematic illustration of a peel sample is shown in Figure 3.9. The test paper strip runs from A to G. End segments *AB* and *FG* correspond to the location of the double sided tape which fixes the paper to the wheel. Segments *BC* and *FO* denote the bare paper surfaces; segment *CO* corresponds to the region where the PSA tape is laminated on the paper surface; segment *OH* is the tail end of the tape strip which is attached to the Instron grips; point *I* is the center of wheel; point *O* is the debonding point of PSA tape and paper; O^* is the projection of O on the wheel surface; and, *D* and *E* are two tangent points between the paper and wheel surface.

For simplicity, it is assumed that the surface force is applied only on point *O*. A force balance at the point *O*, as illustrated in Figure 3.10, leads to the following relationship between surface force F_s (N/m) and the reacting force of paper f (N/m), where θ is the supplementary angle between *OD* or *OE* and *OH*.

$$F_s = 2f\cos(\theta) \qquad \text{Equation 1}$$

The reacting force, f, of paper in peeling is given by equation 2 where σ is paper stress, and h is paper thickness.

$f = \sigma \cdot h$ Equation 2

The fundamental assumption of this analysis is that paper stress σ has a linear relationship with its nominal strain e in peeling. This relationship is mathematically expressed in equation 3 where k is the apparent modulus of paper.

$\sigma = k \cdot e$ Equation 3

The nominal strain is defined as below, where OF is the length of paper sample at the right side of the debonding point O and O^*F is its projected length on the wheel surface.

$$e = \frac{OF - O^*F}{O^*F}$$

Combining equations 1, 2 and 3 gives the following.

$F_s = 2k \cdot h \cdot e \cdot \cos(\theta)$ Equation 4

The e and θ can be approximately expressed as functions of the projected length, L (the O^*F in Figure 3.9) of the bare paper sample on the wheel surface, wheel radius, r, and separation distance, d (the OO^* in Figure 3.9). (see section 3.9 Appendix)

$$\cos(\theta) \approx \sqrt{\frac{2d}{r}}$$ Equation 5

$$e \approx \frac{d}{L} \cdot \sqrt{\frac{2d}{r}}$$ Equation 6

Inserting equation 5 and 6 into 4 leads to the following relationship between surface force, F_s, and separation distance, d.

$$F_s \approx 4k \cdot h \cdot \frac{d^2}{L \cdot r}$$ Equation 7

The model (equation 7) reveals that surface force increases with the square of d for a given paper sample. Furthermore thicker paper (the term h) requires a higher surface peel force to obtain a given separation distance. Finally, equation 7 predicts that during a peeling experiment with a constant F_s, the separation distance d must increase to compensate for increasing L (the O^*F in Figure 3.9). Perhaps this explains the slight increase of d in Figure 3.5 when peel force was constant.

Surface Forces from Separation Distance Calibration Curves

The forces required to stretch the peel samples were directly measured at 25mm/min using the setup in Figure 3.3. The experimental results are shown in Figure 3.11, together with curves calculated with equation 8 where α was a fitting coefficient.

$F_s = \alpha \cdot d^2$ Equation 8

For both papers, the experimental data showed a slightly greater dependence on d than the squared dependence predicted by equation 8. Furthermore, the glassine paper had a bigger α value than newsprint where, according to the model, α is given by the following expression.

$$\alpha = \frac{4kh}{Lr}$$ Equation 9

Based on equation 9, k values were calculated from the fitted α values in Figure 3.11 and are compared with the tensile modulus, E, for two papers in Table 3.2. The calculated k values are about one fifth of the corresponding E values, but the ratios of k to E for the two paper samples are almost same.

Figure 3.12 shows the influence of strain rate on the calibration curve. The influence of strain rate was minor especially over the first 1.5 mm. The curves at 25 mm/min were used as standard calibration curves.

Surface forces were obtained by interpolating the d_I data of Figure 3.8 into calibration curves of Figure 3.11 and are shown as a function of peel rate in Figure 3.13. Only peel results corresponding to interfacial failure are shown. Like the peak peel force, the log of surface peel force increased linearly with the log of peel rate. A comparison of surface forces to their corresponding peel forces is shown in Figure 3.14 where the three distinct data sets from Figure 3.13 have collapsed to a single line. That is, the surface and overall peel forces are linearly related and the two tapes on the two paper types gave results that fell on the same line. In nearly every case, the overall peel force was greater than the surface peel force with the maximum difference of about 25% occurring at the highest peel force. Interestingly, most of the data for two tapes and two papers fell on the same line in Figure 3.14. Nevertheless, the reader is reminded that the two tapes in Figure 3.14 had the same paper backing and the difference in their adhesive layers thickness was about 30%. Commercial tapes with stiffer backing are likely to deviate from the line in Figure 3.14.

3.4 Discussion

The ultimate goals of our work are to understand peeling from paper and to develop a robust test for paper surface strength. Peeling is an attractive process for estimating paper surface strength because paper surface failure often occurs during printing, calendaring, and converting operations which inflict stresses on paper which are similar to peeling. It is interesting that the two types of PSA tapes and two paper surfaces gave approximately the same correlation curve between surface force and overall force (Figure 3.14). This suggests that the two different tapes could be used to estimate the same minimum force required for paper surface failure. Note that the corresponding peel rates would be different, reflecting different adhesive rheology. In other words, Figure 3.13 shows that to inflict a specific force on the surface of glassine paper, a higher peel rate would be required for tape 9974B than for tape 400.

A conclusion from this work is that the overall peel force, measured in a conventional manner is a fairly good estimate of the force experienced by the paper surface. The validity of this conclusion depends upon the accuracy of our surface force measurements. The primary measurement was the separation distance, d (see Figure 3.4). The following analysis indicates that d is a sensitive measure of paper strain.

Rearrangement of equation 6 leads to the following relationship between the separation distance d and the length (the product of e and L) by which the paper was elongated.

$$d = (\frac{r}{2})^{1/3} \cdot (e \cdot L)^{2/3} \qquad \text{Equation 10}$$

For example, a typical paper in peeling exhibited a 0.3% nominal strain which gave a separation distance of 1.05 mm, about six times greater than its elongation ($e \cdot L$) which is only 0.18 mm. The estimated accuracy of our optics and image analysis for d was ±0.03mm which is about 3% of typical separation distances.

On the other hand, the peeling methodology was not good for determining the elastic modulus of paper. Indeed, we use the terms nominal strain and elongation length since some of the strain actually was observed to occur in the tape used to mount the paper strip ends to the peel wheel. Stretching within the mounting tape may account for the observation that the apparent modulus, k, calculated based on equation 9, was smaller than the tensile modulus, E, of paper measured by convention methods. Since exactly the same mounting procedure was used for the direct calibration procedure, strain in the mounting tape layer was not considered to be an important effect for the present purposes.

The relationship between separation distance and surface force is theoretically revealed by equation 7, which is based on the assumption of a linear relationship between paper nominal strain and paper stress. This model slightly underestimated the results in the calibration curves (Figure 3.12) at high separation distance d, indicating limitations in the model. Nevertheless the model (equation 7) does reveal how paper properties may influence the measurement of surface force. For example, surface force linearly increases with paper thickness for a given separation distance. The roles of paper sample length, L, and wheel radius, r, are also captured in the model.

3.5 Conclusions

1. Peeling of a pressure sensitive adhesive tape exerts a force (we call the surface peel force, F_s) at the peel crack on the paper surface and this force can be estimated by the induced strain in the paper.
2. The surface peel force is proportional to the overall peel force. By varying peel rates, the two types of forces are shown to have a linear relationship.
3. Although the overall peel force is sensitive to the type of paper, the type of tape and the peel rate, the relationship between surface and overall peel force is independent of paper and PSA tape for the two tape types and two paper types investigated herein.
4. The tendency of a paper surface to fail, either by loss of individual fibers or by catastrophic delamination, can be estimated by extrapolating surface peel force to the peel rate at which paper failure initiates.
5. A force balance model shows that the peel force applied to the paper surface scales with the square of the distance that the paper lifts off the peel wheel during peeling. The model was verified by calibration experiments.

3.6 Acknowledgments

This work was supported by 3M Canada and the Natural Science and Engineering Research Council of Canada. Thanks Elaine Miasek and Luis Anderson for experimental assistances.

3.7 References

1 D. Satas (editor), In: *Handbook of Pressure Sensitive Adhesives*, Van Nostrand Reinhold, pp. 61-96 (1989).

2 A. Koubaa and Z. Koran, *Tappi*, 78(3):103-111 (1995).

3 J. Skowronski and W. Bichard, *J. Pulp Paper Sci.,* 13(5):165-169 (1987).

4 J. Skowronski, *J. Pulp Paper Sci.,* 17(6):217-222 (1991).

5 R. Pelton, W. Chen, H. Li, and M.R. Engel, *J. Adhesion*, 77:285-308 (2001).

6 B. Zhao and R. Pelton, *J. Adhes. Sic. Tech.* 17(6):815-830 (2003).

7 A.N. Gent and R.P. Petrich, *Proc. R. Soc., London, Ser. A,* 310:433-448 (1969).

8 E.H. Andrews, *J. Mater. Sci.*, 9: 887-894 (1974).

9 J. Kim, K.S. Kim and Y.H. Kim, *J. Adhes. Sci. Technol.* 3(3):175-187 (1989).

10 N. Aravas, K.S. Kim and M.J. Loukis, *Mater. Sci. and Eng.*, A107:159-168 (1989).

11 T. Igarashi, In: *Adhesive Joints*, edited by K.L. Mittal, Plenum Press, pp. 419-432, (1984).

12 A.N. Gent and G.R. Hamed, *J. Appli. Polym. Sci.*, 21:2817-2831 (1977).

13 A. J. Kinloch, C.C. LAU and J.G. Williams, *Int. J. of Frac.*, 66(1):45-70 (1994).

14 A. El Maachi, S. Sapieha, and A.Yelon, *J. Pulp Paper Sci.,* 21(10):362-366 (1995).

15 A. El Maachi, S. Sapieha, and A.Yelon, *J. Pulp Paper Sci.,* 21(12):401-407 (1995).

16 A. El Maachi, S. Sapieha, and A.Yelon, *Nordic Pulp Paper Res. J.* 14(1):17-22, 29 (1999).

17 B. Zhao and R. Pelton, *J. Mater. Sci. Letter,* 22:265-266 (2003).

18 T.Yamauchi, T.Cho, R. Imamura and K. Murakami, *Nordic Pulp Paper J.*, 3(3): 128-131 (1988).

3.8 Tables and figures

Table 3.1 **Newsprint and glassine properties. The elastic moduli were measured at 25 mm/min.**

Sample	Thickness (μm)	Density (Kg/m^3)	Elastic Modulus (GPa)
Newsprint	68	662	3.8
Glassine Paper	35	1017	12.1

Table 3.2 **A comparison of the apparent stretching moduli, *k*, with the elastic moduli E of two paper types. The α values were obtained by fitting calibration curves to equation 8 and the corresponding *k* values were calculated with equation 9.**

Sample	α (MPa/m)	*k* (GPa)	*k*/*E*
Newsprint	89.39	0.70	0.18
Glassine	129.81	1.98	0.16

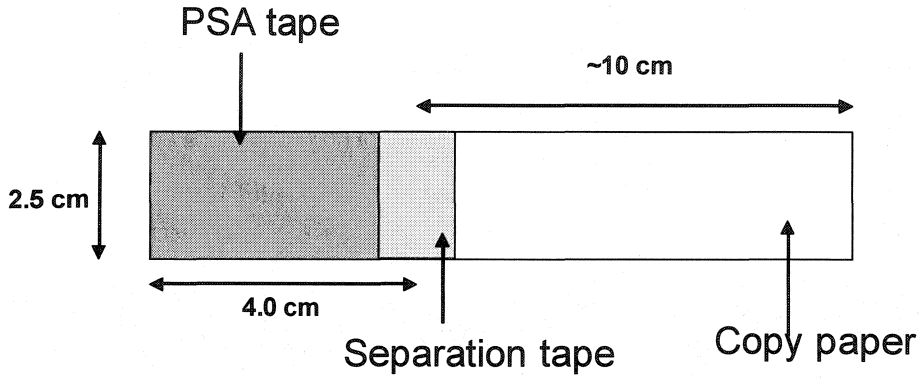

Figure 3.1 Illustration of the construction of a peel strip

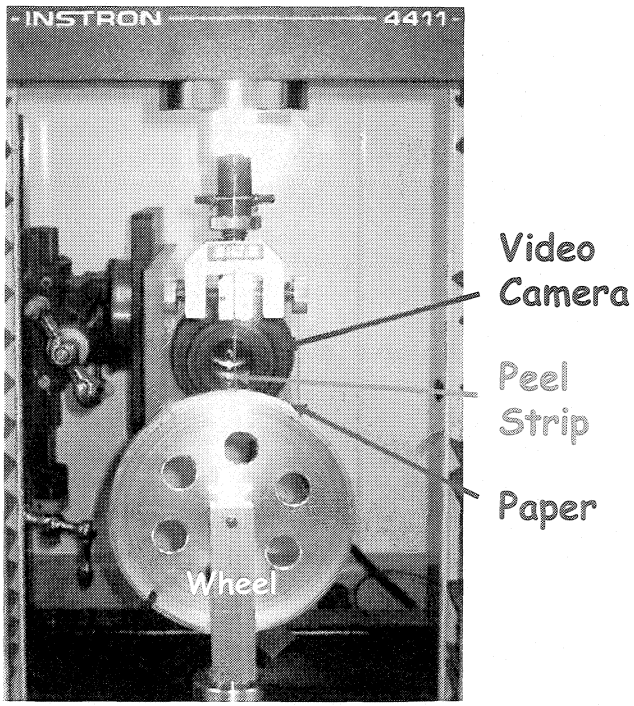

Figure 3.2 **Peeling apparatus. The wheel is freely rotating and peel force is measured using an Instron tester.**

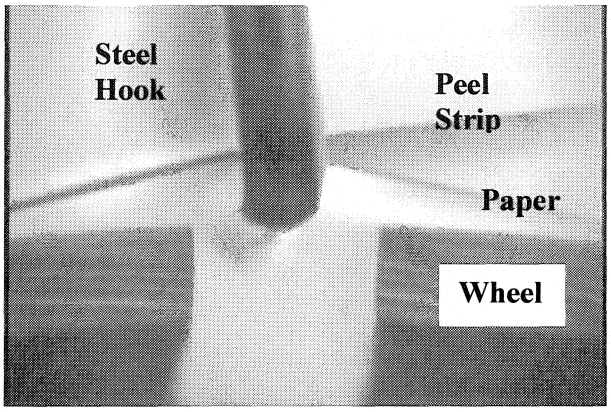

Figure 3.3 **A photograph (side view) of the paper stretching calibration setup. The hook under the paper is lifted up by the Instron and force is measured as a function of separation distance, *d*.**

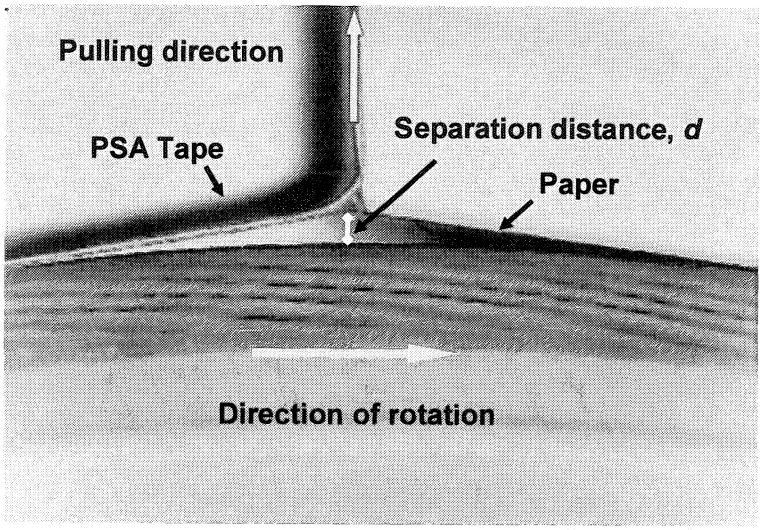

Figure 3.4 A peeling experiment in progress

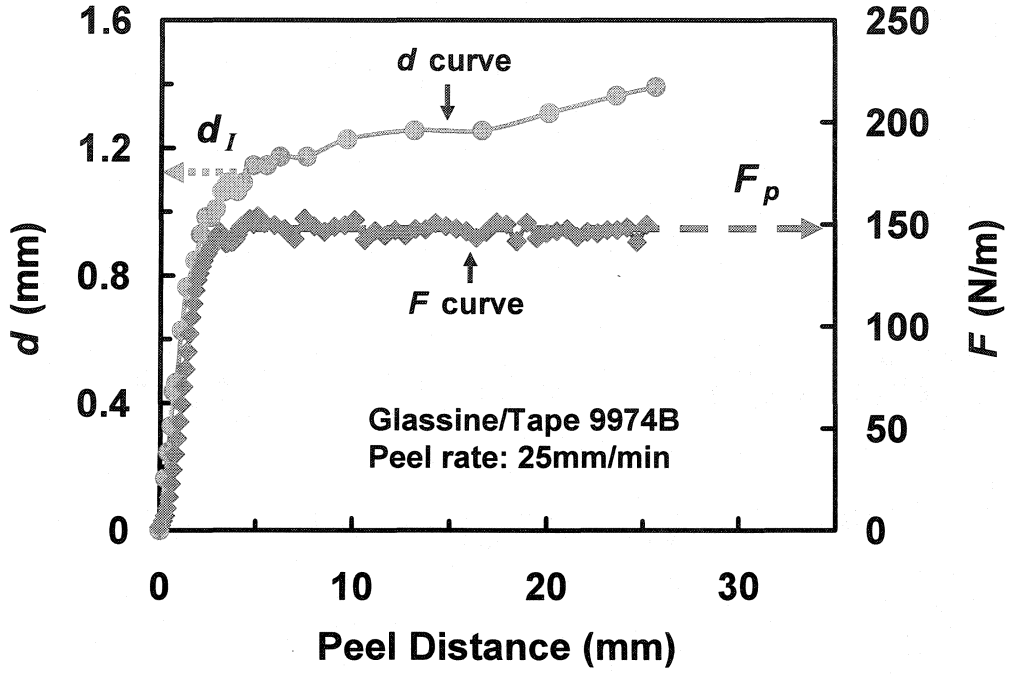

Figure 3.5 **Peeling tape 9974B from glassine paper at 25 mm/min giving interfacial failure**

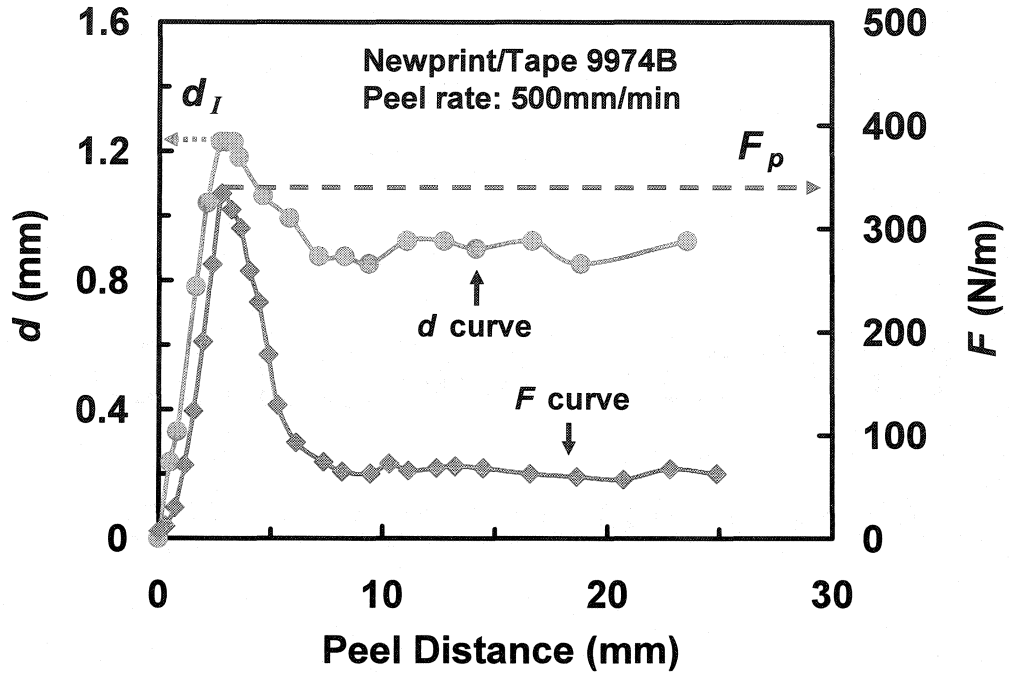

Figure 3.6 **Peeling tape 9974B from newsprint paper at 500 mm/min giving paper failure**

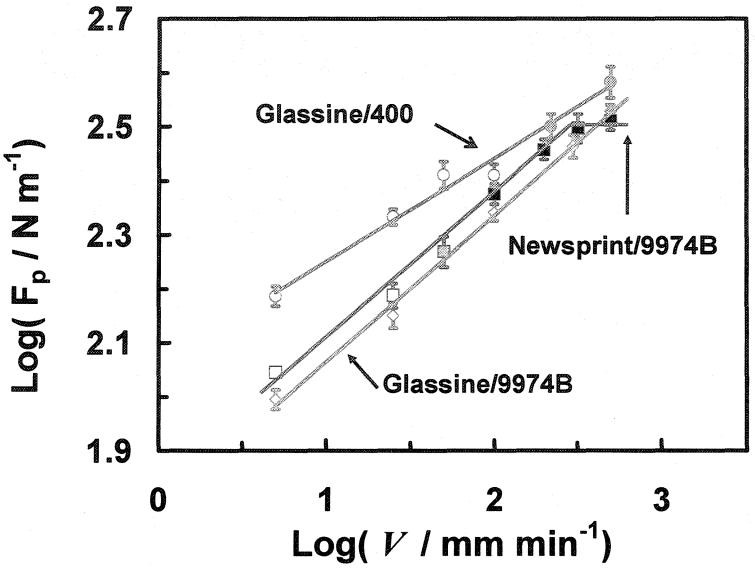

Figure 3.7 **The influence of peel rate and paper/ tape combinations on peak peel force: open symbols denote interfacial failure; gray-filled symbols denote fiber picking; black-filled symbols denote paper failure.**

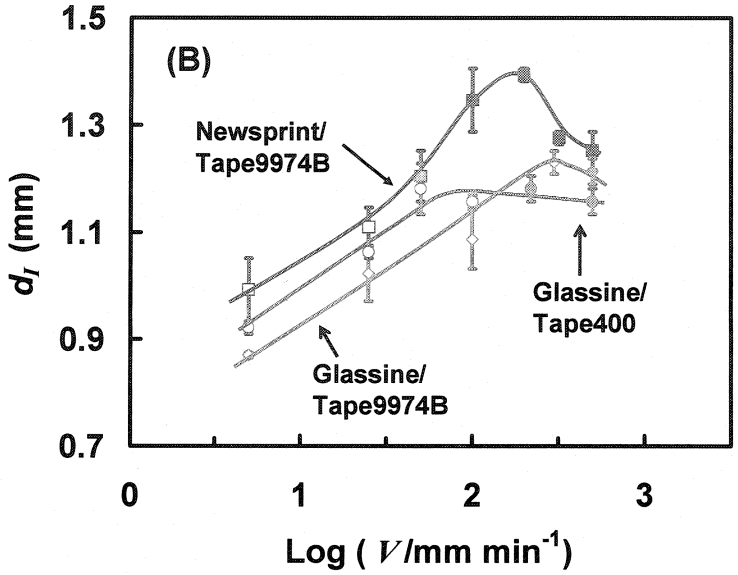

Figure 3.8 **Influences of peel rate and paper/tape combinations on peak separation distance: open symbols denote interfacial failure; gray-filled symbols denote fiber picking; black-filled symbols denote paper failure.**

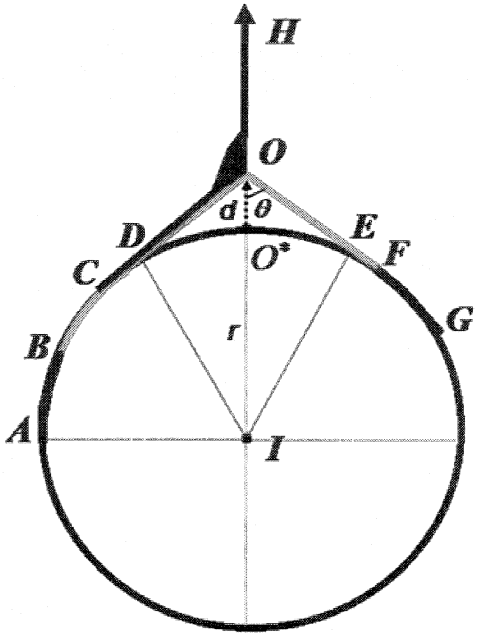

Figure 3.9 Schematic illustration of the construction of peeling

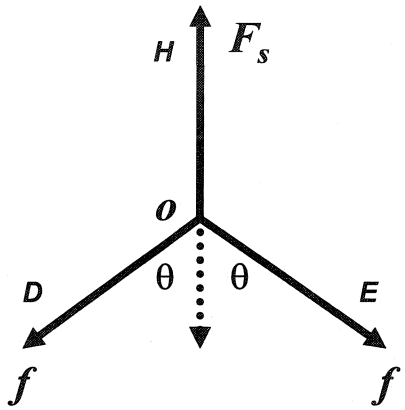

Figure 3.10 Force balance analysis at point *O* in Figure 3.9

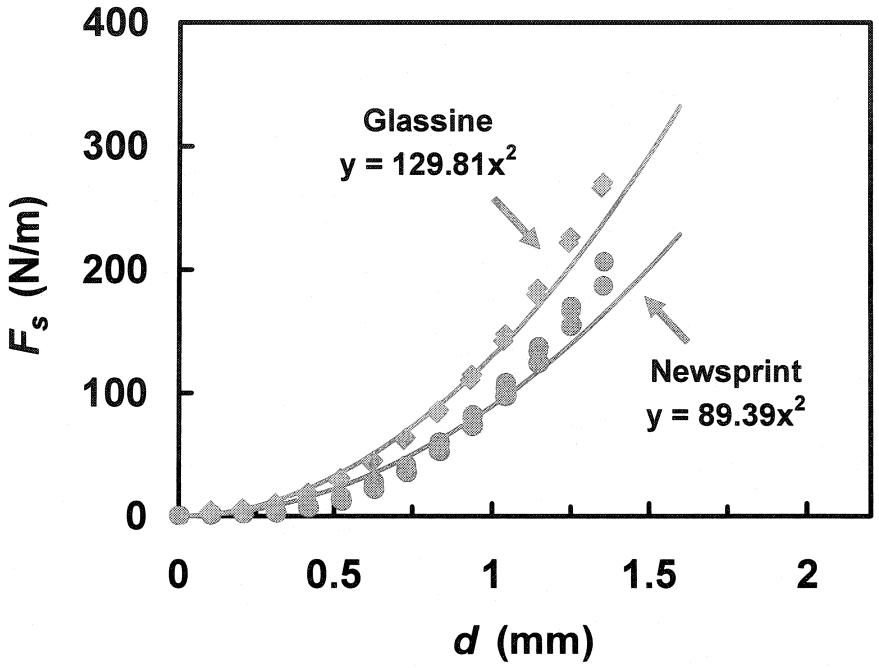

Figure 3.11 **Calibration curve for estimating F_s from measured d values. The experimental data were obtained with the apparatus shown in Figure 3.3 at the strain rate of 25mm/min. The solid lines were calculated with equation 8.**

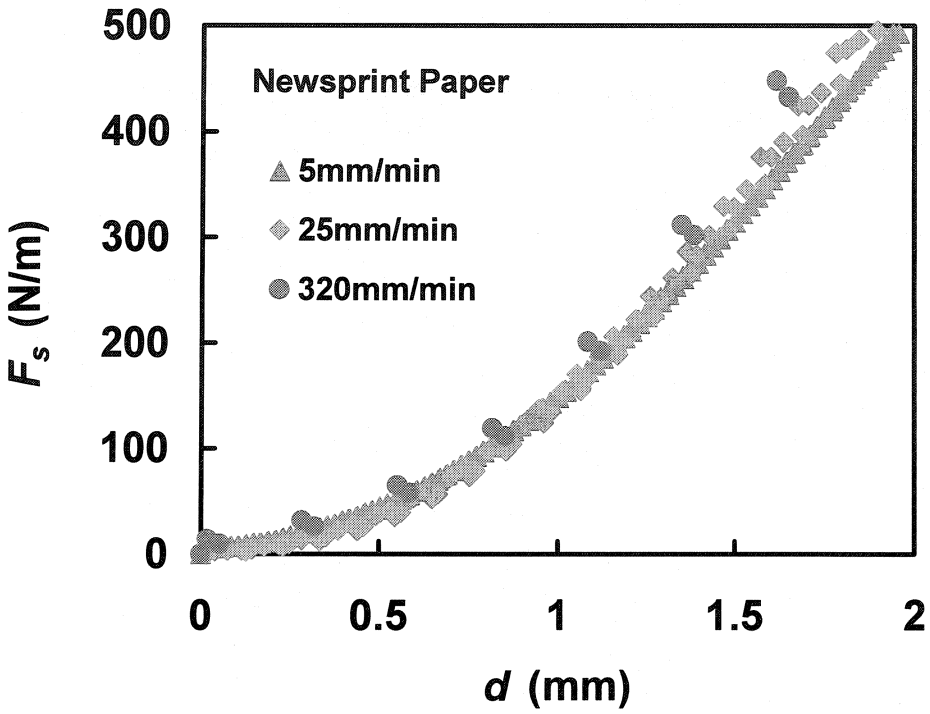

Figure 3.12 The influence of strain rate on calibration curves of F_s as functions of d.

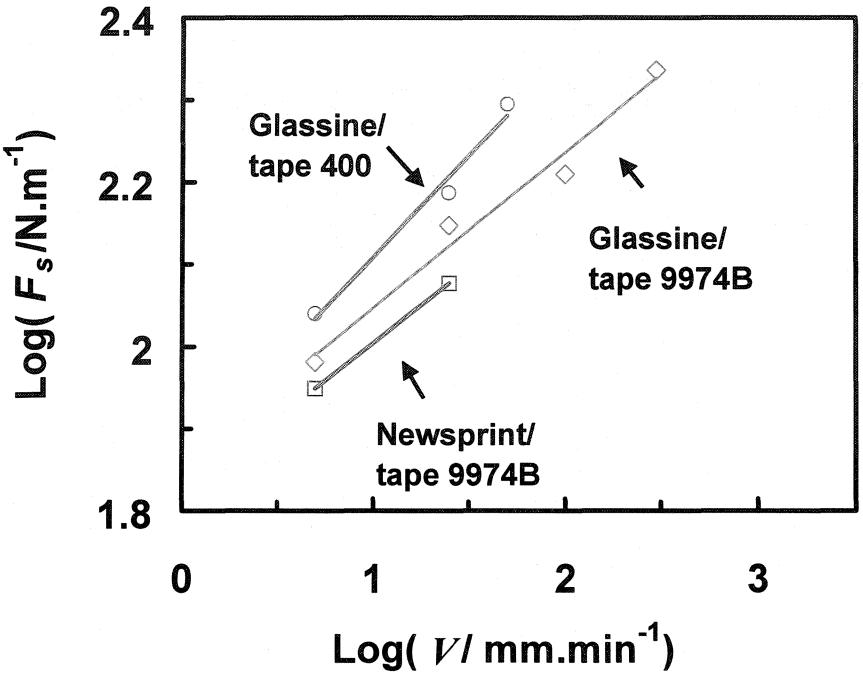

Figure 3.13 Surface force as a function of peel rate

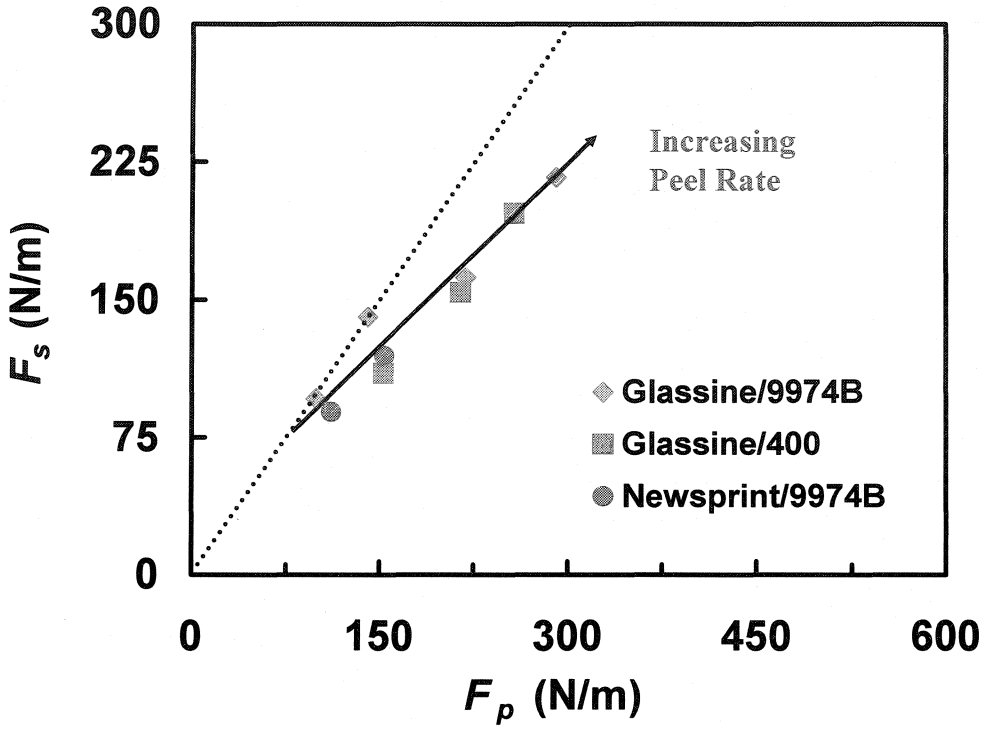

Figure 3.14 The comparison of surface force F_s to overall peel force F_p

3.9 Appendix: calculation of paper nominal strain

The nominal paper strain e is defined as following where OF (see Figure 3.9) is the length of bare paper sample and O^*F is its projected length on the wheel surface, which is also denoted by L.

$$e = \frac{OF - O^*F}{O^*F} \qquad \text{Equation A 1}$$

Since $OF = OE + EF$ and $O^*F = O^*E + EF$, then $OF - O^*F = OE - O^*E$. Thus,

$$e = \frac{OE - O^*E}{O^*F} \qquad \text{Equation A 2}$$

$$O^*E = r \cdot (\frac{\pi}{2} - \theta) \qquad \text{Equation A 3}$$

$$OE = (r + d) \cdot \cos(\theta) \qquad \text{Equation A 4}$$

where r is the radius of supporting wheel (r = O^*I=EI =DI); and d is the separation distance (d=O^*O). When θ is close to $\frac{\pi}{2}$, let's say $\frac{\pi}{3} < \theta \leq \frac{\pi}{2}$, $\cos(\theta)$ approximately equals $\frac{\pi}{2} - \theta$.

$$\cos(\theta) \approx \frac{\pi}{2} - \theta \qquad \text{Equation A 5}$$

Thus,

$$OE - O^*E \approx d \cdot \cos(\theta) \qquad \text{Equation A 6}$$

Inserting this equation into equation A1 leads to the following.

$$e \approx \frac{d \cdot \cos(\theta)}{O^*F} \qquad \text{Equation A 7}$$

If we use L to represent O^*F, then

$$e \approx \frac{d \cdot \cos(\theta)}{L} \qquad \text{Equation A 8}$$

The triangle OEI with right angle at point E gives the following relationship.

$$\sin(\theta) = \frac{EI}{OO^* + O^*I} = \frac{r}{d + r} \qquad \text{Equation A 9}$$

Thus,

$$\cos(\theta) = \sqrt{1 - \sin^2(\theta)} = \sqrt{1 - \frac{r^2}{(r+d)^2}} = \sqrt{\frac{2rd + d^2}{(r+d)^2}} \qquad \text{Equation A 10}$$

Since $d << r$ (d <2mm and r =71mm), the following relationships exist

$$\frac{d^2}{(r+d)^2} \approx 0 \qquad \text{Equation A 11}$$

$$(r+d)^2 \approx r^2 \qquad \text{Equation A 12}$$

Inserting the above two expressions into the equation A10 leads to the following.

$$\cos(\theta) \approx \sqrt{\frac{2d}{r}} \qquad \text{Equation A 13}$$

Inserting this expression into equation A8 gives the following.

$$e \approx \frac{d}{L} \cdot \sqrt{\frac{2d}{r}} \qquad \text{Equation A 14}$$

Chapter 4

The Initiation of Paper Delamination in Peeling

Abstract

The primary goal of the research summarized in this chapter was to identify the processes leading to the delamination of paper when a pressure sensitive adhesive tape is peeled from a paper surface. A secondary objective of this work was to determine the influence of wet pressing pressure, pulp beating and fiber length on the propensity for handsheets to delaminate in peel. It was found that the paper delamination is characterized by a high initiation (peak) peel force and a lower steady-state peel force. Furthermore, the peak peel force is more than two times higher than the steady delamination force for a broad range of paper properties. Microscopic observation of the peeling front revealed that paper delamination involved three sub-processes: 1) the initial delamination of the top fiber layer from the paper sheet; 2) the rupture of that delaminated top layer so it remains with the tape in peeling; and, 3) the continuous separation of the top fiber layer from the paper sheet in the steady-state peeling region.

The peak peel force is a measure of the propensity of a paper to delaminate – the higher the peak peel force, the more difficult it is to induce delamination. Peak peel forces of the softwood kraft pulp handsheets increase linearly with internal bond strength and tensile strength of the paper.

4.1 Introduction

Most of us have tried to unwrap presents without damaging the decorative paper wrapping. Usually the act of peeling the pressure sensitive adhesive tape (PSA) causes the paper surface to delaminate. The goal of the work described in this chapter is to identify the critical events leading to the initiation of paper delamination when a tape is peeled from a paper surface. It will be shown that the delamination of the paper surface is relatively difficult to start; however, once started, steady-state delamination in peel is relatively easy due to the layered structure of paper [1]. Understanding the initiation of delamination is important because unwanted delamination is problem in many paper coating, printing and converting operations [2,3].

Many methods have been developed to characterize the resistance of paper to delamination, including the Scott bond test [4], the STFI z-toughness test [5] and the peel-wheel test [6]. All of these give an estimate for paper delamination strength, but none of them provide information on the initiation of the paper delamination.

Following the pioneer work of Bikerman [7] and Yamauchi et al. [8,9], we carried out systematic studies on peeling adhesive tapes from paper surfaces. The overall goal of our research is to understand how paper properties influence the performance of adhesive/paper laminates. This paper focuses on the initiation of paper delamination. Our approach was to quantify the initial portions of the peel force versus peel distance curves measured using a series of well defined papers. The force measurements were augmented with video imaging of the peel front in order to identify structural changes during the initiation of paper delamination.

4.2 Experimental

4.2.1 Materials

Scotch brand 3M 9974B pressure sensitive adhesive (PSA) tape was chosen from various tape samples provided by 3M (London, Canada) because 9974B gave paper delamination over a convenient range of peel rates. The tape consisted of a blue adhesive layer (77μm) coated on both sides of a bleached tissue carrier and with a stiff white release backing (90μm). In addition, a commercial single-sided transparent tape (Grand &Toy Ruban Invisible) was applied as a separation layer to facilitate the folding of the peel strip – see the description in peel test.

Previously dried bleached softwood kraft pulp was obtained from Avenor (now Bowater, Thunder Bay, Canada). Following Tappi Method (T205), a series of handsheets (basis weight 60g/m^2) were made from this pulp using deionized water and a semi-automatic sheet machine (model 300-1, Labtech Instruments Inc., Laval, Canada).The beating of pulp was conducted with an automated laboratory beater (PFI type, Labtech Instruments Inc.). The wet pressing was applied to handsheets of beaten fibers by an automatic sheet press (model 400-1, Labtech Instruments Inc.), whereas unbeaten handsheets were pressed with a hydraulic press (model 3891, Carver Inc., Wabash,

Indiana, U.S.). Fiber lengths were varied by cutting pulp sheets into small squares and the length-weighted fiber lengths were determined by a fiber quality analyzer at the University of British Columbia, Canada.

4.2.2 Physical properties test

All paper handsheets were conditioned for at least a week at 23°C and 50% relative humidity. Paper density was determined by measuring paper caliper (thickness) following Tappi method (T411) and grammage (mass per unit area). Average values were used by measuring the caliper (Precision Micrometer, Testing Machines Inc.) and mass (Mettler Toledo, Laboratory& Weighing Technologies) of a pile of 5 sheets. Mechanical properties of paper samples were measured using Tappi methods: Paper in-plane strength was measured by an Instron machine (model 4411, Instron Canada Inc., Burlington, Canada) following Tappi method (T494); paper z-strength was measured by internal (Scott) bond strength tester (HUYGEN Corporation, Mauconbo, Illinois, U.S.) following Tappi method (T833).

4.2.3 Peel test

The peel forces were measured with the Instron (model 4411) located in a Tappi standard temperature and humidity room. A 50N load cell was used in all the experiments. For most experiments, a peel rate of 300mm/min was used to delaminate paper samples.

The peel test samples were prepared following our previous work [10]. Figure 4.1 shows a schematic illustration of the peel sample construction. First the PSAs tape backings were replaced by strips of Canon copy paper. For this, tape strips 2.5cm x 4cm were placed across a sheet of Canon copy paper. The paper was trimmed to 2.5cm (i.e. to match the tape width) yielding a paper tail which extended about 10cm beyond the tape. This tail was used to attach the strip to the clamps of the Instron machine.

The original white backing was removed from the other surface of the test tape. Then a strip of commercial single-sided transparent tape (Grand &Toy Ruban Invisible) was put on the front edge of the PSAs surface to serve as a separation layer or release layer to help initiate the peel crack.

Most peel tests in this work were carried out with a peel angle of 180°, in which a paper sample was fixed to a 7.5cm x 10cm stainless steel panel by the double-sided tape 9974B. The Canon copy paper backed strip was placed onto the paper substrate and a 2.04kg rubber coated roller (ChemInstruments, Ohio, US) was hand rolled over the sample ten times. Note that tape was placed so that it was not near an edge of the paper substrate. In the final step, the top copy paper backing was gently folded back at the position of the "separation tape" and fixed to the top Instron clamp. Peel tests were performed within two minutes of lamination.

In order to observe and record the peeling process, we built an assembly as shown in Figure 4.2. The assembly consisted of a free-rotating wheel, an Instron machine, and a video camera equipped with a macroscopic lens. The wheel (25mm wide, 142 mm in diameter with a SKF 6, 8-2 RSI radial bearing) was based on a PAPRICAN design [10].

The video camera (Panasonic wv-CL320) fitted with a macroscopic lens (Markozoom, Wild Heerbrugg) was placed behind the peel-wheel and focused on the peeling region. The camera was connected through a digital converter to a computer, and video clips were collected and analyzed with Ulead VideoStudio 4.01 software. The construction of the peel-wheel test sample was similar to that of 180° peel test except that the metal plate in Figure 4.1 was replaced by the surface of the free-rotating wheel. As before, the dimensions of the paper substrate were greater than the tape strip (25mm wide) to avoid edge effects.

4.3 Results

PSA tape strips were peeled at constant velocity from the surface of handsheets made from bleached kraft softwood pulp. Typical peel curves measured at low (25mm/min) and high (300mm/min) rates are shown in Figure 4.3. The lower peel rate gave interfacial failure, whereas the higher peel rate caused paper failure. In the case of the interfacial failure, the peel curve is noisy but approximately constant, resembling the peeling of a PSA tape from stainless steel. The peel curve at the higher peel rate is more complicated. The peel force initially rises to a maximum point and then drops to a low steady-state value, corresponding to catastrophic failure (paper delamination). Herein, paper failure is defined as the presence of at least one fibers layer embedded in the tape surface after peeling.

Two parameters, the peak peel force, F_p, and the lower steady-state force, F_{ss}, were extracted from the peel curves to facilitate the comparison of the results of varying peeling conditions. These parameters are illustrated in Figure 4.3; the paper failure curve (i.e. at high peel rate) is characterized by a high peak force, F_p, and a lower steady-state delamination force, F_{ss}. Note, the low peel rate curve is not of interest in the present work because the peel forces were too low to induce delamination.

3M 9974B pressure sensitive adhesive was peeled from the surface of a handsheet (0.3MPa wet pressing, 1000 PFI revolutions) at a nominal peel angle of 90° and the peel front was photographed with a video camera (see Figure 4.2). Figure 4.4 shows three typical images of the peel front taken at a peel rate of 50mm/min. Figure 4.4A, which corresponds to the beginning of peeling, shows the adhesive layer stretching to form threads which the adhesion technologists call fibrils. Fibril formation is a documented behavior of PSA tape during peeling [11].

Figure 4.4B is the image just before the start of paper delamination. The adhesive fibrils are highly elongated and the top layer of paper fibers has separated from the bulk of the paper. Interestingly, all of the fibers appear to have lifted the same extent from the paper sheet suggesting that the top fiber layers initially lifts as a single unit.

Figure 4.4C corresponds to the steady-state paper delamination. At this point there was a complete layer of fibers embedded into the tape surface and no adhesive fibrils appear in the peel front. Furthermore, there was no evidence of broken fibers suggesting that the major event in the peel front was interfiber debonding of the top fiber layer.

At some point between Figure 4.4B and Figure 4.4C the top layer of fibers must rupture. Top fiber layer rupture can be seen in Figure 4.5 which shows a photograph of paper after the 9974B tape was peeled at 300mm/min from right to left hand along the surface of a handsheet (4.9MPa wet pressing, no PFI beating) at a peel angle of 180°. In the middle is the rupture line where the top layer of fibers was pulled into two parts. Under steady-state peeling, the left part was continually removed with the PSA tape leaving a rough surface whereas the right part of the fiber layer was still attached to the paper.

These observations suggest that there are three sub-processes in the peeling-induced paper delamination: 1) at the start of peeling, the top layer of fibers beneath the peel front is debonded and separated from the remainder of the paper sheet; 2) also at the initial stages, the top fiber layer must rupture so that, downstream from the rupture line, the top fiber layer could be peeled away with the tape whereas, upstream from the rupture line, the top fiber layer remains with the paper; and, 3) steady-state peeling where propagation of the peel front only involves the delamination of the top fiber layer with no evidence of fiber failure. These three processes are illustrated in Figure 4.6. When considering the initiation of paper delamination, the first two processes are critical.

We hypothesize that it is the cohesive strength of the top layer of surface fibers which must be overcome in process 2 that accounts for the difference in the peak force (F_p) in Figure 4.3 and the steady-state delamination force (F_{ss}). To test this hypothesis, a through-thickness cut was made on the paper surface across the peel path before the paper and tape were laminated. Figure 4.7 compares the 180° peel curves for cut and uncut samples measured at the relatively slow peel rate of 25mm/min. The uncut paper surface did not fail because of the low peel rate whereas the cut sample did fail after the cut. When peel front reached the cut, the peel force decreased to a lower level and the paper delaminated. By pre-cutting the top fiber layer we eliminated the peak force before the onset of paper delamination. These results provided strong evidence for the hypothesis that the difference between the peak and steady-state delamination forces is the force required to rupture the top fiber layer.

In Figure 4.7, the peel force did not immediately decrease to the delamination plateau when the peel front met the cut line. Instead, it took a distance of about 2mm for the force to decline to the lower steady-state value. It is proposed that this reflects the fact that the peel front is not a thin line but instead spans a couple of millimeters in the peeling direction. Thus, the leading edge of the peel front meets the cut 2mm before the trailing edge. The details of peel fronts have been discussed in the peel mechanics literature, and the peel force was found to be proportional to the sum of the tensile stresses within the peel front [12,13].

The peak peel force F_p and the steady delamination force F_{ss} were investigated further by conducting 180° peel tests for a series of paper handsheets at a peel rate of 300mm/min. The handsheets were made from the same pulp fibers, but under varying beating and wet pressing conditions yielding a range of paper properties summarized in Table 1. The fiber length for one series of sheets was varied by cutting dried pulp sheets. As expected, beating and wet pressing gave denser and stronger paper which required higher peel forces to initiate (F_p) and propagate (F_{ss}) delamination. Reducing fiber length

resulted in weaker paper giving lower peel forces, but did not display significant effects on paper density.

The results in Table 4.1 show that the F_p was always greater than F_{ss}. Figure 4.8 shows a plot of F_p against F_{ss}, revealing a roughly linear correlation between F_p and F_{ss} with a slope of about 2.6. This observation indicated that the two peel characteristics were controlled by same factors. Since no broken fibers were observed, we propose that both of F_p and F_{ss} are related to the strength of interfiber bonds. Evidence for this is given in Figure 4.9 which shows that the peak force F_p was linearly correlated with the internal (Scott) bond strength. In addition, Figure 4.9 shows the effects beating, fiber length and wet pressing. The data for handsheets of varied beating level and fiber length fell into the same trend line – roughly linear correlation between F_p and tensile and internal bond strengths, whereas the data for handsheets of varied wet-pressure showed a non linear relation.

4.4 Discussion

A paper surface can display a variety of responses to peeling-induced stresses. At sufficiently low peel rates, the adhesive tends to separate with little damage to the paper. Higher stresses resulting from higher peel rates induce failure in the paper surface. The sheets used in this work were based on long, strong chemical pulp fibers so the entire top layer of fibers tended to delaminate as a unit. In work presented in previous chapters (papers) it was shown that newsprint tends to release individual fibers before the entire top layer of fibers delaminates because of the presence of stiff, poorly bonded mechanical pulp fibers. At the other extreme, coated papers can blister which means the top layer delaminates but does not fracture [14]. Thus the top layer remains with the paper sheet after peeling.

While most peel studies in paper science focused on the steady delamination force [6,8,9,10,15,16,17], this work revealed that the force to initiate the delamination is much higher than the steady-state delamination force. Our microscopic observation of the delamination process indicated three processes: 1) the initial delamination of the surface fiber layer from the rest of the paper, a process which is sensitive to the interfiber bond strength (Figure 4.6A); 2) a cohesive failure leading to the rupture of that delaminated surface layer (Figure 4.6B) which is linked to the tensile strength of the top fiber layer; and, 3) the steady-state delamination which is also sensitive to interfiber bond strength (Figure 4.6C).

Most of the experiments were preformed with handsheets made with lightly beaten, strong, chemical pulp fibers. Thus, both the delamination and tensile properties should be dominated by the interfiber bond strength. This explains the strong linear correlation between the peak peel force and the internal bond strength (see Figure 4.9) when paper properties were varied by changing the extent of beating, wet pressing and by using shorter fibers. Of these, only wet pressing showed significant nonlinearity. Wet pressing had a greater positive effect on peak peel force than on internal bond strength. A possible explanation is that wet pressing induces more bonding in the top fiber layers than in the interior of the sheet.

We propose that the initiation of peel induced delamination follows the steps illustrated in Figure 4.6. This qualitative mechanism is now extended to predict the relationship between the F_p and F_{ss} and that between F_p and the tensile strength of the paper. Figure 4.8 shows that the peak peel force, F_p, was about 2.6 times greater than the corresponding steady-state peel force, F_{ss}, for a wide range of handsheets. This observation can be rationalized in the following way. Initially, the top fiber layer must be debonded on both sides of the peel front (Figure 4.6A) and the top layer must be fractured (Figure 4.6B) whereas in steady-state peeling (Figure 4.6C) only the interlayer fiber-fiber bonding in one direction must be overcome. Therefore delamination in both directions (Figure 4.6A) should require twice the force as peeling in one direction (i.e. $F_p = 2F_{ss}$). However, we observed (in Figure 4.8) that $F_p \approx 2.6F_{ss}$ which suggests that both delamination (Figure 4.6A) and surface layer fracture (Figure 4.6B) contribute to the peak peel force.

We estimated the tensile strength of the top layer as calculated from the overall tensile strength and the paper thickness using the following equation where: TS1 is the tensile strength of one fiber layer (N/m); T is the standard paper tensile strength (N/m^2); h is paper thickness (m); and, c is the number of fiber layers forming the sheet of paper and we assumed that c =10. TS1 values are also shown in Table 4.1.

$$TS1 = \frac{T * h}{c} \qquad \text{Equation 4.1}$$

We propose that one of the reasons that the peak peel force is greater than the steady-state peel force is the need to rupture the top layer of fibers. This relationship was tested by plotting F_p-F_{ss} as a function of TS1 in
Figure **4.10**. The difference in the peel forces was linearly related to the estimated tensile strength of the top fiber layer. Furthermore, the two quantities were of the same order of magnitude although the TS1 values were somewhat greater than F_p-F_{ss}.

The practical implication of this work is that the peak peel force, F_p, is a measure of the propensity of paper to delaminate. Indeed, in future work we compare peeling to more traditional surface strength measurement techniques. Furthermore, this work suggests that delamination resistance can be improved by increasing the internal bond and the tensile strength of the paper.

4.5 Conclusions

The main conclusions from this work are

1. The peeling-induced paper delamination involves processes: 1) the initial delamination of the top fiber layer from the paper sheet starting at the peel front and propagating in all directions; 2) the rupture of that delaminated top layer permitting a layer of fibers to remain embedded in the tape; and 3) the steady-state delamination of the paper. Process 1 and 2 only occur in the initiation, whereas delamination (process 3) occurs continuously during peeling. The need to rupture the top layer (process 2) accounts for the observation that the initiation force is more than twice the steady-state delamination force.

2. The peak peel force is a measure of the propensity of a paper to delaminate in peeling.
3. Increasing the beating level, wet pressing pressure and fiber length resulted in higher peeling resistance reflecting the increase in interfiber bond strength and the tensile strength of the top fiber layer.
4. The peak peel force, F_p, the steady-state peel force, F_{ss}, and the paper tensile strength were related by the following approximate expressions where TS1 is the tensile strength of a single fiber layer which was calculated from the overall tensile strength. $F_p \approx 2.6F_{ss}$ and $F_p - F_{ss} \approx TS1$.

4.6 Acknowledgements

This work was supported by 3M Canada and the Natural Science and Engineering Research Council of Canada. Thanks are given to Anna-Karin Ahlman at the University of British Columbia for helping on fiber length measurement, and Kaarlo Niskanen, Atsushi Tanaka at KCL, Finland for useful discussions.

4.7 References

1 I. Kajanto, "Structural mechanics of paper and board", In: *Paper Physics*, K. Niskanen, ed., Fapet Oy, Finland, pp. 192-221(1998).

2 G.N. Ionides, *Paperi ja Puu*, 4 :298- 306 (1984).

3 P.J. Mangin, *Proceedings of technical association of the graphic arts*, p397 (1987).

4 Tappi test method T833, Tappi press (1999).

5 A. Lundh and C. Fellers, *Nordic Pulp Paper Res. J.,* 16(4):298-305 (2001).

6 J. Skowronski and W. Bichard, *J. Pulp Paper Sci.* 13(5):165-169 (1987).

7 J.J. Bikerman, *Tappi* 44(8):568-571 (1961).

8 T. Yamauchi, T. Cho, R. Imarnura, and K. Murakarn, *Nordic Pulp Paper Res. J.,* 3: 128-131 (1988).

9 T. Yamauchi, T. Cho, R. Imarnura, and K. Murakarn, *Nordic Pulp Paper Res. J.,* 1: 43-47 (1989).

10 R. Pelton, W. Chen, H. Li, and M.R. Engel, *J. Adhesion*, 77:285 (2001).

11 A. Zosel, *Inter. J. Adhes. Adhes.,*18: 265 (1998).

12 A.N. Gent and R.P. Petrich, *Proc. Roy. Soc.* A310:433-448 (1969).

13 S.F. Christensen, H. Everlan, O. Hassager, and K. Almadal, *Inter. J. Adhes. Adhes.*,18:131-137 (1998).

14 J. A. Perry, *Tappi,* 55(5):722-728 (1972).

15 A. El Maachi, S. Sapieha, and A.Yelon, *J. Pulp Paper Sci.* 21(10): 362-366 (1995).

16 A. El Maachi, S. Sapieha, and A.Yelon, *J. Pulp Paper Sci.* 21 (12): 401-407 (1995).

17 A. El Maachi, S. Sapieha, and A.Yelon, *Nordic Pulp Paper Res. J.* 14 (1): 17-22, 29 (1999).

4.8 Tables and figures

Table 4.1 **Handsheets properties and peel data. Here, h denotes thickness, *p* denotes density, T denotes overall tensile strength, TS1 denotes the tensile strength of one single fiber layer, E_{in} denotes paper internal (Scott) bond strength, F_p denotes peak peel force, and F_{ss} denotes steady-state peel force.**

Varied papermaking conditions		h (μm)	*p* (kg/m^3)	T (MPa)		TS1 (N/m)	E_{in} (N/m)		F_p(N/m)		F_{ss}(N/m)		F_p-F_{ss} (N/m)
				Mean	SD		Mean	SD	Mean	SD	Mean	SD	
Beating revolution (x1000)	0	120	548				80	7	141	10	50	7	91
	1	103	600	16.9	0.9	173.7	115	9	207	12	80	9	127
	5	99	643	25.9	1.5	257.0	188	7	277	29	108	11	169
	15	89	689	41.9	2.0	374.9	286	15	405	17	140	13	265
	30	83	719	52.9	2.1	437.6	370	21	448	46	186	21	262
Wet pressing (Mpa)	0.0	183	314	4.3	1.7	78.0	48	8	135	18	37	5	97
	0.5	125	474	9.6	0.5	120.1	66	8	136	17	58	7	79
	2.5	103	594	14.7	1.0	152.0	94	7	168	17	77	8	90
	4.9	96	647	17.6	0.6	168.0	130	18	238	20	92	11	146
	8.8	90	678	17.6	1.6	158.2	153	12	264	17	99	10	165
	11.1	90	696	21.4	1.6	191.7	174	27	336	42	107	12	229
Fiber length (mm)	2.14	96	647	17.6	0.6	168.0	130	18	238	20	92	11	146
	2.05	95	637	16.7	1.0	157.9	135	20	223	18	97	6	126
	1.92	93	652	17.9	1.2	165.6	143	20	211	13	90	9	120
	1.47	96	625	12.6	0.5	121.3	113	15	171	18	69	8	102
	1.44	97	622	11.1	0.6	106.9	106	13	170	25	77	11	93

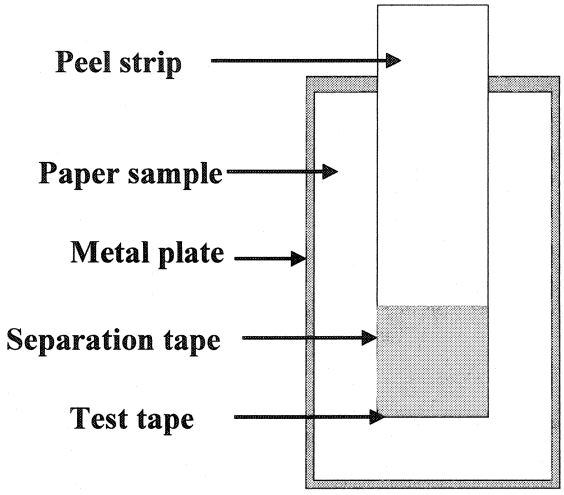

Plain View

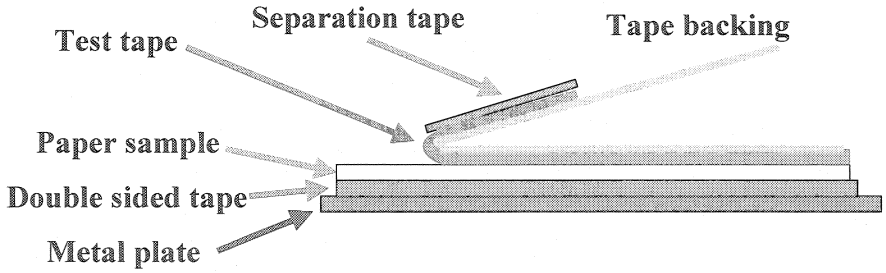

Side view

Figure 4.1 Construction of 180° peel samples

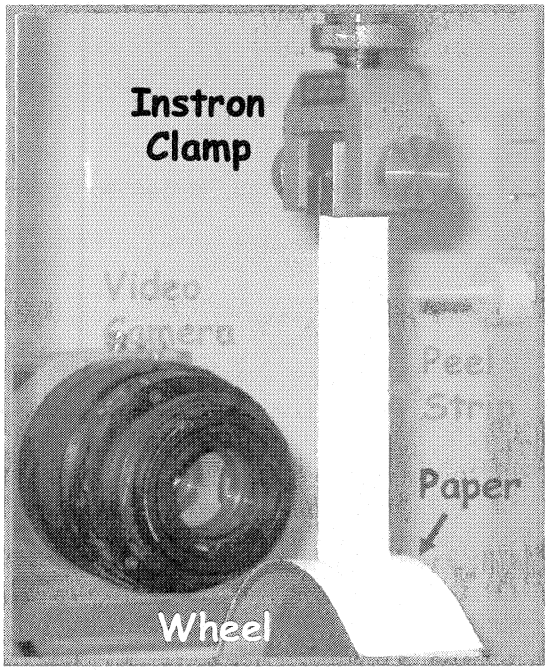

Figure 4.2 **Peel wheel setup consisting of a freely rotating wheel, a microscopic camera and an Instron machine. The camera focuses on the peeling front.**

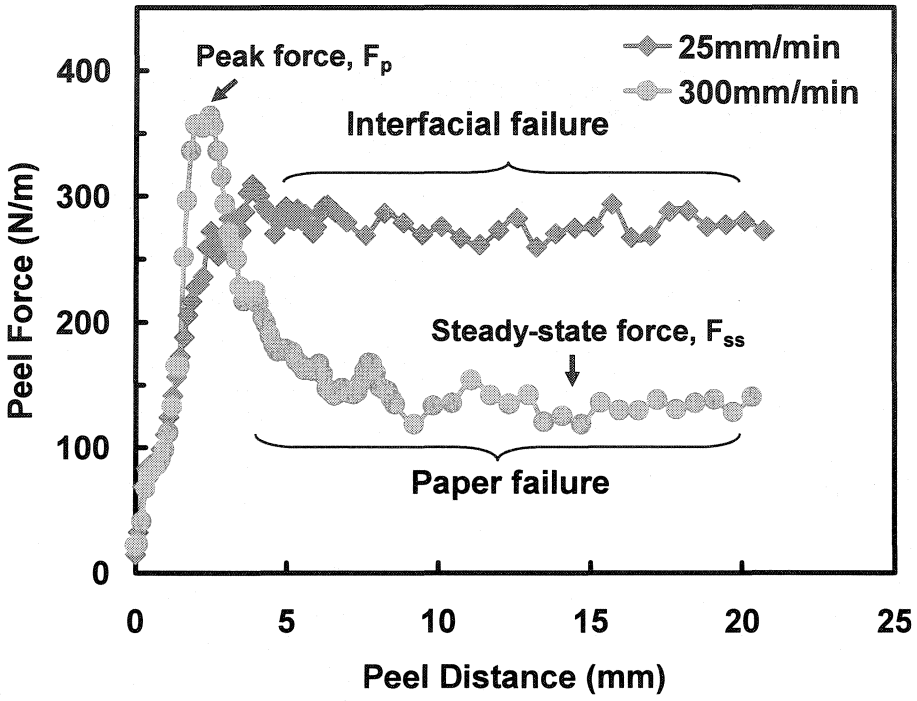

Figure 4.3 Typical curves of peeling tape from paper handsheets

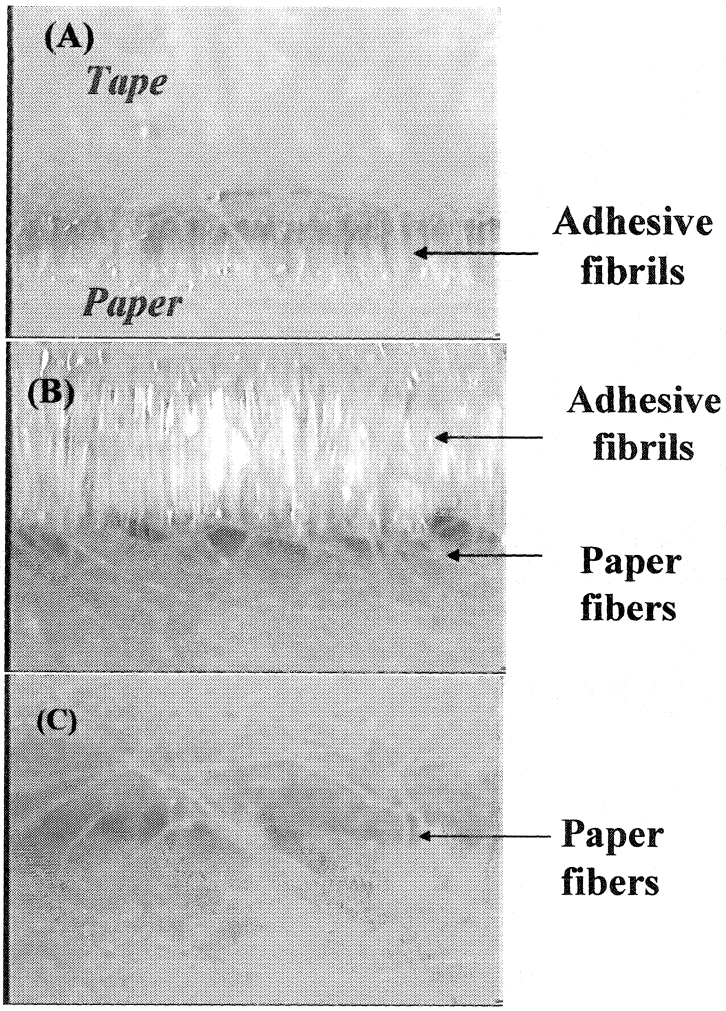

Figure 4.4 **Three stages of peeling tape from paper handsheet (0.3MPa wet pressing and 1000 PFI revolutions): (A) The start of peeling; (B) the start of paper delamination; (C) the progress of paper delamination**

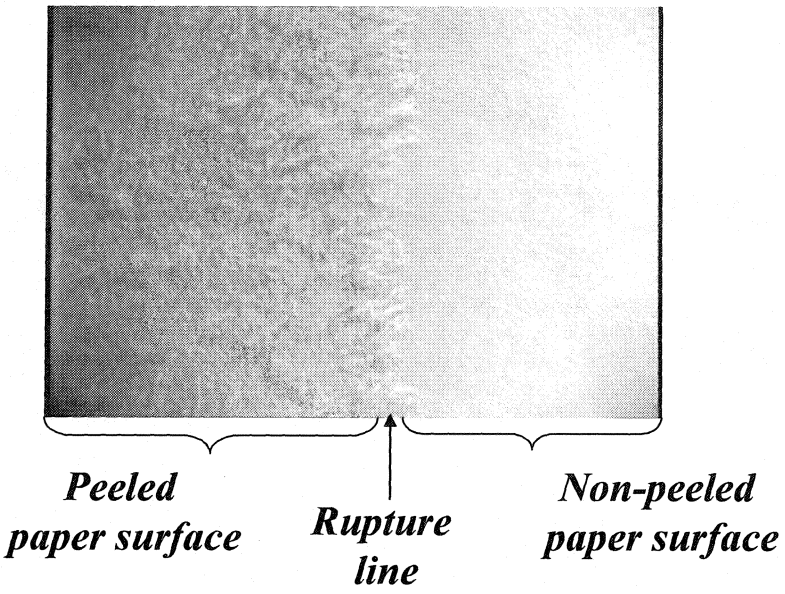

Figure 4.5 **Peeled paper surface of a handsheet (4.9MPa wet pressing, no beating) at 300mm/min and 180° peeling.**

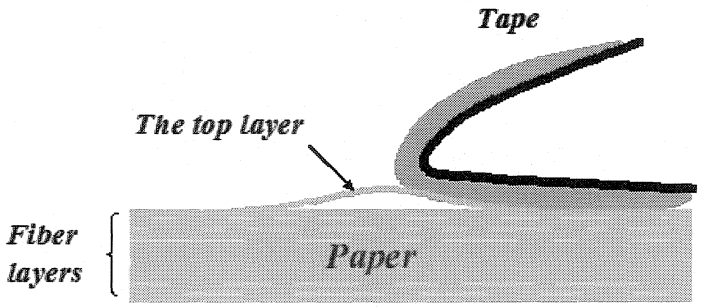

A) the initial delamination of the top fiber layer

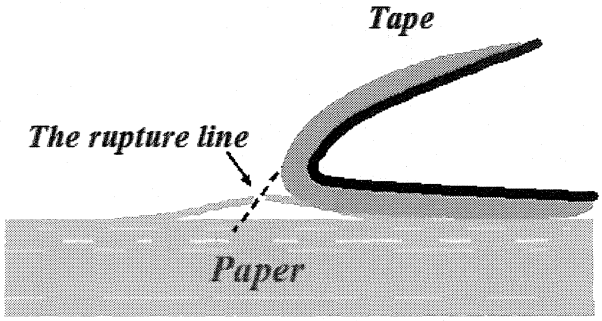

B) the rupture of the top fiber layer

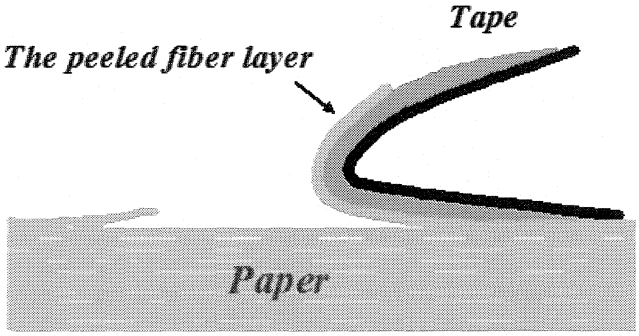

C) the steady-state delamination

Figure 4.6 Illustration of the sub-processes of the peeling-induced paper delamination

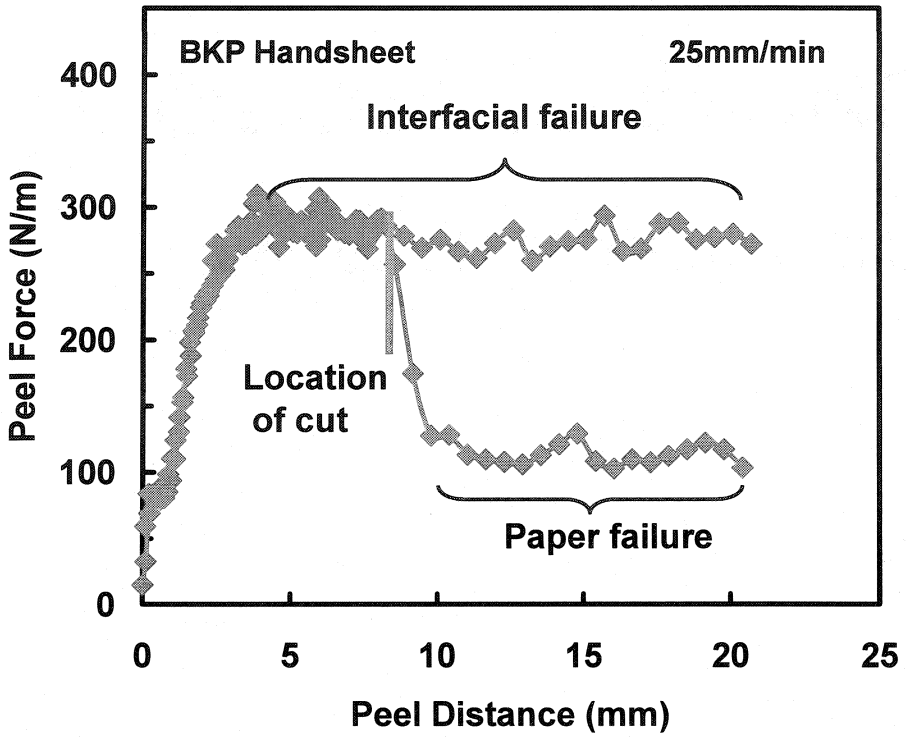

Figure 4.7 **A cut leads to paper failure from interfacial failure.**

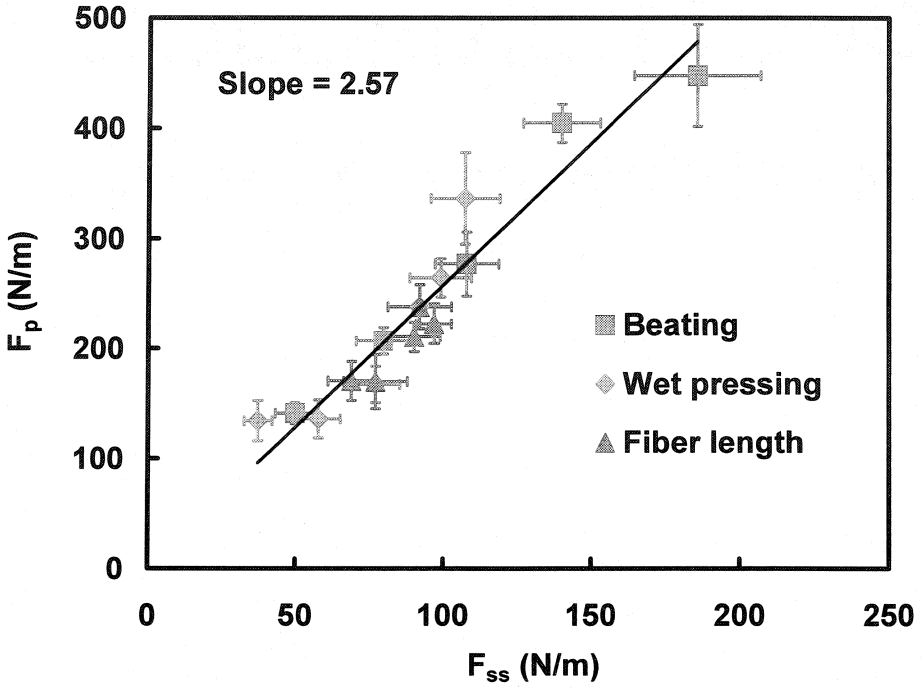

Figure 4.8 **Peak peel force F_p versus steady-state peel force F_{ss} for three sets of handsheets of varied beating level, wet pressing or fiber length.**

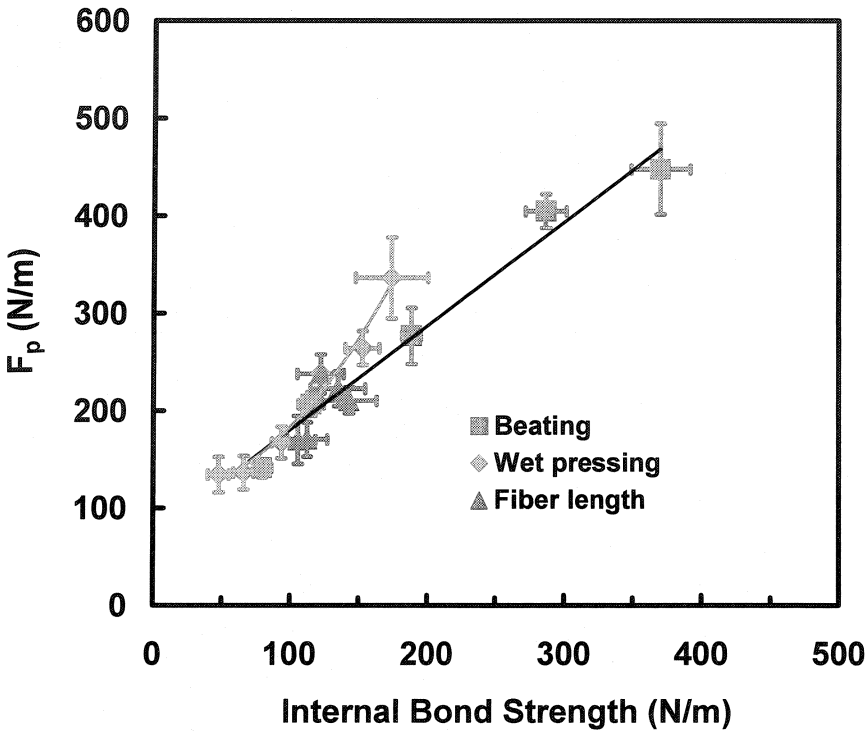

Figure 4.9 **Comparison of F_p with paper internal bond strength for three sets of handsheets of varied beating level, wet pressing or fiber length.**

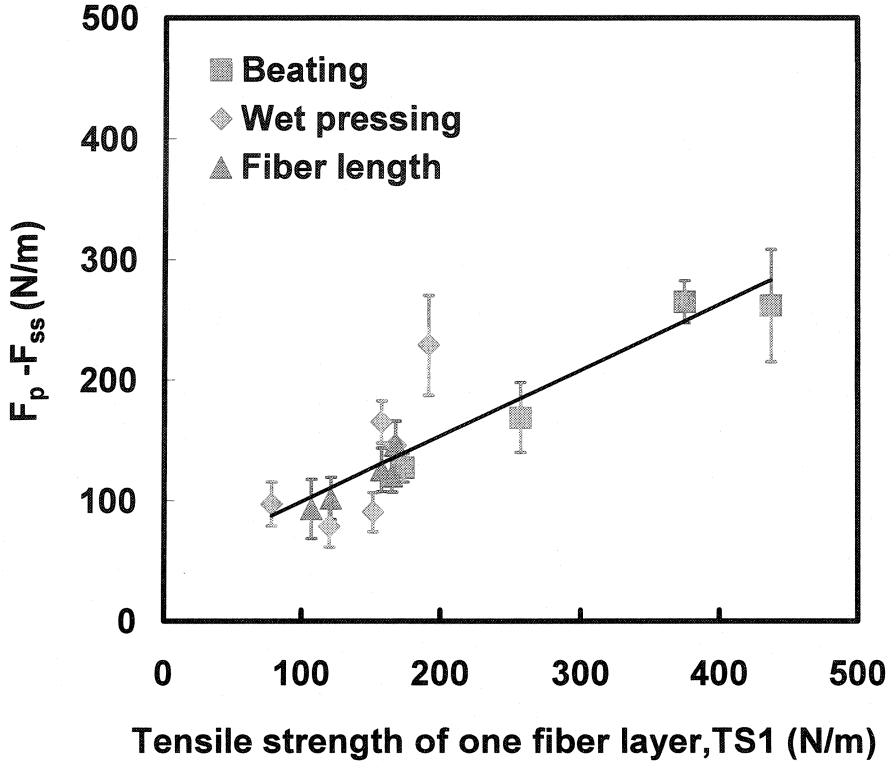

Figure 4.10 **Comparison of F_p-F_{ss} with the tensile strength of one single fiber layer for three sets of handsheets of varied beating level, wet pressing or fiber length**

Chapter 5

Paper Properties Affecting Tape Adhesion

Abstract

The interplay between paper and pressure sensitive adhesive was investigated by using peel adhesion testing as a probe. The paper/adhesive peel curves were analyzed by plotting the logarithm of the peak peel force (i.e. the maximum value) against the logarithm of the peel rate yielding two linear segments - a peel rate-dependent interfacial failure domain and rate-independent paper failure domain. Three independent parameters were extracted from these plots - the interfacial peel force (F_{in}) at a low peel rate of 1mm/min, the maximum peel force (F_c) and the slope (Sp) of the interfacial peel force in the plot of log (interfacial peel force) versus log (peel rate).

The paper properties influencing peel force in interfacial failure domain were found to be, primarily, the paper surface chemistry characterized by oxygen/carbon ratio (determined by XPS) and, secondarily, paper surface roughness. The peel force increased with oxygen/carbon ratio and with the surface roughness. The log-log slope in the interfacial failure domain was found to be independent of paper properties; it is determined by the adhesive rheology. The governing paper property in the paper failure domain was found to be the paper internal bond strength as measured by a paper internal (Scott) bond test.

5.1 Introduction

Paper/adhesive interactions are important in many applications such as packaging and lamination, where a proper control of adhesion at the paper base/adhesive and adhesive/tape backing or paper base is required. For example, splicing tapes used to join paper rolls require rapid adhesion, giving a strong splice at papermachine speeds which are usually more than 1000m/min [1].

Although it has been long realized that paper properties affect tape adhesion, the detailed links between properties of paper and those of paper/adhesives laminate are unknown. This is partly because of the complicated nature of paper and adhesives, and because of the lack of an appropriate method to quantify the interaction between adhesives and paper. Presented in this work are the results of an experimental study which identify the key paper properties which influence paper adhesion to pressure sensitive adhesives. The critical features of our work are the use of multivariate data analysis methods and a newly developed approach for analyzing paper/adhesive peel curves.

Multivariate data analysis is a widely used, powerful statistical technique. In paper science, it had been used to predict paper properties from fiber properties [2]. In the present work, we apply the multivariate analysis methods of principal component analysis (PCA) and partial least squares analysis (PLS) to explore relationships between the peel data and the paper properties. The power of these analyses lies in that they can show the relationships between the paper properties and peel data simultaneously. Our purpose was not to build a statistical model to predict tape adhesion responses from paper properties, which certainly needs much more data, but to get some insight into the relationships among paper properties and tape peel adhesion responses.

Peel adhesion testing is often employed to assess the bonding strength of laminated materials when at least one of the layers is flexible [3]. Indeed, "peel" is one of the design criteria for pressure sensitive adhesive development. Typically, the adhesive industry employs 90 or 180 degrees peel tests from well defined stainless steel surfaces, and the results of peel tests are characterized by a single number, i.e., the steady-state peel force. However, this practice is not suited to peeling from paper because, unlike stainless steel, the paper often fails, and the resulting peel force versus peel distance curve is complex [4,5,6].

In a recent note, we proposed paper-tape interactions in peeling are best accessed by conducting a set of peeling experiments at varying peel rates, and the log peak (i.e. the maximum) peel forces are plotted as a function of the log peel rate [7]. This analysis resulted in a generalized peel curve which consisted of two linear segments (on the log/log plots) intersecting when the failure mode changed from interfacial to paper failure. The influence of PSA type and peel angle on the generalized peel curve was further determined in our previous publication [8]. It was found that the peel angle shifted the generalized peel curves vertically, whereas the adhesive properties influenced the slope of the interfacial failure segment, but had no significant effect on the paper failure segment.

The objectives of this work were to identify the most important paper properties influencing the log peak force versus log peel rate plots. Peel adhesion tests were conducted for a series of 21 well-defined, machine-made paper samples. Multivariate statistical analyses were applied to explore the relationships between paper properties and peel adhesion responses.

5.2 Experimental

5.2.1 Materials

The pressure sensitive adhesive (PSA) tape, Scotch brand 9974B, was provided by 3M (London, Canada). The tape consisted of a blue adhesive layer (77μm) coated on both sides of a bleached tissue carrier and with a white backing (90μm).

The paper samples included 12 pilot-papermachines-made fine papers and 9 commercial papers. The pilot-papermachines-made samples were originally prepared for the ASTM committee conducting the Paper Aging Program, so we named these samples as ASTM paper. The commercial samples included 3 newsprint, 3 filter papers, 1 glassine (wrapping) paper and 2 copy papers. These paper samples are listed in Table 5.1 with their pulp types and papermaking conditions.

5.2.2 Paper characterization

The paper samples were conditioned for at least one week in a room of constant temperature (23°C) and relative humidity (50%) and tested in the same conditions. Many paper properties were measured referring to TAPPI standard methods: thickness (h) – TAPPI 411, basis weight (BW, i.e., mass per unit area) – TAPPI 410, density (p) calculated as the ratio of basis weight to thickness, tensile strength (T) – TAPPI 494, elastic modulus (E) – TAPPI 494, tensile energy absorption (TEA) – TAPPI 494, internal bond strength (E_{in}) –TAPPI 833 and surface pH – TAPPI 529. Paper thickness was measured by a micrometer (Testing Machines Inc.), and mass was measured by a microbalance (Mettler Toledo Inc.). Paper tensile properties were measured by an Instron machine (Model 411, Instron Corporation); paper internal bond strength was measured by a Scott bond tester (HUYGEN Corporation); and paper surface pH was measured by a surface pH meter (Extech Instruments).

Paper surface roughness was characterized by a surface profilometer (Surftest 211, Series 178) at three cut-off (sampling) lengths: 0.25mm, 0.8mm and 2.5mm. The samples were measured on the smooth side along the paper machine direction. For each sample, 5 sheets with 4 points each were measured; the average values were reported.

Paper surface chemistry was characterized by X-ray photoelectron spectroscopy (XPS). Three sheets of each sample were randomly picked from a stack of 500 sheets; a square (about 10 x 10mm) was cut from the paper sheet, and mounted on the XPS sample stand with its smooth side facing up using double-sided adhesives. XPS was carried out at both low and high resolution. The resulting spectra were recorded with a photoelectron takeoff angle of 90° relative to the paper surface. The low resolution spectra revealed the

atomic composition of the paper surface region down to 10Å, while the high resolution spectra focused on the carbon signal to investigate its oxidation states.

5.2.3 Peel adhesion test

The 180° peel tests were performed along the paper machine direction using the Instron machine located in a room of constant temperature (23°C) and humidity (50%). A 50N load cell was used in all the experiments. A computer interface was used to control peel conditions and restore the peel data in the form of force versus displacement curve. Peel rates ranged from 5mm/min to 500mm/min.

The peel test samples were prepared following our previous work [6]. The paper substrate was fixed to a 7.5 cm x 10cm stainless steel panel with the double-sided tape (Scotch brand 3M 9974B). The PSA tape strip was placed onto the paper substrate and a 2.04kg rubber coated roller (ChemInstruments, Ohio) was hand-rolled over the sample ten times. A schematic illustration of the 180° peel samples is shown in Figure 5.1. Note that the tape was placed so that it was not near an edge of the paper substrate. In the final step, the tape backing was gently folded back at the position of the "separation tape" (see Figure 5.1). Peel tests were performed within two minutes of lamination.

5.2.4 Multivariate statistical analysis

The multivariate data analysis methods of principal component analysis (PCA) and partial least squares (PLS) analysis were applied to explore the relationships among paper properties and peel responses [9]. In these approaches, all the data in Tables 5.2, 5.3 and 5.4 were converted to dimensionless relative values by subtracting each variable value with its average, and scaled to unit variance. Thus, it was assumed that all of the variables were equally important before the analysis.

In the PCA analysis, the data in Tables 5.2, 5.3 and 5.4 were combined into a single matrix. Two new, orthogonal variables, *t1* and *t2*, which are called *PCA components,* were calculated from the following equation where: subscript *i* refers to the paper sample (*i* ranges from 1 to 21); subscript *j* refers to the property (*j* ranges from 1 to 25). Thus, v_{ij} is the *jth* property for *ith* paper sample; w_j1 is the *weight* which determines how much property *j* contributes to the *t1*; and, w_j2 is the weight which determines how much property *j* contributes to *t2*.

$$t_i1 = \sum_j (w_j1 \cdot v_{ij}) \qquad t_i2 = \sum_j (w_j2 \cdot v_{ij}) \qquad \text{Equations 1 and 2}$$

Thus, all the data for each paper sample is reduced to *t1* and *t2* value which are called *score values*. Every paper sample has a different pair of score values.

The Partial Least Squares (PLS) analysis was used to reveal the relationships between paper and peel properties. In this analysis, the paper properties data in Tables 5.2 and 5.3 were combined to form a single paper data matrix. Unlike PCA analysis described above, this data matrix does not contain the peel data. The nitrogen and inorganic elemental data, from XPS, were also removed from the data matrix because they had no impact on peel. Two PLS score values (*t1* and *t2*) as well as the corresponding variable weightings (*w1* and *w2*) were then calculated from the paper score

matrix using equations 1 and 2 with the maximum value of *j* equaling 17 reflecting the absence of peel and the inorganic composition data. Note, that these score values and the corresponding PLS weighting values are different from the PCA counterparts because the PLS parameters do not contain the peel results.

Each peel parameter was than separately regressed against the two PLS score values for all the paper samples to yield the PLS weights, *c1* and *c2*. For example, the vector of parameterized F_c values is related to the PLS score values by the following equation.

$$F_{ci} = c1 \cdot t_i 1 + c2 \cdot t_i 2 \qquad \text{Equation 3}$$

The final step can be understood by referring to Figure 5.5 in which each triangle represents a paper property plotted on the w1 versus w2 surface. Also plotted in Figure 5.5 is the c1 and c2 weights (from equation 3) for the peel strength, F_c. The contribution of each paper property is obtained by projecting the variables position onto the line drawn from the origin through the F_c point. This procedure is illustrated in Figure 5.5 for the internal bond strength, E_{in}. The distance from the origin along the line to the projected point is called the PLS coefficient, X_j in Figure 5.5, which, in this example, is a relative measure of the contribution of the internal bond strength to the paper peel strength.

The statistical calculations were carried with SIMCA-P+ 10.0 (UMETRICS) statistical software. A cross-validation technique [10] was used to show that two principal components were sufficient to explain the variation in our data set. More details are given in the appendix.

5.3 Results and Discussion

5.3.1 Paper properties

The physical properties of the paper samples were measured according to TAPPI standard methods. These properties are tabulated in Table 5.2. Of the 21 paper samples, the glassine paper is the smoothest and strongest paper with the highest density. The internal bond strength of the glassine could not be determined. The filter papers are the roughest papers with the lowest densities. Surface pH measurements could not be made with filter paper because the water drops were quickly absorbed. It was also noted that the three roughness parameters seem to be positively correlated with the roughness measured at higher cut-off length having the higher values.

The chemical composition of the paper surfaces were analyzed by low and high resolution XPS and the results are summarized in Table 5.3.. Low resolution analyses revealed that carbon and oxygen were abundant, accounting for more than 98% of paper surface elemental composition. This reflects the chemical nature of paper whose major components are cellulose and lignin. In addition, there were small amounts of nitrogen and the inorganic elements: sodium, aluminum, silicon and calcium. High resolution analyses examined the fine structure of the carbon, which was divided into four categories (C1– C4) according to their oxidation level. C1 refers to un-oxidized carbon (C-C or C-H); C2 refers to carbon with one bond to oxygen (C-O); C3 refers to carbon with two bonds to oxygen (O-C-C or C=O); and C4 refers to carbon with three bonds to

oxygen (O-C=O). Of the four components, C4 accounted only for a small fraction of the total carbon. It had been found in paper chemistry literature that C2 and C3 are mainly from cellulose, while C1 and C4 are mainly from lignin and other extractives [11,12,13,14].

5.3.2 Peel data analysis

The 180° peel tests were performed on these paper samples for a series of increasing peel rates. The peeling behaviour was summarized by plotting the peak peel force F_p (i.e. the maximum force in each peel curve) versus the peel rate, V, on logarithmic scales. Figure 5.2 shows three example plots. The error bars were calculated as $\log((F_p \pm SD)/F_p)$ where F_p is the mean force of at least 6 measurements and SD is its standard deviation. It can be seen that the log (F_p) increases linearly with log (V) in the interfacial failure domain and levels off when paper failure starts.

Most uncoated papers display the peeling behavior summarized in Figure 5.2. Therefore, a specific tape/paper interaction can be summarized by three parameters, which is the minimum number required to describe two line segments with one having zero slope. The three adhesion parameters we chose are the maximum peel force (F_c) in the paper failure domain, the interfacial peel force (F_{in}) at a peel rate of 1mm/min, and the log-log slope (Sp) in the interfacial failure domain. These three peel parameters are tabulated in Table 5.4 with their percentage standard errors. Here F_{in} and Sp and their standard errors SE were obtained by linear regression analysis in the interfacial failure domain. The maximum peel force F_c was calculated as the mean of the peak peel force values (F_p) at peel rates which induced paper failure. The corresponding standard errors (SE) were calculated as $\sqrt{\left(\sum_1^m (SD^2/n)\right)/m}$, where SD is the standard deviation of F_p of n (n = 6) replications at each peel rate which induced paper failure; m is the number of paper failure points. For example, consider the ASTM 11 peel results in Figure 5.2. Only the results from the highest three peel rates (i.e. m =3) induced paper failure, so these were used to calculate F_c and the corresponding SE. There were 6 paper types without F_c values, because they displayed only the interfacial failure.

5.3.3 Principal component analysis (PCA) of relationships amongst all properties

The PCA analysis was performed on the database consisting of both paper properties and the three peeling parameters resulting in two unique scores (t1 and t2) for each sample. The relationships between the various paper samples are revealed in Figure 5.3 which plots the t2 values against the corresponding t1 values. Similar paper types appear as groups on the t2-t1 planes. As expected, the filter papers and the glassine paper are separated from the others. The remaining papers form three groups except ASTM 2 and 8 which were isolated.

The scores (t values) for each paper, shown in Figure 5.3, were calculated as a linear combination (equations 1 and 2) of the data in Tables 2, 3 and 4. However, each

type of data contributed a different weighting (*w* value) to scores. Figure 5.4 is the scatter plot of the variable *weights* on the PCA components t1 and t2. The most important information revealed in Figure 5.4 is the relationships among the 25 variables. The rules for interpreting this figure are: variables contributing similar information are grouped together; the impact of a particular variable increases with distance from the origin; and, negatively correlated variables are positioned on opposite sides of the plot origin in diagonally opposed quadrants.

The parameters approximately fall into four groups of paper properties as shown in Figure 5.4. The first group consists of tensile strength (T), modulus (E), internal bond strength (E_{in}) and density (p), clustered at the top center. The second group consists of elements O, C2, C3 and surface pH which are clustered at the top right of the plot. The third group consists of paper roughness (R1, R2 and R3), basis weight (BW) and thickness (h) clustered at the bottom right. The fourth group: C, C1 and C4, are clustered at the bottom left. Note that the fourth group of variables is inversely correlated to the second group of O, C2 and C3 which are in the opposing quadrant; and it seems that these two groups could be captured by considering the oxygen/carbon ratio. Finally, the inorganic elements and N and TEA are close to the origin indicating they are not important to the analysis.

The three peel responses, F_{in}, F_c and Sp, are not grouped together in Figure 5.4, indicating they are independent and linked to different paper properties. F_{in} (i.e. the low speed peel force in the interfacial failure domain) lies on the right side of the plot origin between the roughness and O, C2, C3 groups, opposite to the group of C, C1 and C4. This implies that F_{in} is sensitive to paper surface chemistry and roughness. By contrast, the maximum peel force, F_c, lies at the top centre of the plot and is grouped with the paper mechanical properties implying that mechanical properties have the major influence on F_c. The slope of the interfacial peel domain, Sp, is close to the origin of the plot indicating that Sp is independent of paper properties.

The variable weighting plots of PCA in Figure 5.4 help illustrate the physical significance of the two new variables (t1 and t2) in Figure 5.3. The t1 is located near two groups of paper surface properties – the paper surface chemistry variables(C, O, C1, C2, C3, C4 and surface pH) and the paper surface roughness parameters (R1,R2 and R3); while the t2 is grouped with the mechanical properties (E_{in}, T, E and p).

5.3.4 Partial least Squares (PLS) linking peel to paper properties

The PLS analyses were performed for ranking paper properties with regards to their influence on the three peel responses F_{in}, F_c and Sp. The PLS analysis was conducted separately for each peel response because the results in Figure 5.4 show that the three peel parameters are independent. The inorganic elements and nitrogen were discarded from these analyses since they did not influence peel (Figure 5.4).

As explained in the experimental section and illustrated in Figure 5.5, the results of the PLS analysis are PLS coefficients which give an indication of relative contribution a paper property to a peel property. Figure 5.6 ranks the PLS coefficients relating paper properties to the maximum peel force, F_c. The paper internal bond strength (E_{in}) had the

highest positive coefficient indicating that E_{in} was the most important paper properties to F_c. Next to E_{in} is paper surface pH; apparently the alkaline papers in this data set had a higher surface strength. The tensile strength, elastic modulus and the total energy adsorption often scale with the internal bond strength and so these also contribute to peel strength. The remaining paper properties display small coefficients indicating their influences on F_c are negligible.

The PLS coefficients for the low speed interfacial peel force, F_{in}, are ranked in Figure 5.7. The paper surface oxygen content, O, had the highest positive coefficient whereas the surface carbon content, C, had a large negative coefficient indicating that the two parameters are inversely correlated. Of the subtypes of carbons, C1 and C4 had the largest negative effect. It seems reasonable that alkane species (C1) will lower surface energy and thus interfacial peel force. Similarly, the C4 groups are carboxyl groups associated with most conventional hydrophobic sizing chemicals. The surfaces roughness parameters were also important – the higher the roughness, the greater the interfacial peel force. Interestingly, the internal bond strength, E_{in}, was the least important parameter for interfacial peel whereas it was the most important paper property for the paper delamination strength, F_c.

5.3.5 Proposed predictors of paper properties for tape adhesion

It was anticipated that paper surface properties would influence peel force in the interfacial failure domain. The statistical analyses confirm that the interfacial peel force is related to both paper surface chemistry and surface roughness. This is illustrated in Figure 5.8 by plotting F_{in} against the O/C ratio. The O/C ratio, measured by X-ray photoelectron spectroscopy, is used as the indicator of paper surface chemistry, since the oxygen and carbon contents are inversely related. The general trend is that F_{in} increases with the O/C ratio, which explains the 50% of the variation of F_{in}.

The O/C ratio can be considered to reflect the relative content of cellulose in the paper surface region. Cellulose with the molecular formula of $(C_6O_5\ H_{12})_n$ has a high O/C ratio (~0.83), while lignin has a low O/C ratio due to the fact that it consists mainly of aliphatic and aromatic carbon with a few reactive groups such as hydroxyl, carbonyl and carboxyl groups [15]. In addition, paper sizing agents are often added in paper to reduce the ink penetration. Like lignin, such sizing agents are hydrophobic having a very high carbon and low oxygen content from a few functional groups such as carboxyls.

It is interesting to explore further the scattering of the data in Figure 5.8 by considering a line orthogonal to the correlation line of F_{in} and O/C. For the commercial papers whose roughness displayed significant differences, the smoothest glassine paper lies below that correlation line and the roughest filter papers lie above. It seems that the orthogonal line is related to paper surface roughness; the smoother paper displayed the lower interfacial peel force. For the ASTM samples which display similar roughness, most of them follow the trend line except for two sized samples ASTM 1 and ASTM 5; the origin of this scatter is not known.

The interfacial peel force was found to increase with peel rate until paper failure. This rate-dependent behavior mainly reflects the viscoelastic properties of adhesion tapes

[16,17]. In this work, we peeled one tape from different paper samples and the resulting slopes were independent of the paper properties. However, our previous work showed that peeling different tapes from one paper surface displayed different slopes [8]. Thus the slope in Figure 5.2 was mainly determined by the rheology of adhesive.

High peel rates gave paper failure/delamination, which was captured in the parameter F_c. Figure 5.4 shows that F_c was associated with a group of paper strength properties. This is because all paper strength properties are determined by fiber strength and fiber-to-fiber bonding strength. However, at a finer level, various tests measure different features. For example, paper scientists have long known that paper is very resistant to in-plane stresses (tensile strength), whereas paper is very sensitive of out-of-plane or Z-directional stresses [18]. Thus paper is very susceptible to delamination. Because paper failure in peeling is a delamination process, we propose that the internal (Scott) bond strength, which measures the energy to delaminate paper sample, is the most relevant standard paper property when considering the maximum peel force, F_c. Figure 5.9 shows the correlation between internal bond strength and F_c. Although the data points were scattered, F_c increased linearly with paper internal bond strength for all types of paper. This relationship had been demonstrated in other laboratories [19].

In early work from our laboratory, it was proposed that paper surface roughness may have some effect on F_c by affecting the contact area [6]. This work revealed that the effect of surface roughness on F_c was negligible (Figure 5.6). This is understandable, considering that F_c is governed by paper cohesive strength and the contact area is not very relevant.

5.4 Conclusions

This work used multivariate statistical analyses to probe the linkages between uncoated paper and peeling properties. The conclusions from this work are:

1. Tape adhesion on paper can be characterized by three independent parameters derived from a series of peel experiments at varying rates. The parameters are (1) the interfacial peel force F_{in} at the low peel rate of 1mm/min, (2) the maximum peel force F_c, and (3) the slope Sp of the interfacial peel force in the plot of log (interfacial peel force) versus log (peel rate).
2. The interfacial peel force, F_{in}, reflecting events in the interfacial failure domain, is dominated by the paper surface chemistry characterized by the oxygen/carbon ratio (determined by XPS); the higher this ratio, the greater the interfacial peel forces. Of secondary importance is surface roughness; F_{in} increases with roughness.
3. The governing paper property in the paper failure domain is the fiber-to-fiber bond strength as measured by the paper internal (Scott) bond test.
4. The log-log slope (Sp) in the interfacial failure domain was independent of paper properties. It is dominated by the adhesive rheology.

5.5 Acknowledgements

This work was supported by 3M Canada and NSERC. We thank Alison Banks and Luis Anderson for experimental assistance, Bruce Arnold for providing ASTM paper samples from ASTM Paper Aging Research program, and Dr. Yu and Dr. MacGregor for providing the statistical software and helping on the analysis.

5.6 References

1 Goetz, W.J., Alheld, R.J., Ehrnrooth, H.G. and Landskroener, P.A., *Tappi,* 68 (2):113-115 (1985).

2 A. Marklund, J. B. Hauksson, U. Edlund and M. Sjöström, *Nordic Pulp Paper Res. J.* 13(3), 211-219 (1998).

3 D. Satas, In: *Handbook of Pressure Sensitive Adhesive Technology*, D. Satas (Ed), pp. 61-96, Van Nostrand Reinhold (1989).

4 J.J. Bikerman, *Tappi,* 44 (8), 568 - 571 (1961).

5 T. Yamauchi, T. Cho, R. Imarnura, and K. Murakarmi, Nordic Pulp Paper Res. J. 3 (3), 128-131 (1988).

6 R. Pelton, W. Chen, H. Li, and M.R. Engel, *J. Adhesion* 77, 285-308 (2001).

7 B. Zhao and R. Pelton, *J. Mater. Sci.* 22, 265-266 (2003).

8 B. Zhao and R. Pelton, *J. Adhesion Sci. and Tech.* 17 (6), 815-830 (2003).

9 L. Eriksson, E. Johansson, N. Kettaneh-Wold, and S. Wold, *Introduction to Multi- and Megavariate Data Analysis Using Projection Methods (PCA &PLS)*, Umetics AB, Sweden (1999).

10 S. Wold, *Technometrics,* 20(4), 397-405 (1978).

11 G.M. Dorris and D.G. Gray, *Cell. Chem.Tech.* 12, 9-23 (1978).

12 G.M. Dorris and D.G. Gray, *Cell. Chem. Tech.*12,721-734 (1978).

13 A. Koubaa, B. Riedl and Z. Koran, *J. Appl. Polym. Sci.* 61: 545-552 (1996).

14 M. Kazayawoko, J.J. Balatinecz, R.T. Woodhams, and R.N.S. Sodhi, *J. Wood Chem. Technol.* 18(1):1-26 (1998).

15 E. Sjostrom, In: *Wood Chemistry, Fundamentals and Applications*, pp. 71-89, Academic Press (1993).

16 A.N. Gent and J. Schultz, *J. Adhesion* 3: 281-294 (1972).

17 K. R. Shull, *Mat. Sic. and Eng. R.,* 36(1): 1-45 (2002).

18 I. Kajanto, In: *Paper Physics,* K. Niskanen (Ed), pp. 192-221, Fapet Oy, Finland (1998).

19 A. Koubaa and Z. Koran, *Tappi*, 78(3), 103-111 (1995).

5.7 Tables and figures

Table 5.1 Paper samples and their composition. Here, BNSWK denotes bleached softwood kraft, BNHWK denotes bleached hardwood kraft, SW-BCTMP denotes bleached ChemiThermoMechnical softwood pulp, HW-BCTMP denotes bleached ChemiThermoMechnical hardwood pulp, SGW denotes stone ground wood, TMP denotes ThermoMechanical pulp, and PCC denotes precipitated calcium carbonate.

Paper sample	Pulp Type 1	Pulp Type 2	Fillers	Internal Size
ASTM paper 1	100% BNSWK	None	None	2#/T Rosin
ASTM paper 2	100% BNSWK	None	5%PCC	None
ASTM paper 4	100% SW-BCTMP	None	5%PCC	None
ASTM paper 5	100% Cotton fiber	None	None	2#/T Rosin
ASTM paper 8	20%BNSWK	80%SLUSH-SGW	5%PCC	None
ASTM paper 9	20%BNSWK	80% HW-BCTMP	None	None
ASTM paper10	20% BNSWK	80% HaW- BCTMP	5%PCC	None
ASTM paper 11	50% BNSWK	50% BNHWK	None	None
ASTM paper 12	50% BNSWK	50% BNHWK	5%PCC	None
ASTM paper13	50% BNSWK	50% HW- BCTMP	5%PCC	None
ASTM paper 14	50% BNSWK	50% HW-BCTMP	None	2#/T Rosin
ASTM paper 15	50% BNSWK	50% BNHWK	5%PCC	4#/T AKD
Copy paper 1	-	-	-	-
Copy paper 2	-	-	-	-
Glassine paper	Chemical pulp	None	-	-
Filter paper 1	100% Cotton fiber	None	-	-
Filter paper 4	100% Cotton fiber	None	-	-
Filter paper 5	100% Cotton fiber	None	-	-
Newsprint 1	100% TMP	None	-	-
Newsprint 2	100% TMP	None	-	-
Newsprint 3	100% TMP	None	-	-

Notes:
1 - Most ASTM paper samples were made by the Herty Foundation pilot paper machine except for ASTM paper 5 which was made by Crane & Co. Inc. All these samples were provided through the ASTM Paper-Aging Program.
2 - Copy paper 1 is a commercial copy paper sold by Canon (Ontario, Canada), and Copy paper 2 is Domtar copy paper sold by Domtar (Montreal, Canada). Glassine paper is the commercial MasterpakTM glassine paper #2-11. All newsprint were made and provided by Donohue Inc. in Montreal, Canada. The filter papers 1, 4 and 5 are the commercial Whatman Filters No.1, 4 and 5.

Table 5.2 **TAPPI standard paper properties and paper roughness. Here, BW denotes paper basis weight (i.e., mass per unit area), h denotes thickness, p denotes density. T denotes tensile strength, E_{in} denotes internal bond strength, R1 denotes roughness with cut-off length 0.25mm, R2 denotes roughness with cut-off length 0.8mm, R3 denotes roughness with cut-off length 2.5mm, pH denotes surface pH, E denotes tensile modulus, and TEA denotes tensile energy absorption.**

Paper sample	BW (g/m^2)	h (mm)	p (kg/m^3)	T (MPa)	E (GPa)	TEA (N/m)	E_{in} (J/m^2)	pH	R1 (μm)	R2 (μm)	R3 (μm)
ASTM paper 1	78	0.12	649	47.9	5.0	61.3	173	4.9	2.64	3.49	4.63
ASTM paper 2	72	0.11	658	60.9	5.5	83.7	203	8.0	2.49	3.21	3.88
ASTM paper 4	75	0.16	471	28.2	2.5	57.5	318	8.1	3.41	5.26	6.43
ASTM paper 5	77	0.12	642	32.3	4.0	37.0	383	6.8	3.28	4.56	5.87
ASTM paper 8	77	0.19	405	17.8	1.7	34.2	207	7.2	4.76	5.41	6.99
ASTM paper 9	76	0.12	635	39.2	3.5	63.9	351	7.1	2.97	3.75	4.56
ASTM paper10	79	0.13	609	33.1	3.6	36.9	295	8.2	3.00	3.83	5.01
ASTM paper 11	82	0.12	680	36.5	4.0	52.9	229	5.8	2.57	3.33	4.19
ASTM paper 12	77	0.13	593	28.9	3.9	26.4	164	7.9	2.66	3.25	4.04
ASTM paper13	74	0.12	614	37.6	3.8	51.9	258	8.2	2.98	3.76	4.64
ASTM paper 14	76	0.12	631	54.5	4.8	85.6	240	5.8	2.97	3.81	4.82
ASTM paper 15	77	0.14	550	30.6	2.7	62.0	252	8.6	3.20	4.17	5.21
Copy paper 1	77	0.10	796	21.5	1.8	99.2	581	8.5	1.68	2.34	3.03
Copy paper 2	76	0.10	772	58.5	4.9	92.9	457	9.0	1.96	2.60	3.32
Glassine paper	40	0.04	1106	108.7	9.5	53.3	-	7.4	1.01	1.53	2.56
Filter paper 1	87	0.17	505	8.7	0.9	39.8	191	-	4.81	5.91	7.01
Filter paper 4	91	0.20	459	5.9	0.7	22.2	144	-	5.71	7.15	8.44
Filter paper 5	98	0.18	534	17.5	2.2	45.9	320	-	4.69	6.61	8.02
Newsprint 1	45	0.07	662	35.6	4.1	19.2	223	5.3	1.97	2.89	3.71
Newsprint 2	49	0.07	683	31.3	3.6	14.9	154	4.5	2.07	2.76	3.51
Newsprint 3	49	0.08	624	30.4	3.4	16.1	144	4.6	2.07	2.76	3.51

Table 5.3 Paper surface chemistry analysis

Paper sample	C%	O%	N%	Na%	AL%	Si%	Ca%	C1%	C2%	C3%	C4%
ASTM paper 1	68.4	29.9	0.1	0.1	1.2	0.3	0.0	35.0	21.0	9.5	3.0
ASTM paper 2	56.7	42.8	0.0	0.0	0.0	0.0	0.4	9.0	32.6	13.3	1.7
ASTM paper 4	62.6	36.3	0.3	0.3	0.0	0.1	0.4	19.1	29.1	12.3	2.2
ASTM paper 5	61.7	37.0	0.2	0.1	0.7	0.2	0.1	20.6	28.3	11.4	1.6
ASTM paper 8	66.3	32.5	0.2	0.1	0.4	0.1	0.3	27.2	25.1	10.5	3.6
ASTM paper 9	62.1	37.3	0.2	0.3	0.0	0.0	0.1	17.1	30.4	12.4	2.2
ASTM paper10	60.8	38.4	0.2	0.1	0.1	0.1	0.3	16.3	30.5	11.8	2.2
ASTM paper 11	57.9	42.1	0.0	0.0	0.0	0.0	0.0	10.8	32.3	12.9	1.8
ASTM paper 12	58.1	41.5	0.1	0.0	0.0	0.1	0.2	10.5	33.7	12.0	2.0
ASTM paper13	60.9	38.7	0.0	0.0	0.0	0.0	0.4	14.5	32.9	11.2	2.4
ASTM paper 14	63.8	34.6	0.2	0.1	0.7	0.5	0.0	24.8	26.6	8.7	3.7
ASTM paper 15	60.4	39.1	0.3	0.0	0.0	0.0	0.3	15.3	32.1	10.9	2.2
Copy paper 1	61.4	37.3	0.3	0.1	0.0	0.3	0.6	19.4	28.7	11.4	1.9
Copy paper 2	61.2	37.5	0.4	0.3	0.0	0.2	0.6	19.1	28.7	11.6	1.8
Glassine paper	57.8	41.5	0.1	0.2	0.0	0.3	0.2	11.0	33.0	12.5	1.3
Filter paper 1	56.4	43.1	0.3	0.1	0.0	0.2	0.0	9.8	32.5	12.7	1.4
Filter paper 4	55.7	43.5	0.3	0.3	0.0	0.3	0.1	9.3	32.5	12.6	1.2
Filter paper 5	55.3	43.5	0.1	0.2	0.0	0.1	0.9	8.1	34.0	11.7	1.5
Newsprint 1	62.7	33.9	0.5	0.1	1.0	1.4	0.4	27.2	23.1	10.1	2.3
Newsprint 2	69.3	30.1	0.3	0.2	0.0	0.1	0.0	31.2	24.2	10.5	3.4
Newsprint 3	70.1	29.4	0.2	0.1	0.0	0.1	0.1	32.1	28.1	7.6	2.3

Table 5.4 Peel data

Paper sample	F_{in}		F_c (N/m)		Slope	
	(N/m)	SE (%)	(N/m)	SE (%)		SE (%)
ASTM paper 1	103.5	4	430	3	0.266	5
ASTM paper 2	128.0	5	506	4	0.237	6
ASTM paper 4	92.4	3	>500	-	0.235	4
ASTM paper 5	179.4	5	620	2	0.221	6
ASTM paper 8	69.8	15	>360	-	0.262	14
ASTM paper 9	85.6	2	>500	-	0.285	2
ASTM paper10	122.9	8	545	3	0.256	9
ASTM paper 11	113.8	-	383	2	0.275	-
ASTM paper 12	114.6	-	347	4	0.273	-
ASTM paper13	111.5	3	518	2	0.267	3
ASTM paper 14	68.4	0	459	3	0.363	0
ASTM paper 15	99.6	3	595	2	0.282	3
Copy paper 1	104.8	8	>547	-	0.274	6
Copy paper 2	111.1	2	>538	-	0.252	2
Glassine paper	118.0	7	>491	-	0.218	8
Filter paper 1	208.7	6	399	3	0.188	14
Filter paper 4	186.6	-	295	3	0.266	-
Filter paper 5	175.1	2	481	4	0.214	3
Newsprint 1	125.9	5	494	2	0.230	5
Newsprint 2	72.6	7	398	2	0.279	6
Newsprint 3	66.7	16	401	4	0.299	15

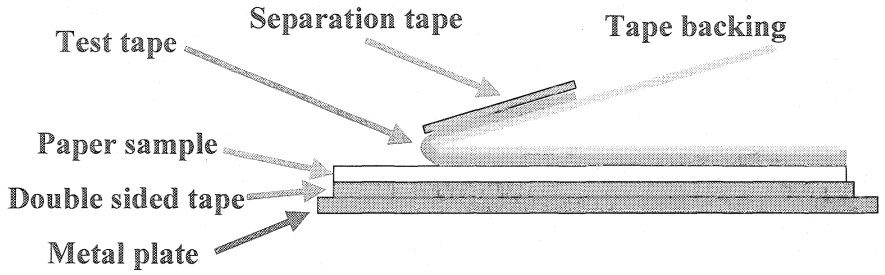

Figure 5.1 Construction of 180° peel samples

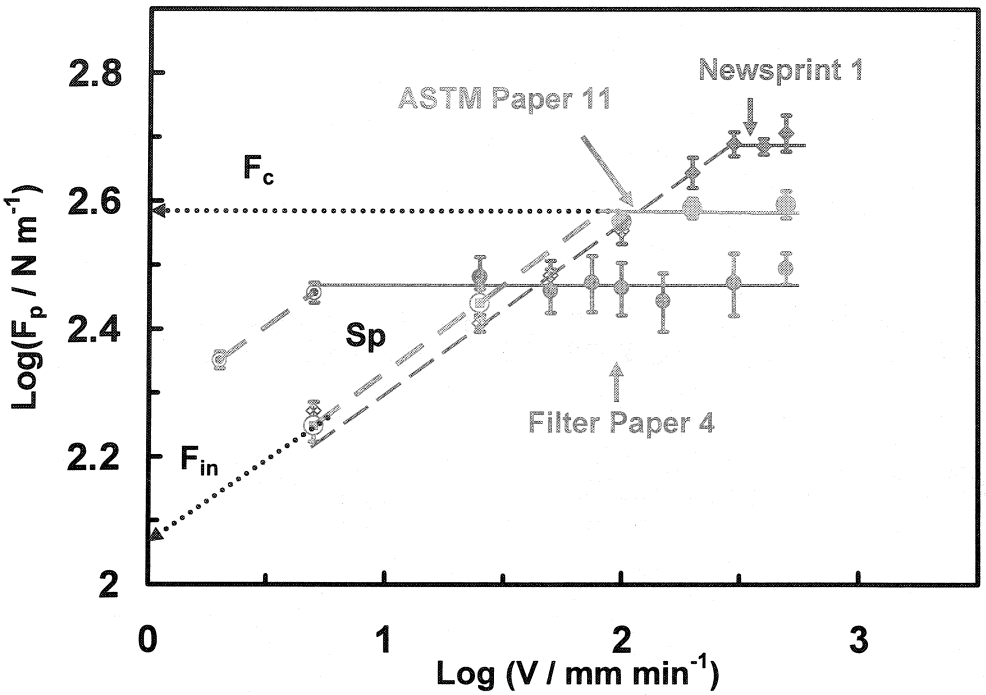

Figure 5.2 **Illustration of peel data analysis of plotting log (F_p) against log (V). F_p is the peak peel force, i.e. the maximum force in peel traces. V is the peel rate. Open symbols are for interfacial failure; solid symbols are for paper failure. Three parameters are defined in the plot of ASTM paper 11: the maximum peel force (F_c), the peel force at a peel rate of 1mm/min (F_{in}) and the slope (Sp) of the interfacial failure line.**

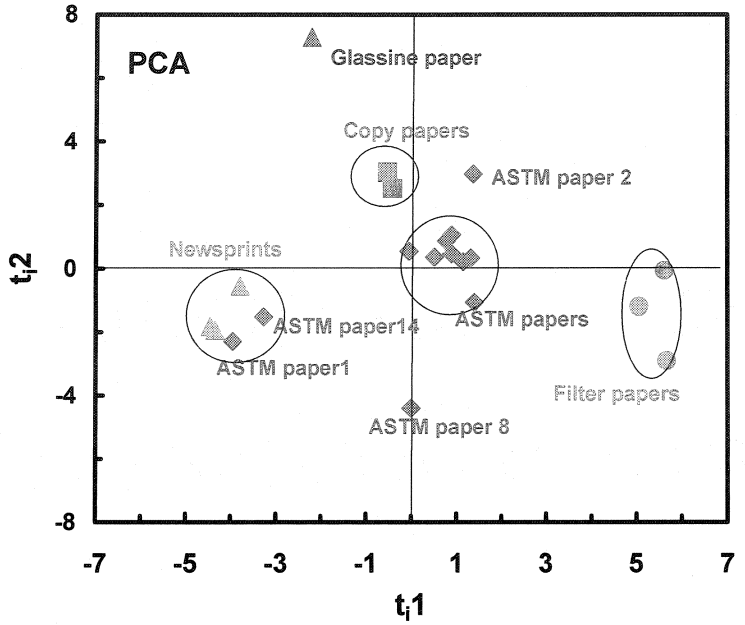

Figure 5.3 **Scatter plot of PCA scores t_i1 versus t_i2. Numbers 1 and 2 represent the first and second PCA component respectively. The subscript *i* refers to the paper sample (*i* ranges from 1 to 21).**

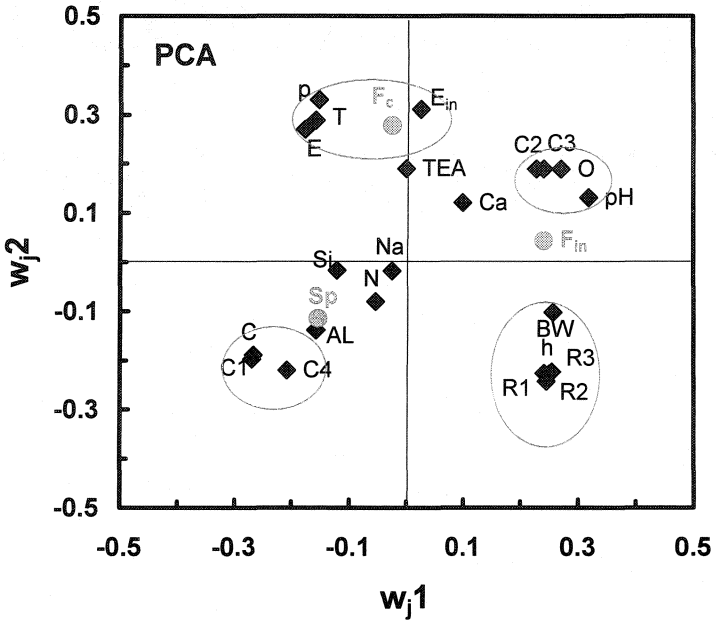

Figure 5.4 **Scatter plot of PCA weights w_j1 versus w_j2. The labels 1 and 2 represent the first and second PCA component respectively, and the subscript j refers to a specific property.**

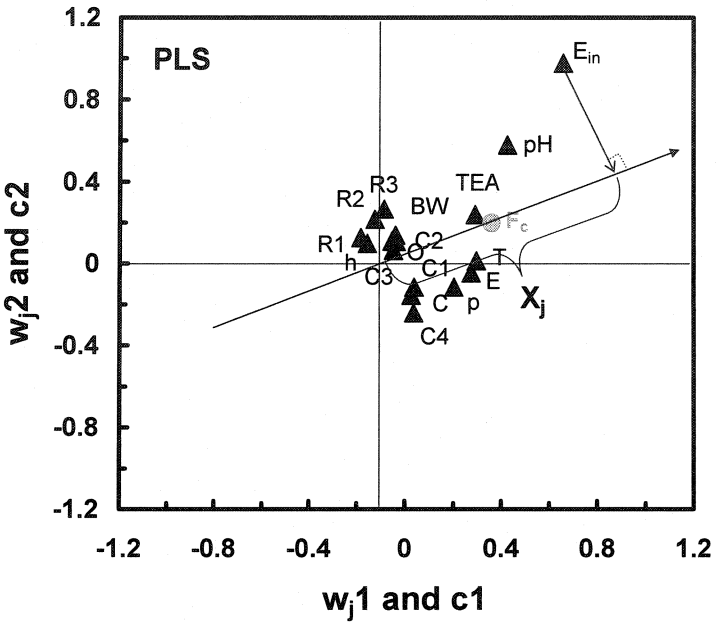

Figure 5.5 **Illustration of the determination of the PLS coefficients (X_j) of paper properties on F_c by plotting the weights w_j1 and c1 versus w_j2 and c2. w denotes the weight of paper properties and c denotes that of the peel response F_c. 1 and 2 represent the first and second new variables respectively. j denotes each of the paper property variables.**

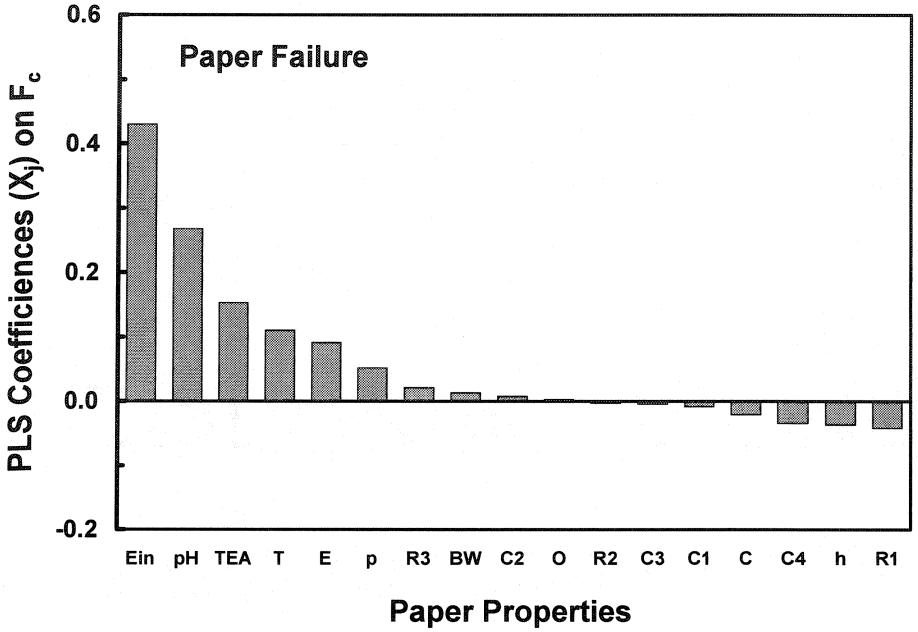

Figure 5.6 **The PLS coefficients (X_j) showing the relative contributions of paper properties to paper peel strength, F_c**

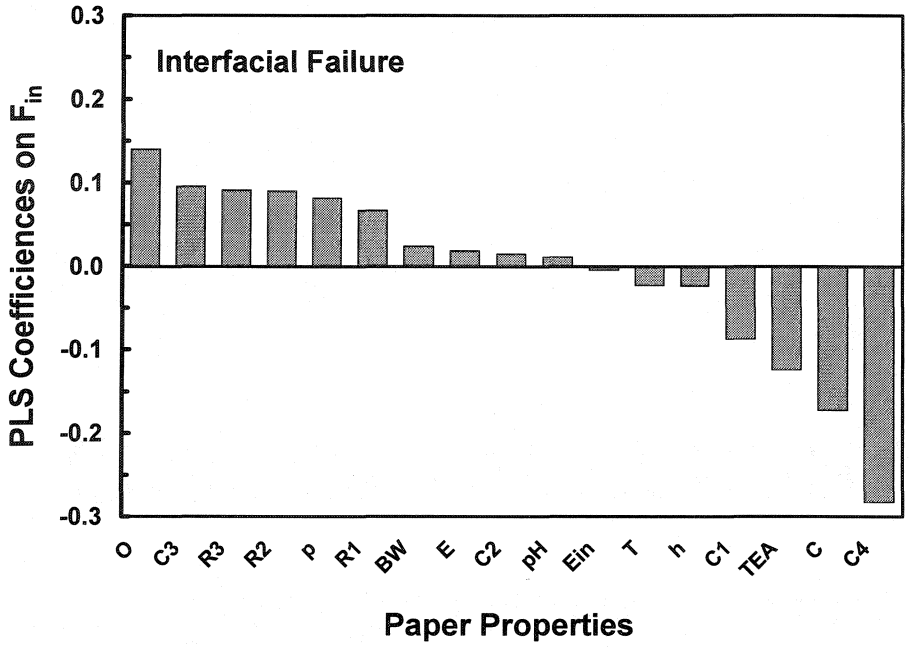

Figure 5.7 **The PLS coefficients showing the relative contributions of paper properties to the low speed, interfacial peel strength, F_{in}**

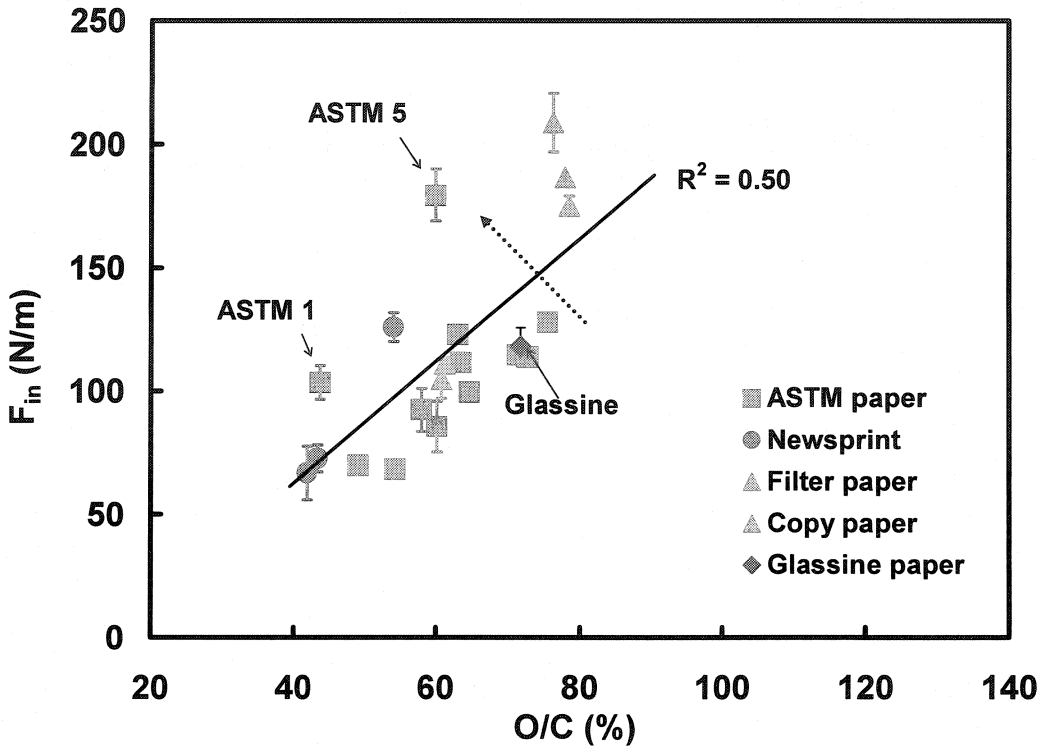

Figure 5.8 **Interfacial peel force F_{in} as a function of O/C, the ratio of surface oxygen to carbon.**

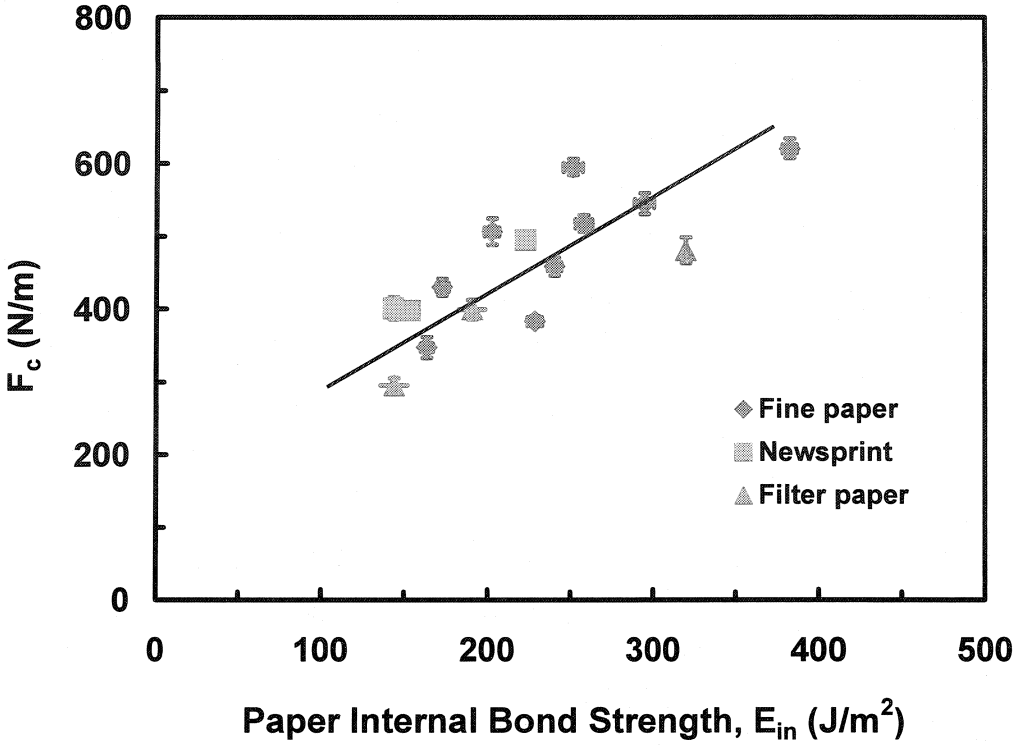

Figure 5.9 **The maximum peel force F_c as a function of paper internal bond strength.**

5.8 Appendix: Scores and weights of the PCA, PLS analyses

In the PCA analysis, two new variables (t1 and t2) were calculated to represent the original properties (both paper properties and peel responses); they were found to explain 59% variation of the data in table 5.2, 5.3 and 5.4. The scores values (t1 and t2) for each sample and the weights of the original properties to the new variables are listed in Table 5.5.

In the PLS analysis to F_c, the two new variables t1 and t2 were found to be able to explain 73% variation of the paper property data in Table 5.2 and 5.3, and 67% variation of F_c. The score and weight values are listed in table 6, as well as the PLS coefficients (X_j) of paper properties on F_c.

In the PLS analysis to F_{in}, the two new variables t1 and t2 were found to be able to explain 66% variation of the paper property data in Table 5.2 and 5.3, and 69% variation of F_{in}. The score and weight values are listed in table 7, as well as the PLS coefficients of paper properties on F_{in}.

Finally, the PLS analysis on Sp didn't yield any new variable. This suggests that the influence of paper properties on Sp was not significant.

Table 5.5 PCA scores (t_i1 and t_i2) and weights (w_j1 and w_j2). Here, the subscript i refers to a specific paper sample, and j refers to a specific property.

PCA Scores			PCA Weights		
Paper Sample	t_i1	t_i2	Property	w_j1	w_j2
ASTM paper 1	-3.950	-2.292	BW	0.257	-0.102
ASTM paper 2	1.371	2.981	h	0.255	-0.224
ASTM paper 4	1.396	-1.064	p	-0.152	0.330
ASTM paper 5	0.510	0.360	R1	0.246	-0.243
ASTM paper 8	-0.002	-4.390	R2	0.251	-0.227
ASTM paper 9	-0.049	0.540	R3	0.242	-0.226
ASTM paper10	0.895	0.466	T	-0.158	0.289
ASTM paper 11	0.894	1.059	E	-0.176	0.270
ASTM paper 12	1.311	0.324	TEA	0.000	0.190
ASTM paper13	0.775	0.868	E_{in}	0.026	0.310
ASTM paper 14	-3.270	-1.526	pH	0.319	0.131
ASTM paper 15	1.144	0.209	C	-0.266	-0.189
Copy paper 1	-0.411	2.533	O	0.271	0.189
Copy paper 2	-0.519	3.038	C1	-0.269	-0.197
Glassine paper	-2.209	7.289	C2	0.241	0.189
Filter paper 1	5.058	-1.199	C3	0.229	0.189
Filter paper 4	5.673	-2.908	C4	-0.207	-0.219
Filter paper 5	5.626	-0.060	N	-0.053	-0.080
Newsprint 1	-3.789	-0.549	Na	-0.025	-0.018
Newsprint 2	-4.446	-1.821	Al	-0.157	-0.138
Newsprint 3	-4.341	-1.944	Si	-0.121	-0.016
			Ca	0.100	0.121
			F_{in}	0.241	0.043
			F_c	-0.024	0.277
			Sp	-0.153	-0.115

Table 5.6 PLS scores (t_i1 and t_i2), weights (w_j1, c1, w_j2, c2) and coefficient (X_j) on F_c. Here, the subscript i refers to a specific paper sample, and j refers to a specific paper property.

PLS Scores			PLS Weights			PLS Coefficients	
Paper sample	t_i1	t_i2	Property	w_j1 and c1	w_j2 and c2	Property	X_j
ASTM paper 1	0.573	-2.617	BW	-0.038	0.138	E_{in}	0.430
ASTM paper 2	1.922	0.737	h	-0.156	0.099	pH	0.267
ASTM paper 5	1.588	2.484	p	0.204	-0.115	TEA	0.152
ASTM paper 10	1.044	1.578	R1	-0.184	0.127	T	0.110
ASTM paper 11	0.385	0.016	R2	-0.124	0.216	E	0.090
ASTM paper 12	-0.426	-0.404	R3	-0.086	0.266	p	0.051
ASTM paper 13	1.105	1.055	T	0.297	0.014	R3	0.021
ASTM paper 14	1.603	-0.713	E	0.275	-0.045	BW	0.013
ASTM paper 15	0.550	1.701	TEA	0.292	0.239	C2	0.008
Filter paper 1	-3.276	0.934	E_{in}	0.660	0.978	O	0.002
Filter paper 4	-4.973	0.531	pH	0.426	0.578	R2	-0.003
Filter paper 5	-1.251	3.726	C	0.026	-0.155	C3	-0.005
Newsprint 1	0.540	-2.319	O	-0.053	0.109	C1	-0.009
Newsprint 2	-0.399	-4.304	C1	0.039	-0.115	C	-0.021
Newsprint 3	-0.711	-4.000	C2	-0.037	0.107	C4	-0.034
			C3	-0.048	0.064	h	-0.037
			C4	0.036	-0.241	R1	-0.042
			F_c	0.361	0.196		

Table 5.7 PLS scores (t_i1 and t_i2), weights (w_j1. c1, w_j2, c2) and coefficient (X_j) on F_{in}. Here, the subscript i refers to a specific paper sample, and j refers to a specific paper property.

PLS Scores			PLS Weights			PLS Coefficients	
Paper Sample	t_i1	t_i2	Property	w_j1 and c1	w_j2 and c2	Property	X_j
ASTM paper 1	-3.950	-2.292	BW	0.236	-0.159	O	0.140
ASTM paper 2	1.371	2.981	H	0.203	-0.304	C3	0.095
ASTM paper 4	1.396	-1.064	P	-0.072	0.383	R3	0.091
ASTM paper 5	0.510	0.360	R1	0.257	-0.020	R2	0.090
ASTM paper 8	-0.002	-4.390	R2	0.277	0.045	p	0.082
ASTM paper 9	-0.049	0.540	R3	0.270	0.056	R1	0.067
ASTM paper10	0.895	0.466	T	-0.145	0.066	BW	0.024
ASTM paper 11	0.894	1.059	E	-0.131	0.208	E	0.019
ASTM paper 12	1.311	0.324	TEA	-0.086	-0.375	C2	0.015
ASTM paper13	0.775	0.868	E_{in}	0.013	-0.031	pH	0.011
ASTM paper 14	-3.270	-1.526	pH	0.178	-0.147	E_{in}	-0.005
ASTM paper 15	1.144	0.209	C	-0.360	-0.271	T	-0.023
Copy paper 1	-0.411	2.533	O	0.341	0.166	h	-0.024
Copy paper 2	-0.519	3.038	C1	-0.302	-0.008	C1	-0.087
Glassine paper	-2.209	7.289	C2	0.227	-0.184	TEA	-0.124
Filter paper 1	5.058	-1.199	C3	0.271	0.072	C	-0.173
Filter paper 4	5.673	-2.908	C4	-0.377	-0.664	C4	-0.282
Filter paper 5	5.626	-0.060	F_{in}	0.280	0.266		
Newsprint 1	-3.789	-0.549					
Newsprint 2	-4.446	-1.821					
Newsprint 3	-4.341	-1.944					

Chapter 6

Using Peel as a Measure of Paper Surface Strength

Abstract

The force required to initiate delamination of paper when peeling a strip of adhesive tape is proposed as a measure of paper surface strength. Employing a 180° peeling geometry in which only the test tape was allowed to bend resulted in measurements which were insensitive to tape properties, peeling direction and peeling velocity. Peel surface strengths were compared to IGT surface strength velocities (a current industrial measure) for 15 uncoated papers, which included machine made fine papers, newsprint and filter paper. The newsprint and fine papers surface peel strengths were linearly correlated with the IGT results, whereas the filter paper data were poorly correlated. We propose that the IGT test was compromised by excessive liquid pickup in the very porous filter paper. The peeling measurements offer the advantages that a force is directly measured, measurements from vastly different paper types can be directly compared and the procedure does not require operator assessment of the onset of paper failure.

6.1 Introduction

Paper surface strength is an important property for printing, coating and converting operations because these processes apply significant stresses to paper surfaces. Paper failure in these operations can take many forms including linting, fiber picking, blistering or catastrophic delamination [1]. One approach to optimizing surface strength is to simply optimize bulk paper strength on the assumption that similar fiber strength and bonding properties determine both the surface and bulk properties, such as tensile and burst. However, it seems more appropriate to measure surface strength directly by methods which, to some extent, mimic the stresses applied during printing. Although many methods have been proposed for measuring the surface strength of paper, the IGT test appears to be the most widely employed. The IGT test consists of accelerating a strip of paper through a nip consisting of a drive wheel contacting a disk coated with a test fluid. During a test, the drive wheel is accelerating, which means the forces applied to the paper surface increase with distance along the test strip of paper. The operator determines the location along the paper strip where the first fibers are picked. Thus, the output of the IGT test is a velocity. Since paper and paperboard span a large range of surface strengths, IGT provides three test fluids covering a range of viscosities and according to IGT Method - W31, the results are expressed as a product of the pick velocity and the test fluid viscosity. An advantage of the IGT test is that it simulates some types of printing nips. However, reading the IGT strength from a picked paper surface is operator-dependent, and the reproducibility was found to be poor among different laboratories [2]. There may also be issues associated with trying to compare results from different test fluids.

In this work we compare IGT to a modified peeling test as an assessment of surface strength. Using peel to measure paper properties has a long history in paper science. Half a century ago, the Graphic Arts Research Laboratory in Sweden proposed peeling pressure-sensitive adhesive tapes from paper as a measure of paper surface strength [3]. Their method used a peeling geometry similar to the T-peel test used in adhesives technology. The maximum peel force was used as the paper surface strength. It was also reported that the measured forces were dependent on peel rate, suggesting that measured forces were sensitive to the viscoelastic properties of the adhesive. We suspect that this is because the peel geometry in their testing was not fixed and because energy was consumed in bending both the test paper and the adhesive tape. Our approach uses a peeling geometry in which the paper does not bend. The results presented show that it is possible to achieve a peel-rate independent measure of paper surface strength which is strongly correlated to the IGT strength while offering some advantages.

6.2 Experimental

6.2.1 Materials

Table 6.1 describes the 15 uncoated papers employed in this work, including fine paper, newsprint and filter paper. The fine paper samples were made elsewhere on pilot papermachines for an ASTM paper-aging research program.

Each peel test involved three adhesive tapes: 1) the "peeling adhesive tape" (3M Scotch Brand 9974B, 25 mm wide, 77 μm thick) which was used to apply stress to the test paper surface; 2) a double-sided "fixing tape" (tape 9974B) which was used to fix the test paper to a metal panel; and, 3) the single-sided transparent "separation tape" (Grand &Toy Ruban Invisible) which was used to facilitate the initiation of peeling – see below.

6.2.2 Peel tests

The preparation of peel test samples was based on our previous work [4] and each test sample involves two types of paper and three adhesive tapes. The two papers are the "test paper" whose surface strength is being measured, and the "backing paper" (Canon copy paper, 0.1 mm thick, basis weight 77g/m^2) which is used to cover the peeling adhesive (see below). The test sample construction is illustrated in Figure 6.1.

2.5cm x 4cm strips of peeling tape were placed across a sheet of Canon copy paper which was trimmed to 2.5cm (i.e. to match the adhesive width) yielding a paper tail which extended more than 10cm beyond the tape. Next, the white backing was removed from the other surface of the adhesive tape. A strip of the separation tape, 2.5cm x 1cm, was placed across the front edge of the adhesive surface with the sticky side facing the adhesive layer to serve as a separation or release layer to help initiate the peel crack. The resulting tape strip consisted of 4cm adhesive layer, 10cm bare paper backing tail and 1cm separation tape across the front edge of the adhesive surface. The paper backing offered little resistance to folding and also gave much stronger adhesion between the backing and the adhesive.

A conditioned (23 °C, 50% RH) test paper strip was trimmed to 5cm x 6 cm so that the peeling direction corresponded to the machine direction. The paper strip was fixed onto the surface of a stainless steel panel (1mm x 7.5cm x 10 cm) using the fixing tape. The strip of peeling adhesive tape was applied to the middle of the mounted test paper (see Figure 6.1A) and the laminate was pressed by 10 passes with a 2.04 kg rubber coated roller (ChemInstruments, US).

The metal panel was clamped into the lower crosshead of an Instron machine (Model 411) located in a Tappi standard controlled temperature and humidity room. The separation tape facilitated the final step, which was gently to fold back the test tape tail and fix it to the top crosshead giving a 180° peeling geometry - see Figure 6.1B. The initial distance between the lower and top crossheads was 11cm.

Peel tests were performed within two minutes of lamination. The peel trace for an individual experiment was recorded in form of a force/distance curve. Each paper sample was tested at least 6 times at a given peel rate. The methods of data analysis and error estimation are described in the results section.

6.2.3 IGT surface strength test

The IGT surface strengths of the paper samples were measured on an IGT (model A1C2) tester in the Paprican Printability Laboratory in Montreal following the standard method of ISO 3783 as closely as possible. The test oil was applied to inking rollers of the IGT inking systems, and about 10 minutes was allowed for evenly distributing the test oil. Then, the IGT printing disk was placed against the inking rollers for 1 min. Next, the inked disk was attached to the IGT tester against the paper sample mounted on an acceleration wheel; the paper was then printed under acceleration from zero to a preset end-velocity, V_{final}. It was found that the standard IGT oil of middle viscosity (IGT Testing Systems, Inc.) was suitable for all of the samples in this study.

Paper samples were cut into strips around 5cm x 35cm along their machine direction. The paper strip was then mounted on the IGT acceleration wheel with the smooth side facing up. Preliminary tests were performed to identify an appropriate end-velocity so that the fiber picking would occur near the middle of the strip. The print surface was examined for picked fibers under low angle illumination. The velocity at which the first pick occurred, V_{pick}, was reported as the surface strength of the paper.

6.3 Results

Virtually everyone who has tried to peel tape from paper knows that the tape will cleanly separate from the paper (i.e. interfacial failure) if one peels very slowly, whereas rapid peeling causes catastrophic failure of the paper surface. Examples of peel curves illustrating these two cases are shown in Figure 6.2. The interfacial failure curve is characterized by a force plateau, while the paper failure curve is characterized by a peak force F_p and a lower steady-state force. Herein, interfacial failure is defined as the absence of a fiber layer on the adhesive surface after peeling whereas paper failure corresponds to at least one fiber layer embedded in the tape surface after peeling. The mixed failure region shown in Figure 6.2 is a transitional region leading to complete delamination.

It has been long known that the tendency of a paper to delaminate in peel can be very sensitive to peeling direction, apparently reflecting whether the fiber ends are orientated up or down in the z-direction, which in turn is a function of the drag-to-rush ratio [5, 6, 7]. Figure 6.3 shows replicated peeling traces obtained with ASTM paper #5 at 100mm/min. One half of the data was obtained by peeling one way in the machine direction (MD1) whereas the other half was peeled in the opposite machine direction (MD2). The MD2 peels all lead to paper delamination with a reproducible steady state peel force. By contrast, the MD1 peels gave reproducible interfacial peel curves with a much higher steady-state peel force. Fortunately, the peak force F_p for the MD2 experiments corresponded to the steady-state MD1 results suggesting the F_p is a direction-independent parameter.

In previous work, we showed that peak force F_p increases monotonically with peel rate until paper failure after which peak force is independent of peel rate [4]. This behavior is illustrated in Figure 6.4 which shows plots of log (F_p) versus log (V), where F_p equals the stable interfacial force in the interfacial failure domain and the peak force in

the paper failure domain and is the mean of at least 6 observations. The error bars in the Figure 6.3 were calculated as $Log((F_p \pm SD)/F_p))$ where SD is the standard deviation of F_p based on 6 replicates.

The results for each tape/paper combination in Figure 6.4 consisted of two linear segments on the log-log plots. The segment with the positive slopes corresponded to interfacial failure (open points in Figure 6.4) whereas the horizontal segments corresponded to paper failure (solid points). The intercept of the segments gives the critical peel rate at which paper failure starts. Previous work showed that the critical peel rate was difficult to identify accurately for papers with weak surfaces like newsprint [4]. By contrast, F_c, the peak peel force corresponding to paper failure can be measured accurately. Therefore we propose to use F_c, which we call *surface peel strength,* as a measure of paper surface strength.

The paper surface strengths as measured by the Peel and IGT tests are summarized in Table 6.2. The surface peel strength (F_c values) were calculated as the mean of the peak peel force values (F_p) for those peel rates which induced paper failure. The corresponding standard errors (SE) were calculated as $\sqrt{\left(\sum_1^m (SD^2/n)\right)/m}$ where SD is the standard deviation of F_p of n (n >= 6) replications at each peel rate, at which paper failure occurred; m is the number of paper failure points. For example, consider the newsprint peel results in Figure 6.4. Only the results from the highest three peel rates induced paper failure so these were used to calculate F_c (i.e. m=3) and the corresponding SE.

The IGT results in Table 6.2 consist of V_{pick} values, the mean of the wheel velocity corresponding to the initiation of fiber picking. The corresponding standard errors were based on 5 replicates of each paper sample.

The percentage standard errors of the peel and IGT results in Table 6.2 span the same range. The peel surface strengths are plotted against the corresponding IGT values in Figure 6.5. For newsprint and the uncoated fine papers, although the data points were scattered, there was a good linear correlation between F_c and V_{pick} with correlation coefficient (R^2) 0.71. For the three filter papers, there was no correlation between the methods. The IGT results suggested that the filter papers had the highest surface strengths whereas the peel tests ranked the filter papers in the bottom half of surface strengths and included the weakest paper.

6.4 Discussion

We propose that the peak peel force required to delaminate paper in peel can be used as a measure of paper surface strength. The advantage of using the peak force is that it is related to the initiation of failure at the paper surface. By contrast, past peel studies [7,8, 9,10,11,12,13] have focused on the steady-state delamination force. Because of its layered structure, paper is relatively easy to delaminate once the failure has been initiated. Indeed, the steady-state delamination force is highly correlated to the internal bond strength and other measurements of z-direction strength [14].

Our peeling geometry differs from previous work [3]. By employing 180° peeling with the test paper fixed to the stainless steel plate (Figure 6.1), the paper is not required to bend which means the results should be independent of the stiffness of the paper or paperboard.

Only peeling experiments which lead to paper failure give a measure of paper surface strength. Previous work with a series of tapes indicated that the surface strengths were insensitive to the tape type, lamination pressure or dwell time [15]. This conclusion is reasonable since the adhesive layer does not fail during the tests of interest. However, we expect departures from tape independence with extremely thick tapes or tapes with stiff backings which require significant work to bend. We recommend replacing the commercial tape backing with paper because the commercial backings are stiff and designed to easily separate from the adhesive layer. By contrast, the replacement paper backing strongly adheres to the adhesive and is flexible enough to ensure a stable 180° peeling.

The results in Figure 6.4 show that in the paper failure domain, the results are insensitive to peel rate. Therefore in a routine testing situation, surface strengths could be measured at only one peel rate. In this situation, sample preparation and testing could be completed within ten minutes.

Surface strength determined by peel showed a reasonable correlation with the IGT results. The largest discrepancies were with filter papers where we propose the IGT results were poor due to excessive fluid pickup.

To summarize, we have shown that peak peel forces measured with 180° peel give a measure of the propensity of a paper surface to initiate failure. The advantages of using peel to characterize surface strength are that the method is rapid, there is little penetration of the adhesive into the paper structure, the result is a force, and the results are independent of operator judgment.

6.5 Conclusions

From this work, we can conclude that

1. The peak peel force required to initiate delamination when a tape is peeled from a paper surface is a measure of surface strength we call the *paper surface peel strength*. The critical elements of the method are: a) the stiff release backing used for most double sided tapes was replaced with a flexible paper backing; b) the test paper was fixed to metal panel so the paper did not bend during the test; and, 3) only peak peel forces leading to paper delamination were used.
2. *Paper surface peel strength* is independent of peel rate up to 500 mm/min, the limit of our test equipment.
3. *Paper surface peel strengths* were linearly correlated with the IGT surface strengths for uncoated fine paper and newsprint. By contrast, filter paper gave poor correlations possibly because excess penetration of IGT test fluid into the filter paper gave erratic results.
4. The advantages of the peel-based test are that the procedure is rapid and operator independent giving a quantitative force.

6.6 Acknowledgements

This work was supported by 3M Canada and NSERC. We thank Alison Banks and Luis Anderson for experimental assistance, Anthony Manfred for helping with IGT testing, and Bruce Arnold (Chair of the ASTM Paper Aging Research Program) for providing the ASTM paper samples.

6.7 References

1 P.J. Mangin, 1987 *Proceedings of technical association of the graphic arts*, p. 397

2 J.S. Aspler, S. Davis, S. Ferguson, N. Gurnagul, and M.B. Lyne, *Tappi,* 68 (5):112 (1985).

3 A. Arname, I. Olsson and L. Pihl, *Svensk Papperstidning*, 18(30):709 (1952).

4 B. Zhao and R. Pelton, *J. Adhesion Sci. and Tech.* 17(6):815 (2003).

5 Derek Page, personal communication.

6 K. Niskanen, I. Kajanto and P. Pakarinen, "Paper structure", In: *Paper Physics*, edited by K. Niskanen, Fapet Oy (1998).

7 R. Pelton, W. Chen, H. Li and M.R. Engel, *J. Adhesion*, 77:285 (2001).

8 T. Yamauchi, T. Cho, R. Imarnura and K. Murakarn, *Nordic Pulp Paper Res. J.*, (3):128 (1988).

9 J. Skowronski and W. Bichard, *J. Pulp Paper Sci.,* 13(5):165 (1987).

10 J. Skowronski, *J. Pulp Paper Sci.,* 17(6):217 (1991).

11 A. El Maachi, S. Sapieha and A. Yelon, *J. Pulp Paper Sci.*, 21(10): 362 (1995).

12 A. El Maachi, S. Sapieha and A. Yelon, *J. Pulp Paper Sci.* 21(12): 401 (1995).

13 A. El Maachi, S. Sapieha and A. Yelon, *Nordic Pulp Paper Research J.*, 14(1):17 (1999).

14 A. Koubaa and Z. Koran, *Tappi* 78(3):103 (1995).

15 B. Zhao, *PhD thesis*, McMaster University, *in preparation* (2004)

6.8 Tables and figures

Table 6.1 Paper samples.

Sample	*Pulp Type 1*	*Pulp Type 2*	*pH*	*Ph Control Chemical*	*Calcium Carbonate*	*Internal Size*	Paper Density (Kg/m^3)
ASTM paper 1	100% BNSWK	None	5	Alum	None	2#/T Rosin	649
ASTM paper 2	100% BNSWK	None	8.1	Na_2CO_3	5%PCC	None	658
ASTM paper 5	100% Cotton	None	5	Alum	None	2#/T Rosin	642
ASTM paper 10	20%BNSWK	80% HW-BCTMP	8.1	Na_2CO_3	5%PCC	None	609
ASTM paper 11	50%BNSWK	50% BNHWK	8.1	Na_2CO_3	None	None	680
ASTM paper 12	50%BNSWK	50% BNHWK	8.1	Na_2CO_3	5%PCC	None	593
ASTM paper 13	50%BNSWK	50% HW- BCTMP	8.1	Na_2CO_3	5%PCC	None	614
ASTM paper 14	50%BNSWK	50% HW-BCTMP	5	Alum	None	2#/T Rosin	631
ASTM paper 15	50%BNSWK	50% BNHWK	8.1	Na_2CO_3	5%PCC	4#/T AKD	550
Newsprint 1	100% TMP	-	-	-	-	-	662
Newsprint 2	100% TMP	-	-	-	-	-	683
Newsprint 3	100% TMP	-	-	-	-	-	624
Filter paper 1	100% Cotton	-	-	-	-	-	505
Filter paper 4	100% Cotton	-	-	-	-	-	459
Filter paper 5	100% Cotton	-	-	-	-	-	534

Note:
1 - symbol list
BNSWK: bleached softwood Kraft
BNHWK: bleached hardwood Kraft
BCTMP: bleached chemi-thermomechnical pulp
SGW: stone ground wood
TMP: thermomechanical pulp
2 - Most ASTM paper samples were made by Herty Foundation pilot paper machine except of ASTM paper 5 which was made by Crane & Co. Inc. All these samples were provided through the ASTM paper-aging program.
3 - All newsprint samples were provided by Donohue Inc. in Montreal, Canada. The filter papers 1, 4 and 5 are Whatman Filter No.1, No. 4 and No. 5.

Table 6.2 Paper surface strength as measured by Peel and IGT tests

	Peel		IGT		
Sample	F_c (N/m)	SE(%)	V_{final} (cm/s)	V_{pick} (cm/s)	SE(%)
ASTM paper 1	430	3	300	128	4
ASTM paper 2	506	4	300	142	4
ASTM paper 5	620	2	600	234	8
ASTM paper 10	545	3	500	246	3
ASTM paper 11	383	2	200	86	3
ASTM paper 12	347	4	150	86	2
ASTM paper 13	518	2	400	189	2
ASTM paper 14	459	3	400	204	5
ASTM paper 15	595	2	600	300	3
Newsprint 1	494	3	200	86	4
Newsprint 2	398	3	100	55	2
Newsprint 3	401	4	100	53	5
Filter paper 1	399	2	700	327	4
Filter paper 4	295	3	600	360	4
Filter paper 5	481	3	700	522	3

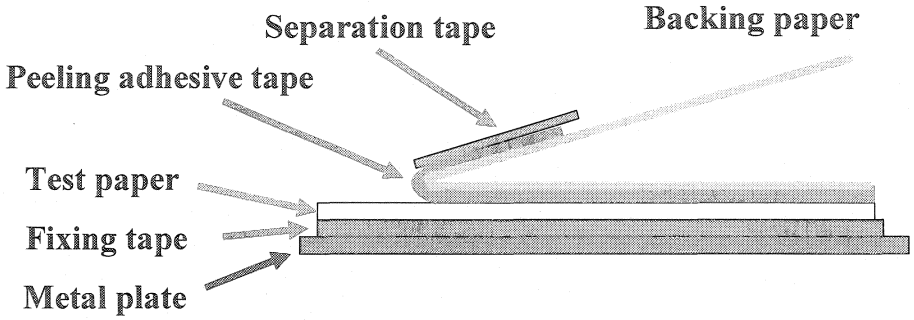

(A) **Construction of the 180° peel test samples**

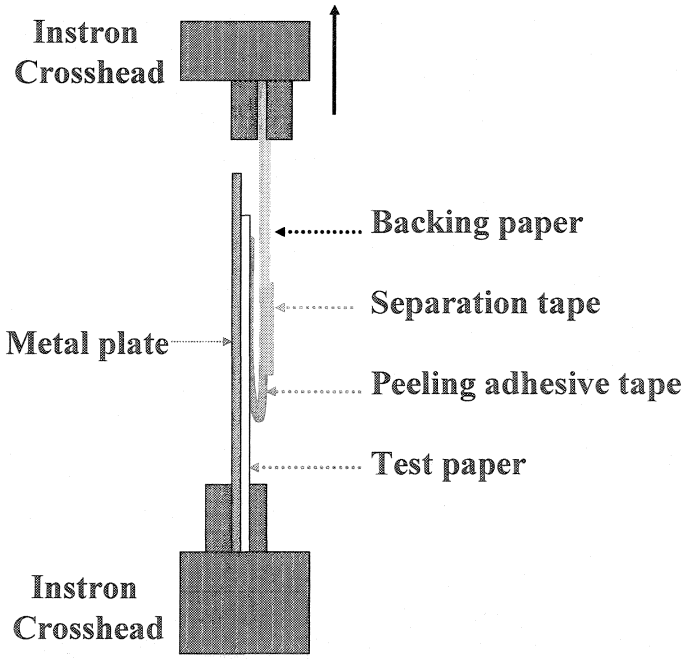

(B) Geometry of the 180° peel test

Figure 6.1 Experimental setup for using Peel as a measure of paper surface strength

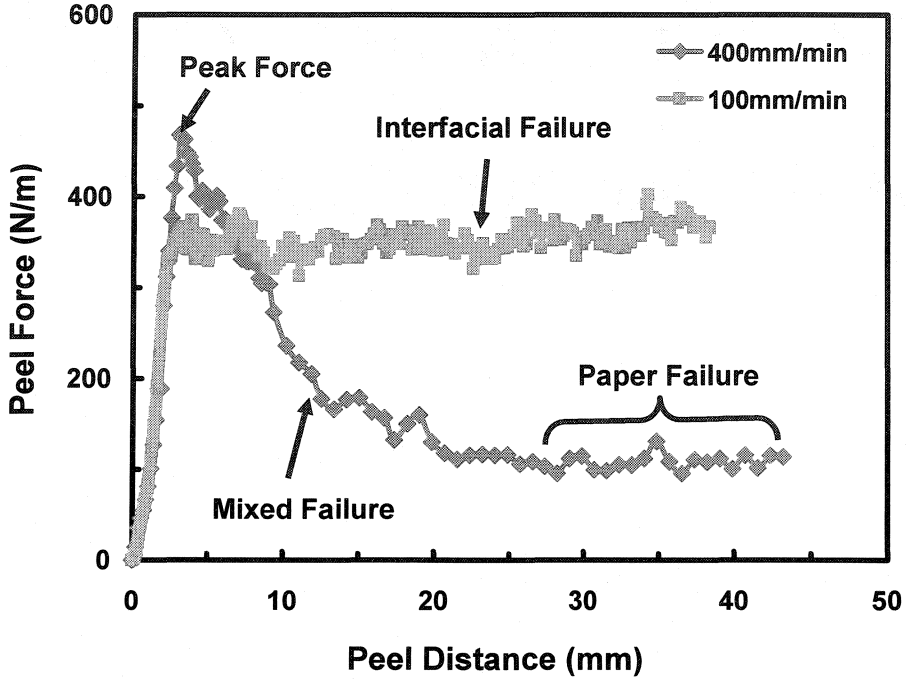

Figure 6.2 **Typical peel curves and failure modes. Peeling PSA tape 9974B from newsprint 1 at peel rates of 100mm/min and 400mm/min. Interfacial failure is defined as the absence of apparent fiber layer picked out from paper surface; paper failure is defined as the presence of at least one fiber layer embedded in the tape surface after peeling; mixed failure is the intermediate state between interfacial and paper failure.**

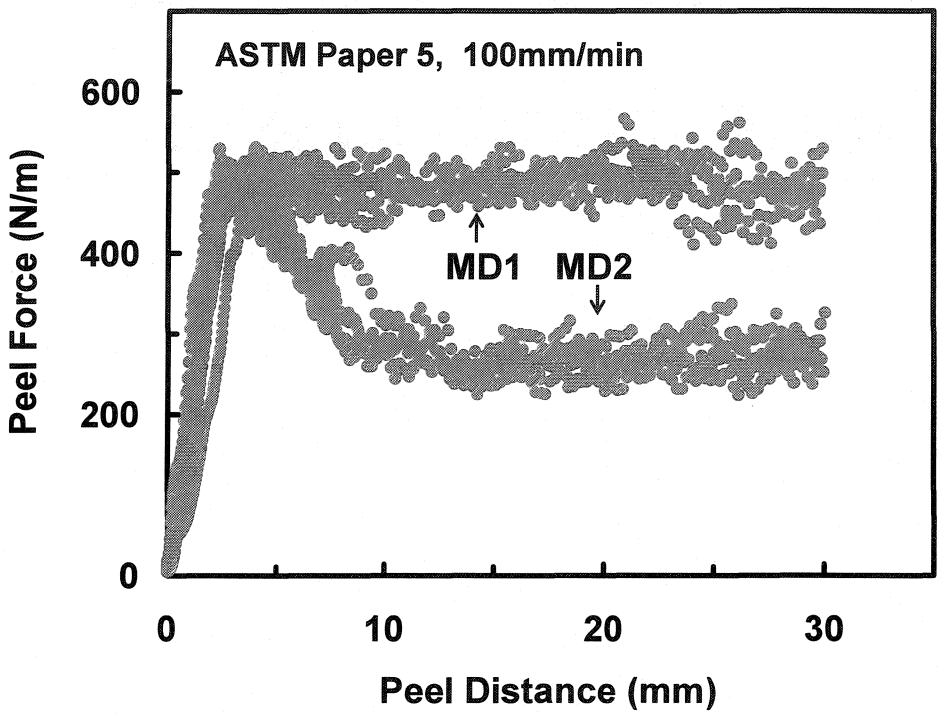

Figure 6.3 **Peeling tape 9974B from ASTM paper 5 along two of its machine directions (MD1 and MD2) at 100mm/min**

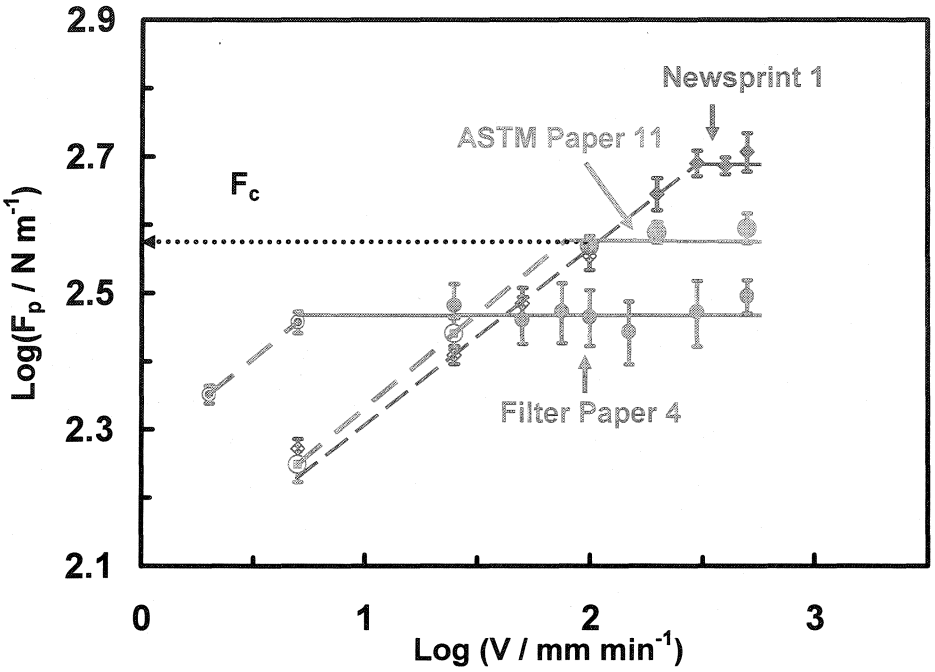

Figure 6.4 **Peel data analysis by plotting log (F_p) against log (V). F_p is the peak peel force, i.e. the maximum force in peel traces. V is the peel rate. Open symbols are for interfacial failure; solid symbols are for paper failure. F_c is the critical force for paper failure.**

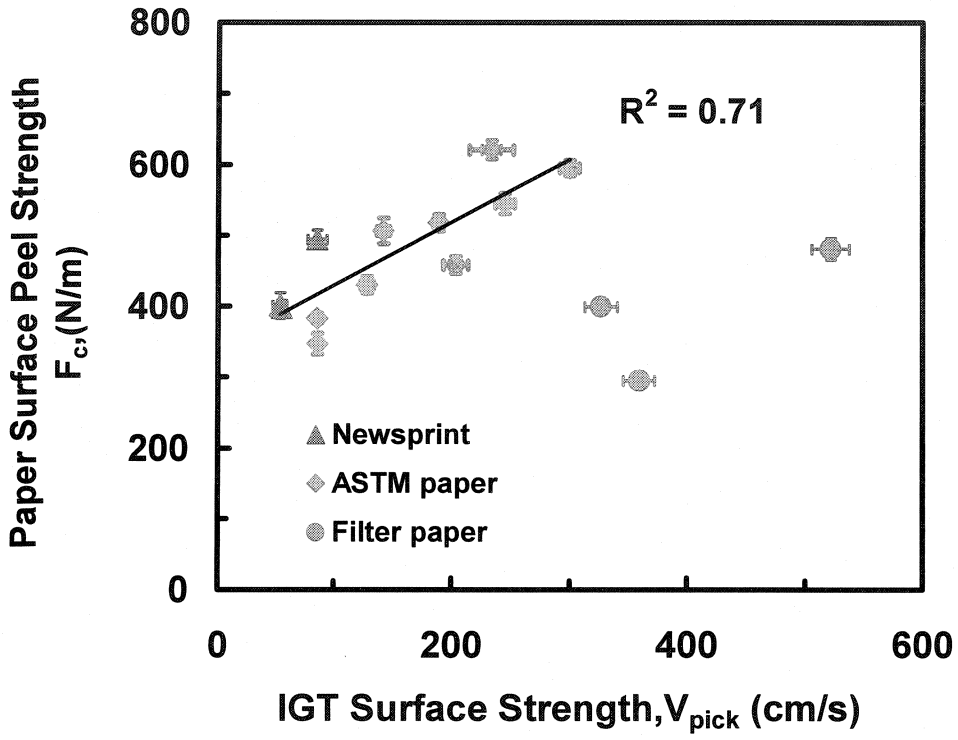

Figure 6.5 **Comparison of paper surface strength by Peel and IGT tests. The error bar is the standard error of the measurements.**

Chapter 7. Conclusions and suggestions

In this thesis, I have investigated the interplay between paper and pressure sensitive adhesive by using peel adhesion testing as a probe. The research objectives set in chapter 1 have been fulfilled. The following provides a review of key findings and a summary of contributions, as well as some suggestions for future work.

7.1 Conclusions

Peeling tapes from paper results in either interfacial failure or paper failure. Interfacial failure is characterized by a stable peel force whereas paper failure is characterized by a high peak force (i.e. the maximum force in a peel curve), a relatively low propagation force and a transition distance over which the failure mode changes from interfacial to paper failure. At the transition region, the paper failure can start from several weak points which then broaden and merge to an entire fiber layer, that is, paper delamination.

Many peeling experiments revealed that the peak force is the most important for studying the adhesive/paper interactions. Based on this, we developed a new peel data analysis method by which the overall peel behavior of a paper/adhesive combination is conveniently summarized by plotting the log peak peel force as a function of log peel rate. This yielded a generalized peel curve consisting of a rate-dependent interfacial failure domain and a rate-independent paper failure domain. The influence of PSA type and peel angle on the generalized peel curve was further determined. It was found that the peel angle shifted the generalized peel curves vertically, whereas the adhesive properties influenced the slope of the interfacial failure segment, but had no significant effect on the paper failure segment.

Three independent parameters were extracted from the generalized peel curve. They are the interfacial peel force (F_{in}) at a low peel rate of 1mm/min, the maximum peel force (F_c), and the slope (Sp) of the interfacial peel force in the plot of log (interfacial peel force) versus log (peel rate). Therefore, the interactions between paper and adhesives can be analyzed by monitoring these three parameters.

The force generated at the paper surface in peeling was analyzed by a new experimental approach in which the induced paper strain in peeling and the peel force were measured simultaneously. By calibrating the induced paper strain, we estimated the force generated at the paper surface which we called the surface peel force. This force was found to be proportional to the overall peel force. By varying peel rates, the two types of forces were shown to have a linear relationship for the two tape types and two paper types investigated. These results proved that we can use the easily-measured peel force as a probe for the real force at the interface. In addition, the experimental technique allowed for examining the peeling region microscopically.

Owning to the peel data analysis method and the microscopic analysis technique, we were able to investigate the fracture mechanism of paper/adhesive laminates in detail. It was observed that, in slow peelings, the adhesives flow away from the paper surface

leaving it intact. However, in rapid peelings, the adhesives are elongated to form many individual fibrils which in turn pull the paper fibers out leading to paper delamination.

The peeling-induced paper delamination was analyzed further by peeling from three sets of paper handsheets made in the laboratory. The delamination was found to be characterized by a high initiation (peak) force and a lower steady force, and the two force characteristics were linearly correlated with a slope of 2.6 independent of the papermaking conditions. Microscopic observations revealed that paper delamination involves three sub-processes: 1) the initial delamination of the top fiber layer from the paper sheet; 2) the fracture of this delaminated top layer so that it remains with the tape in peeling; 3) the continuous peeling of the top fiber layer away from the paper. The need to fracture the top layer (process 2) accounts for the observed peak peel force corresponding to the initiation of paper delamination.

For the first time, links between paper properties and the performance of PSA have been identified by the use of advanced statistical analysis and the newly developed approach for analyzing paper/adhesive peel curves. The paper properties influencing peel force in interfacial failure domain were found to be, primarily, the paper surface chemistry characterized by oxygen/carbon ratio (determined by XPS) and, secondarily, surface roughness; the peel force increased with oxygen/carbon ratio and with the surface roughness. The log-log slope in the interfacial failure domain was found to be independent of paper properties; it is determined by the adhesive rheology. The governing paper property in the paper failure domain was found to be the paper internal bond strength as measured by a paper internal (Scott) bond tester.

Finally, the fundamental research on paper/adhesive interactions was extended to solve a practical problem. We developed a new peel-based test for paper surface strength, in which the force required to initiate paper delamination when a tape is peeled from a paper surface was proposed as a measure of surface strength which we call the *paper surface peel strength*. It was found to be independent of peel rate up to 500 mm/min, the limit of our test equipment, and linearly correlated with the IGT surface strength (an industrial measure of paper surface strength) for uncoated fine paper and newsprint. By contrast, filter paper gave poor correlation possibly because excess penetration of IGT test fluid into the filter paper gave erratic results.

7.2 Summary of contributions

1. A new peel data analysis method was developed for analyzing paper/adhesive interactions.
2. A new technique was developed for measuring the peel force and the induced paper strain simultaneously, by which the force generated at the paper surface was analyzed.
3. For the first time, the initiation of peeling-induced paper delamination process has been analyzed.
4. For the first time, the link between paper properties and the performance of pressure sensitive adhesive was established.
5. A new peel-based approach was developed for measuring paper surface strength.

7.3 Suggestions for future work

The research work in this thesis showed that paper failure can start from several weak points and then transit to the delamination of one fiber layer. It would be interesting to study further this transition phenomenon and the influence of the network structure of paper. For this, it would be helpful to design a series of experiments involving peeling from paper handsheet with varying fiber orientation. Further, man-made flaws on paper surface may help to understand the role of the flaw size.

The relation of paper surface roughness to the interfacial peel force found here suggests that there was not complete contact between paper and adhesives. The paper/adhesive interactions could be better characterized if their contact area could be measured directly. This is a challenge for future work.